

Chemical Characterisation and Source Apportionment of Atmospheric Quasi-Ultra-Fine Particulate Matter (PM_{0.36}): Seasonality and Spatio-Temporal Variability

Kumulative Dissertation

zur Erlangung des akademischen Grades eines doctor rerum naturalium
(Dr. rer. nat.)

vorgelegt der

Mathematisch-Naturwissenschaftlichen Fakultät

der Universität Rostock

von

Fengxia Li

geboren am 04. Mai 1985 in Chongqing

München und Rostock, Mai 2018

ERKLÄRUNG

Ich versichere hiermit an Eides statt, dass ich die vorliegende Arbeit selbstständig angefertigt und ohne fremde Hilfe verfasst habe. Dazu habe ich keine außer den von mir angegebenen Hilfsmitteln und Quellen verwendet und die den benutzten Werken inhaltlich und wörtlich entnommenen Stellen als solche kenntlich gemacht.

Die vorliegende Dissertation wurde bisher in gleicher oder ähnlicher Form keiner anderen Prüfungsbehörde vorgelegt und auch nicht veröffentlicht.

München, Mai 2018

Fengxia Li

Contribution of the Author to Published Papers

The contribution of the author to each publication is briefly summarised as following:

Publication I: Li, F.X., Schnelle-Kreis, J., Karg, E., Cyrus, J., Gu, J.W., Orasche, J., Abbaszade, G., Peters, A., Zimmermann, R. Semi-continuous sampling of health relevant atmospheric particle subfractions for chemical speciation using a rotating drum impactor in series with sequential filter sampler. Environmental Science and Pollution Research 2016; 23, 7278–7287.

For the 1st publication, the author did all the practical work to acquire the data, including the experiments to test the cut-points of 2 RDI, the pilot field sampling as well as the chemical analyses of samples. The author performed all the data processing. The author also undertook the writing, submission and revising of the manuscript.

Publication II: Li, F.X., Schnelle-Kreis, J., Cyrus, J., Karg, E., Gu, J.W., Orasche, J., Abbaszade, G., Peters, A., Zimmermann, R. Organic speciation of ambient quasi ultrafine particulate matter (PM_{0.36}) in Augsburg, Germany: Seasonal variability and source apportionment. Science of The Total Environment 2018; 615: 828-837.

For the 2nd publication, the author carried out a sampling campaign in Augsburg for nearly 1 year and did most of the sampling. The author performed all the chemical analyses of the samples, including organic speciation analysis and elemental carbon/organic carbon (EC/OC) analysis. The author also did all the data processing and analysis, particularly the positive matrix factorization (PMF) modelling. She undertook the writing, submission and revising of the paper.

Publication III: Li, F.X., Schnelle-Kreis, J., Cyrus, J., Wolf K., Karg, E., Gu, J.W., Orasche, J., Abbaszade, G., Peters, A., Zimmermann, R. Spatial and temporal variation of sources contributing to quasi-ultrafine particulate matter PM_{0.36} in Augsburg, Germany. Science of The Total Environment 2018b; 631-632: 191-200.

For the 3rd publication, the author was in charge of the sampling campaign. She did the organic molecular analysis and EC/OC analysis. All the data processing and the PMF analysis were performed by the author. With help from discussion with co-authors, she undertook interpretation of the results and manuscript writing, as well as revision of the paper based on reviewers' comments.

München, May 2018

Fengxia Li

It is the time you have wasted for your rose that makes your rose so important.

If you shed tears when you miss the sun, you also miss the stars.

DANKSAGUNG / ACKNOWLEDGEMENTS

This study was performed within the framework of UIII project “ENVIRONMENTAL NANOPARTICLES AND HEALTH: Exposure, Modeling and Epidemiology of Nanoparticles and their Composition within KORA” in cooperation with Epidemiology Group II of Helmholtz Zentrum München. I was all the time working in the Comprehensive Molecular Analysis (CMA) group of Joint Mass Spectrometry Center (JMSC) of Helmholtz Zentrum München and University Rostock. I would like to express my many thanks to their collaboration and help.

First and foremost, I would like to express my sincere gratitude to my supervisor Prof. Dr. Ralf Zimmermann, for giving me the great opportunity to do scientific research in his group and for his continuously support during this period.

I would also like to give my special thanks to my advisor Dr. Jürgen Schnelle-Kreis. Based on his many years of professional experience in atmospheric particulate matter research and tutoring PhD work, he gave me invaluable suggestions on my research. It is mostly informative and enjoyable to have a discussion with him. Particularly when I was confused or felt difficult to proceed with the scientific writing, it was extremely helpful to have discussions with him. His input never failed to clarify the situation and bring about further progress. He is open-minded, knowledgeable and humorous; it is therefore never boring to listen to his “stories”.

Thank Erwin Karg for his help as an experienced aerosol physicist with the RDI test concept and experimental setup as well as the result interpretation of the tests.

My appreciation also goes to Jürgen Orasche for his help with the sampler setup, and his innovation in devising the original analytical method.

I would also like to thank Geza Koczis for helping me with the transport of samplers between Augsburg and Munich on a weekly basis and relocating the mobile sampler to reference site and other master sites on a 2-weekly basis. Thanks to Kerstin Koch for her help in the laboratory work.

I am also very thankful to colleagues in epidemiology group for their effort and cooperation to carry out the project smoothly. Thank Jianwei Gu for sharing his experience with PMF analysis.

Special thank goes to Chinese Scholarship Council’s financial support to my PhD work for 4 years.

To my parents, thank them for their hard work and support for my education even it is not easy for them. I am also thankful to them for being patient and not giving me extra pressure during my PhD work. I would also like to thank my brother Jiang Li for his support.

Finally, I am extremely grateful to the members of my family, Min and our lovely son Leo. Thank Min for his hard work and for undertaking the responsibility of housekeeping issues as much as he can so that I can focus on my PhD work. Thank Min for always being there and supportive no matter what happened. I am proud of Leo being a healthy, happy, active, curious and smart boy. I hope he will also be proud of me being his mother. This thesis is also an achievement of our family. Particularly, I would like to dedicate it to my boy.

ZUSAMMENFASSUNG

Obwohl die kleinste Fraktion von Partikeln (Ultrafeine Partikel, UFP < 100 nm) nur einen geringen Beitrag zur Massenkonzentration atmosphärischer Partikel (PM) leisten, sind sie der dominierende Anteil der Partikelzahl-Konzentration. Epidemiologische Studien haben Zusammenhänge zwischen der UFP-Exposition und gesundheitsschädlichen Auswirkungen, insbesondere auf das Herz-Kreislauf-System, festgestellt. Auch toxikologische Studien haben UFP oder seine spezifischen Eigenschaften oder Bestandteile mit schädlichen Wirkungen verknüpft. Sowohl Bestandteile als auch die Quellen von quasi-UFP sind mit ihren Wirkungen verknüpft. Die bisher vorliegenden Daten zu Gesundheitseffekten lassen jedoch mangels langfristiger Studien keine klaren Aussagen zu. Langzeit-Studien über organische Aerosolkomponenten und die Quellen von UFP sind selten, da sie kostspielig und aufwendig sind. Die vorliegende Arbeit zielt darauf ab, die saisonale und die räumlich-zeitliche Variabilität der Quellen und Prozesse zu untersuchen, die zur organischen Fraktion von quasi-UFP (hier < 360 nm) in der Umwelt beitragen.

Die Studie umfasste vier Hauptschritte. Im ersten Schritt wurden zwei Rotating Drum Impaktoren (RDIs), hinsichtlich ihrer Partikel Abscheidecharakteristik getestet. In einer Pilotkampagne wurden das Probenahmekonzept, die chemisch-analytische Machbarkeit und die Vergleichbarkeit der Messergebnisse aus parallelen Probenätzen untersucht. Der zweite Schritt war die tägliche parallele PM Probenahme an einem Referenzstandort und jeweils einem von 5 Masterstandorten für nahezu ein Jahr. Der dritte Schritt waren chemische Analysen der gewonnenen PM_{0,36} Proben. Eine in situ Derivatisierung Thermische Desorption Gaschromatographie Massenspektrometrie Methode wurde zur gleichzeitigen Quantifizierung von Markern für primäres und sekundäres organische Aerosol (SOA) angewendet. Spezifische Marker für biogene sekundäre organische Aerosole wurden in die etablierte Methode integriert. Summenfraktionen organischen und elementarem Kohlenstoffs (OC/EC) wurden mit einem thermooptischen Kohlenstoffanalysator bestimmt. Der letzte Schritt der Studie war die Anwendung der Positiv-Matrix-Faktorisierung (PMF) für die Untersuchung der Anteile der unterschiedlichen Quellen am organischen Aerosol auf Basis der organischen Marker und die statistische Analyse der erhaltenen Ergebnisse.

Der Cut-Point der letzten Stufe beider RDIs wurde mit 0,36 µm deutlich über dem nominalen Cut-Point von 0,1 µm gefunden. Die Vergleichbarkeit der Konzentration chemischer Komponenten aus der parallelen Probenahme wurde in der Pilotkampagne gezeigt. Es wurden getrennte statistische Analysen zur Untersuchung der zeitlichen und der räumlichen Variabilität der Aerosolzusammensetzung und der Quellenanteile durchgeführt. Beide PMF-Analysen haben fünf Quellen aufgestellt, die zum OC von PM_{0,36} mit ähnlichem Quellenprofil beitrugen. Identifiziert wurden biogen dominiertes SOA (bioSOA), isopren dominiertes SOA (isoSOA), Verkehr, Biomasseverbrennung (BB) und sekundäres Aerosol aus der Biomasseverbrennung (bbSOA). Im Jahresdurchschnitt leistet das SOA aus biogenen Quellen (bioSOA plus isoSOA) den größten Beitrag zum OC, gefolgt von Verkehr und BB-assoziierten Quellen (BB plus bbSOA). bioSOA und isoSOA-Quellenbeiträge, OC2 und OC3, zeigten die höchsten Konzentrationen im Sommer. BB und bbSOA und OC4 zeigten Winter Maxima. Der Beitrag des Verkehrs zeigte nur sehr geringe saisonale Schwankungen. Die räumlich-zeitliche Variation der Quellenbeiträge wurde durch Berechnung des Pearson-Korrelationskoeffizienten (r) bzw. des Divergenzkoeffizienten (COD) untersucht. Die in dieser Studie gefundene zeitliche und räumliche Variabilität der Quellenbeiträge zeigte Abhängigkeiten sowohl vom Standort als auch von den jeweiligen Aerosolquellen. Daher ist bei Studien zu gesundheitlichen Auswirkungen von quasi-UFP Vorsicht geboten, wenn eine einzige

Beobachtungsstelle verwendet wird, um die Exposition der Menschen im gesamten Untersuchungsgebiet zu approximieren.

Abstract

Although the smallest fraction of particles like UFP < 100 nm, or quasi-UFP up to a few hundred nm, make minor contribution to particulate matter (PM) mass, they account for the dominating fraction of particle number concentration (PNC). Epidemiological studies have observed associations between UFP exposure (often indicated as PNC) and adverse health effects on human, particularly on the cardiovascular system. Toxicological studies have also linked UFP or its specific properties to detrimental biological effect. It has been found that chemical species or sources of quasi-UFP were associated with their adverse effects. However, the existing results of health effect studies do not allow drawing any conclusion due to lack of (particularly long term) studies. Moreover, studies on organic species and their sources of (quasi-) UFP are even rarer as they are costly and tedious. This thesis aims to investigate the seasonal variation of sources contributing to organic fraction of quasi ultrafine particulate matter (quasi-UFP: here specifically refers to particulate matter with an aerodynamic diameter < 360 nm, i.e. PM_{0.36}). It also studies the spatio-temporal variability of source contributions.

The study process included four major steps. The first step involved testing the cut-points of two rotating drum impactors (RDIs) used in the study. In a pilot campaign, the weekly-unattended sampling concept, chemical analytical feasibility and the comparability of chemical concentration from two parallel sampling sets were investigated. The second step was parallel sampling of 24-h size-segregated PM at a reference site and one out of 5 master sites in Augsburg, Germany, for nearly one year. The third step was the chemical analyses. An in situ Derivatisation Thermal Desorption Gas Chromatography Time-of-Flight Mass Spectrometry method was applied to PM_{0.36} for simultaneous quantification of primary and secondary organic aerosol markers. Specific markers for biogenic secondary organic aerosols were integrated into the established method to identify the biogenic secondary organic aerosol (SOA). Thermo-optical carbon analyser was used for organic and elemental carbon fractions analyses. The last steps were positive matrix factorization (PMF) analyses for source apportionment based on the markers from chemical analyses and statistical data analyses.

The 50% cut-point of both RDIs using quartz fibre filter (QFF) as substrate was found to be 0.36 μm , which is much higher than the nominal cut-point of 0.1 μm . The comparability of the chemical species concentrations from parallel sampling in the pilot campaign was verified. This ensured the spatio-temporal study by comparing the samples taken by these two sampling sets from reference site and one of the master sites, respectively. Both PMF analyses resolved five sources contributing to organic carbon (OC) of PM_{0.36} with similar source profile, including biogenic dominated SOA (bioSOA), isoprene dominated SOA (isoSOA), traffic, biomass burning (BB) and biomass burning originated SOA (bbSOA). Based on annual average, modelled biogenic originated SOA (bioSOA plus isoSOA) makes the largest contribution to OC, followed by traffic and BB associated sources (BB plus bbSOA). bioSOA and isoSOA source contributions, OC2 and OC3, showed summer maximum. BB and bbSOA source contributions and OC4 showed winter maximum. Traffic source contribution showed very limited seasonal variation. Spatio-temporal variations of source contributions were investigated by calculating Pearson correlation coefficient (r) and coefficient of divergence (COD), respectively. The temporal and spatial variabilities of source contributions found in this study vary among sites and source types, and demonstrate source-specific characteristics. Thus, caution should be taken in health effect studies (e.g. epidemiological studies) of quasi-UFP when a single monitoring site is used to approximate human exposure within the whole study area.

Contents

Introduction.....	1
1.1 Atmospheric particle number size distribution, sources and physical processing.....	1
1.1.1 Particle size mode and size distributions.....	1
1.1.2 Two major primary sources for (quasi-) UFP.....	3
1.1.3 New particle formation via nucleation.....	4
1.1.4 Particle growth through atmospheric processing.....	4
1.2 Particulate matter (chemical) components and sources.....	5
1.2.1 Carbonaceous material.....	5
1.2.2 Organic carbon and organic matter (OM)/aerosol (OA).....	6
1.2.3 Secondary organic aerosol (SOA).....	7
1.2.3.1 Reactions in the gas phase.....	8
1.2.3.2 SOA formation and aerosol chemical aging occurring in the condensed phase.....	9
1.2.4 Atmospheric organic marker compounds and their relation to sources.....	10
1.2.4.1 PAHs.....	10
1.2.4.2 Hopanes.....	10
1.2.4.3 Anhydrosugars and other polar markers from biomass burning.....	11
1.2.4.4 Low molecular weight dicarboxylic acids.....	12
1.2.4.5 Nitrophenol and 4-nitrocatechol.....	12
1.2.4.6 Isoprene oxidation products.....	13
1.2.4.7 α -/ β -pinene oxidation products.....	14
1.2.5 Size distributions of marker compounds.....	16
1.2.6 Spatial and seasonal variability.....	16
1.3 Health effects of ambient Particulate Matter: particularly UFP.....	18
1.3.1 Epidemiological studies of PM health effects.....	18
1.3.2 Toxicological studies of PM health effects.....	19
1.3.3 The association between PM components and PM's health effect.....	20
1.3.4 Health effects of (quasi-) UFP.....	21
1.4 Source apportionment using receptor modelling.....	23
Methodology.....	26
2.1 Sampling.....	26
2.1.1 Sampling system description.....	26

2.1.2 Impactor theory and rotating drum impactor (RDI).....	26
2.1.3 Test collection characteristic of RDIs	27
2.1.4 Pilot field sampling	28
2.1.5 Sampling campaign.....	28
2.2 Monitoring of meteorological data and measurement of the PNSD	29
2.3 Organic compound speciation	29
2.4 EC/OC analysis	30
2.5 PMF analysis	31
Results and discussion.....	32
3.1 Publication I: Proof of concept and comparability of two sampler sets.....	32
3.1.1 Collection characteristics and comparability of cut-points of the 3 rd stage of RDI.....	32
3.1.2 Influence on collection efficiency when using the QFF substrate	32
3.1.3 Comparability of measured organic species concentrations	33
3.1.4 Size distributions of organic species	33
3.2 Publication II: Seasonality and source apportionment at the reference site	33
3.2.1 Concentration comparison and seasonal trends	33
3.2.2 Correlation matrix between different types of parameters	34
3.2.3 PMF analysis results from the PMF _{ref}	35
3.3 Publication III: Spatio-temporal variability of source contributions	37
3.3.1 Comparison of results from PMF _{ref} and PMF _{mas}	37
3.3.2 Temporal correlation of source contributions between reference and master sites.....	38
3.3.3 Spatial variability of sources contributions	39
Summary of results.....	41
References.....	42
Appendix	56

Introduction

An aerosol is a system (in the sense of a system as used in thermodynamics or chemistry) comprising liquid and/or solid particles (PM) in a carrier gas [2]. Atmospheric PM ranges from a few nanometres (nm) to around one hundred micrometre (μm) in diameter [3]. The effects of aerosols on atmosphere, climate, and public health are among the central topics in current environmental research. Particularly, the fact that PM pollution directly impacts human health has been known for centuries and has been the subject of many researches [4]. Health effects of airborne PM are associated with their properties such as size, surface area, number concentration and chemical composition. These properties vary due to their sources of origin and processes they undergo during atmospheric transport [5].

Therefore, one of the most important research objectives is to identify and characterise the sources contributing to atmospheric particles. This is achieved by source apportionment (SA) studies. Depending on their origin, ambient particles can be classified as primary or secondary, as shown in Fig. 1. Primary particles can be emitted directly by natural (e.g. marine, volcano, wild fire, vegetation and microorganism emissions) or anthropogenic (mainly combustion) activities. Secondary particles are formed during gas-to-particle conversion processes in the atmosphere. Similarly, atmospheric organic aerosol

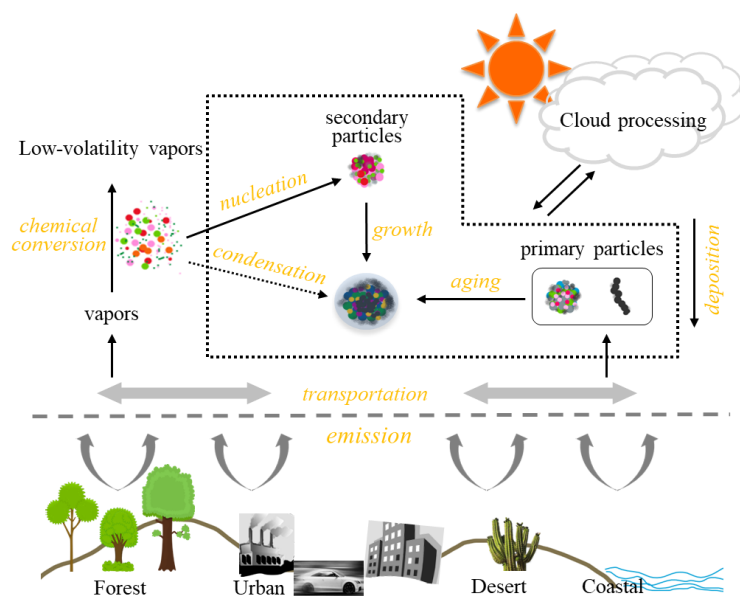


Fig. 1 Schematic image of the formation, growth and processing of atmospheric aerosol. Adapted from Zhang et al. [1].

(OA) can also be divided into primary organic aerosol (POA) and secondary organic aerosol (SOA) as will be further discussed in sections 1.2.3 and 1.2.4 [6]. Based on the above, this thesis focuses on the SA and characterization of atmospheric OA in the quasi-ultrafine size range (see section 1.1.1) through organic molecular analyses.

1.1 Atmospheric particle number size distribution, sources and physical processing

1.1.1 Particle size mode and size distributions

Particle size is one of the most important characteristics that influence a particle's behaviour in the atmosphere and after inhalation. Normally, aerodynamic diameter (D_{Ae}), which indicates a particle's aerodynamic behaviour, is used to denote particle size [7]. The aerodynamic diameter is the equivalent diameter of a spherical particle of unit density that has the same settling velocity as the target particle. Particles having identical aerodynamic diameters may vary in dimension and shape. Based on aerodynamic diameter, atmospheric PM is often categorized into PM_{10} ("inhalable particles"), $\text{PM}_{2.5}$ ("fine particles") or $\text{PM}_{0.1}$ ("ultrafine particles", UFP). Moreover, the term quasi-UFP often refers to PM with a diameter of up to a few hundred nm. In the literature, its definition is not as consistent as UFP of

PM_{0.1}. Particles below 180, 200, 250, 400, 490 nm, etc., have been referred to as quasi-UFP in previous studies [8-13]. It has been used mostly as an operational definition depending on the specific cut-off point of the sampling instrument utilized (e.g. impactors with similar but not identical/slightly different cut-off points). This is also the case for this thesis, as the drum impactors used were tested and have a cut-off diameter of 360 nm. Here all particles below 360 nm are therefore defined as quasi-UFP. Atmospheric aerosol size distribution strongly depends on the sources, formation mechanisms, atmospheric processing, chemical composition, and age of an aerosol. In ambient air, particles are usually distributed across several overlapping “modes” rather than evenly distributed [14, 15], with each mode similar to a log normal distribution. These modes are often classified as the nucleation mode ($D_{Ae} < 30$ or 20 nm), the Aitken mode (20 or 30 nm $< D_{Ae} < 90$ or 100 nm), the accumulation mode (100 nm $< D_{Ae} < 1$ μm) and the coarse mode ($D_{Ae} > 1$ μm). Each mode may be distinct in their formation mechanism (or source) or in atmospheric behaviour. UFP includes both particles in nucleation mode and Aitken mode. Both primary emissions and growth of nucleation mode particles can generate Aitken mode particles. Due to a high diffusion rate, these small particles coagulate rapidly or collide with surfaces; hence, their lifetime is usually short (just minutes to hours long). Particles in accumulation mode originate from primary emissions as well as the growth of smaller particles such as UFP due to the coagulation or condensation of compounds in the gas phase. Particles in this size range tend to accumulate in the atmosphere because they do not diffuse as rapidly as smaller particles and settle down much slower than coarse particles. The main mechanism of their removal from the atmosphere is via wet deposition. In general, accumulation mode particles have a lifetime of 7-10 days, during which they can be transported to sites hundreds to thousands of kilometres away from their sources and have a great chance of forming internally mixed aerosols. The quasi-UFPs investigated in this study, therefore, are Nucleation mode, Aitken mode, and smaller sized accumulation mode particles.

In a typical size distribution of PM in urban environments, the majority of the particle numbers are found in Nucleation and Aitken mode (regarding the UFP size range); the surface area numbers are found in Accumulation Mode and the volume/mass mainly in both Accumulation and Coarse modes (usually in bi-modal distribution) as shown in Fig. 2. Von Bismarck-Osten et al. 2013 [16] reported that more than 80% of all particles

observed in five major European cities were in the Nucleation and Aitken Modes. Due to this distinct distribution of number and mass metrics, particle mass concentrations in urban areas were found to show

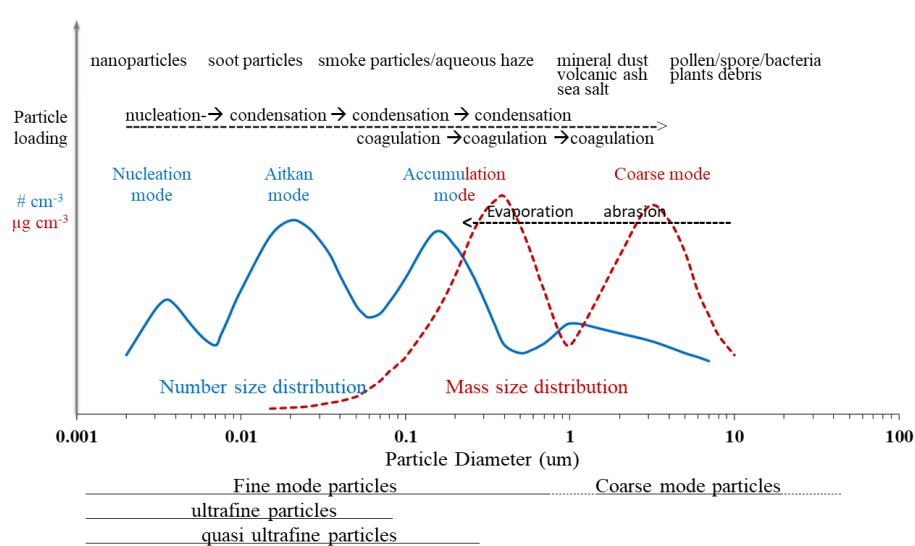


Fig. 2 Schematic example of number and mass size distribution of the same aerosol population. Nucleated fresh particles can increase in size through condensation and coagulation, and decrease through evaporation. Modified from Fuzzi et al. [15].

little to no correlation with the total number or UFP concentration number, and a moderate correlation of accumulation mode particle number concentrations [17] (and literature therein).

1.1.2 Two major primary sources for (quasi-) UFP

The combustion of fossil fuels or biomass often emits sub-micrometre-size aerosols dominated by Aitken Mode or 0.1 - 0.2 μm accumulation mode particles, respectively. It contributes substantially to the quasi-UFP in urban areas. Larger particles mainly come from particle growth or mechanical processes. Of all sources, studies have conclusively shown that motor vehicle emissions are the major source of UFP in urban environments [17, 19-21]. Vehicles contribute to both primary and secondary particles. Primary particles are produced directly in the engine during fuel combustion. Secondary particles are formed either inside the exhaust pipe or in the air one meter after exiting the tailpipe via nucleation and condensation during the dilution and cooling of the hot exhaust (e.g. from lubricating oil vapour) [17]. The combustion-generated particles in the engine consist mostly of solid, graphitic carbon with a small amount of metallic ash, hydrocarbons and sulphur compounds. A schematic example of the composition of UFP is shown in Fig. 3. Particles with elemental carbon core are normally observed in diesel vehicle emissions, particularly in heavy duty diesel vehicles, with the graphitic carbon core originating from the incomplete combustion of the diesel fuel.

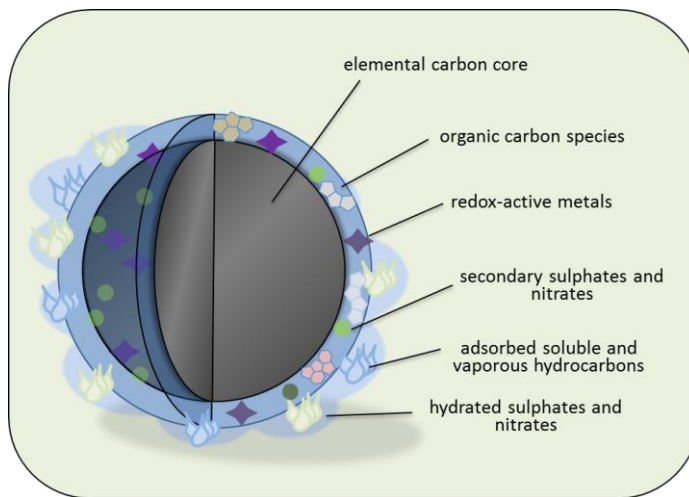


Fig. 3 A schematic example of the composition of UFP (e.g. in urban environment). Adapted from Stone et al. [18].

The Diesel Particulate Filter (DPF) installed in modern diesel vehicles is very efficient in removing these particles. The secondary particles from nucleation accumulate in a smaller size mode (below 30 nm) and usually comprise a small, hydrated, sulphuric acid core coated with condensed hydrocarbons [3]. The overall Particle Number Size Distribution (PNSD) measured in relation to a vehicle's emissions typically shows a unimodal or bimodal lognormal distribution as a result of these two types of particles. In field measurements, traffic-generated particles, which have been measured kerbside, in a tunnel or in a street canyon, show the majority of particles in Nucleation and Aitken Modes, with a peak mode smaller than 30 nm [3].

Biomass burning (BB) used for residential heating contributes substantially to PM pollution during the colder months in Northern Europe. Freshly generated PM from biomass burning measured in field experiments are mostly found to be in accumulation mode, while also appearing in Aitken mode in laboratory studies [3, 22]. Most studies reported similar results of the Count Median Diameters (CMDs) for freshly-emitted BB smoke ranging from 100-160 nm, with an average of about 130 nm. For aged particles, typical CMDs range from 120-230 nm, averaging around 180 nm [22]. The average CMD calculated by Janhall et al. [23] from 20 previous published datasets for fresh smoke was 117 nm, with a geometric standard deviation of 1.7 nm.

1.1.3 New particle formation via nucleation

In the atmosphere, new particle formation events can be observed via nucleation when the vapor pressure in the gas phase exceeds the saturation vapour pressure, leading to a great increase in particles. The main nucleation mechanisms to be discussed are (i) sulfuric acid and water binary nucleation when the vapor pressure of sulfuric acid is higher than the saturation vapor pressure of the sulfuric acid-water mixture, or (ii) ternary nucleation involving a third molecule [24]. Other nucleation mechanisms include ion-induced nucleation and condensation of (Extremely) Low-Volatile Organic Compounds ((E)LVOC) [25, 26]. Nucleation occurs both on a relatively regional scale and at specific hotspots with large amounts of gaseous pollutants from local sources. The traffic-related particles in nucleation mode are typical examples of source-specific and localized nucleation processes [27]. Under natural conditions, new particle formation has been observed in various environments, including urban, rural and remote rural areas, around coastal areas, above forests, on mountaintops and even in the Arctic [28-37]. In addition to temperature and humidity, the rate of new particle formation is mainly influenced by atmospheric gas-phase concentration and the surface area of existing particles [36, 38]. Studies indicate that, in general, particle formation events are favored by low temperatures, which decrease both the saturation vapor pressure. It is also favored by low surface areas onto which the compounds in gas phase condense. The latter is supported by the fact that formation events are often observed in cleaner air after windy or rainy weather, or in the early morning [17, 36, 38]. Nucleation mode particles observed near vehicle exhaust pipes and nucleation events occurring at noon due to gaseous products from photochemical oxidation are two examples of a high gas phase concentration leading to particle formation [27, 34, 38].

1.1.4 Particle growth through atmospheric processing

Within the atmosphere, the size of fresh primary and secondary particles can increase through coagulation or condensation and can decrease through evaporation [39]. Coagulation or condensation growth of the smallest newly-nucleated particles could result in larger Aitken or accumulation mode particles, as shown in Fig. 2. Coagulation happens when particles in rapid motion collide and aggregate to form larger particles. Particle coagulation depends on size, the diffusion coefficient (also size dependent) and the number of particles. Coagulation is more efficient between a small particle and a larger particle, as small particles with a greater diffusion rate tend to merge with larger particles with a larger surface area. Coagulation decreases total particle number but does not change total particle mass. Condensation is the partitioning of semi-volatile compounds from the gas phase into the particle phase as a reverse of evaporation. The condensation rate mainly depends on saturation vapour pressure and the existing particle material onto which the compounds condense. Temperature influences condensation by altering saturation vapour pressure, with low temperatures promoting condensation. Particle size may also influence the saturation vapour pressure due to the Kelvin effect, which suggests that vapour pressure is greater above a convex curved surface of small particles compared to a relatively flat surface of larger particles [36]. Condensation increases the total particle mass but does not change the total particle number. Aside from the condensation of gaseous sulphuric acid, water, ammonia and amines, (E)LVOC from primary emissions or secondary oxidation may also contribute to condensation growth [36, 40, 41]. Particle growth has also been observed worldwide in remote areas, above forests, along coastal areas and in urban environments [36, 42-45].

1.2 Particulate matter (chemical) components and sources

Chemical compositions of atmospheric aerosols are very complex and variable as a result of multiple sources and atmospheric transformations. Therefore, they are location, time, size and meteorological-condition dependent. It is almost impossible to characterize each particle since particles have individual chemical compositions, although some attempts of single particle characterisations have been made [47, 48]. Most studies measure the composition of a population of particles, either on a time resolution of seconds to minutes or on a daily basis. Based on such measurements, the majority of PM mass is classified into

inorganic and organic fractions. Its main components are inorganic ions (mainly sulphate, nitrate, ammonium), carbonaceous substances (organic carbon fractions [OC], and elemental carbon [EC]), sodium, chloride, crustal or mineral elements (i.e. silicon, calcium, magnesium, aluminium, iron), trace elements and water. Putaud et al. [46] summarized data on aerosol characteristics obtained over the past decade at over 60 sites across Europe and categorized them as natural background, rural, near-city, urban and kerbside the major inorganic ions: sulphate, nitrate and ammonium also made substantial contributions. The crustal elements are mostly present in primary coarse particles that arise mainly from traffic-related or wind-driven (re-) suspension/entrainment of soil or mineral material. Its fraction in Europe PM₁₀ was found to increase from rural to kerbside because of traffic-caused soil dust resuspension [46]. Trace elements like Ni, Cr, Zn, Pb, Cd, etc. only constitute a small fraction of particulate mass and may come from multiple or specific sources [49].

1.2.1 Carbonaceous material

The carbon in atmospheric aerosols can be divided into three classes: the class corresponding to i) inorganic carbonates, ii) OC, and iii) EC or black carbon (BC) in terms of light absorption [49]. The last two make up the traditional Total Carbon (TC) content and are also referred to as carbonaceous material of airborne PM. TC is usually determined by thermochemical oxidation and evolved gas analysis (CO₂ detection). It is divided into an OC fraction and an EC or BC fraction (TC=OC+EC or TC=OC+BC) [6]. When applying thermochemical measurement techniques (e.g. thermal-optical carbon analyser), OC could be technically defined as the thermally extractable organic part of PM, while EC as the residue after thermal extraction of the OC fraction. The carbon analyser uses a prescribed thermal protocol to quantify carbon fractions evolved at increasing temperature plateaus. Depending on the temperature protocol applied, thermally-derived sub-fractions of OC and EC are reported. In this thesis, OC1, OC2, OC3 and OC4 with increasing volatility are the four OC temperature fractions quantified by the IMPROVE_A

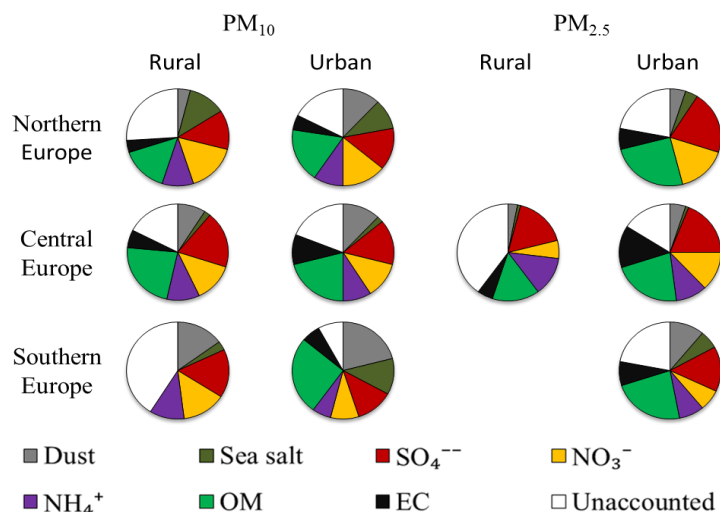


Fig. 4 Average composition of PM₁₀ and PM_{2.5} at rural and urban sites across Europe. OM calculated as OC*1.4, its contribution to PM was therefore probably underestimated. Adapted from Fuzzi et al. [5] and Putaud et al. [46]

protocol (see section 2.4 for the respective temperature plateaus used to extract each OC sub-fraction). IMPROVE and EPA/NIOSH (or STN) are the most widely used thermal-optical protocols in the atmospheric science community [51]. These protocols differ in temperature set points, which are higher for EPA/NIOSH than for IMPROVE, and in the residence time at each temperature step, typically longer for IMPROVE than for EPA/NIOSH [51]. The IMPROVE_A protocol is a slightly modified version of the original IMPROVE protocol first applied in 2005 [52, 53]. Regarding the carbon analyser, the EC is measured only in the presence of O₂ atmosphere due to its refractory property.

BC is measured using optical techniques based on its ability to absorb light [54]. Both the EC and BC consist of the carbon content of a graphite-like material usually contained in soot (technically defined as the black product of an incomplete hydrocarbon combustion or pyrolysis) and other combustion generated particles. These particles can be pictured as more or less disordered stacks of graphene layers or large polycyclic aromatics [6]. Despite the distinct characteristics of BC or EC from OC, a sharp boundary between them does not exist, as shown in Fig. 5 [50]. The thermochemical refractivity and optical absorption continuously decrease from graphite-like structures to non-refractive and colourless organic compounds, respectively. Therefore, the optically- or thermochemically-based measurement techniques may also include the coloured and refractory organic compounds in BC or EC. One more inherent problem of the thermal techniques is that the EC content may be overestimated due to pyrolysis (char formation) of some organic components during temperature rise [55]. In thermal-based carbon analysis, this effect can be corrected by separating EC from OC with a laser-based separation point. This point is when the laser-measured reflectance and/or transmittance of the filter sample return to its initial value, at which time the pyrolysed OC has been removed.

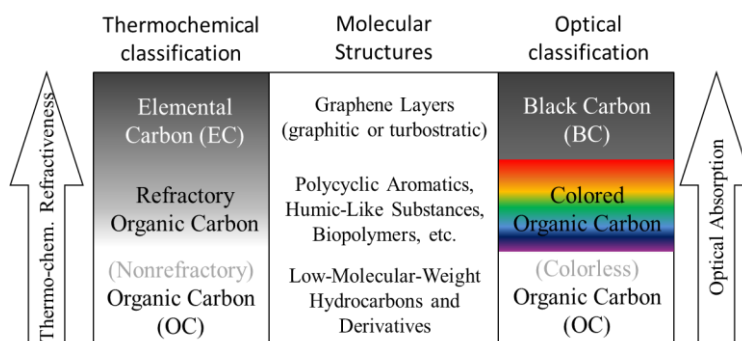


Fig. 5 Thermochemical and optical classification of EC, BC and OC. Adapted from Poeschl et al. [50].

1.2.2 Organic carbon and organic matter (OM)/aerosol (OA)

OC refers to the carbon mass of organic particulate matter (OM, also called organic aerosol, OA). Many sources emit primary OM and gaseous species, which can be converted to secondary organic compounds. OM mass, which accounts for other elements, mainly H, O, N and S, can be estimated from OC by multiplying it with a properly selected ratio [49, 56]. The ratios of different particles or aerosols may vary substantially (e.g. from 1.2 to over 2) based on their composition, origin and oxidation state (or “aging”, as discussed in Section 1.2.3.2). The oxidation state is characterized by an atomic oxygen-to-carbon (O/C) ratio [49]. For an ambient OM, when the N/C ratio is low, the OM/OC ratio is usually correlated with the O/C ratio. The highest OM/OC and O/C ratios (2.5 and 1.0, respectively) are observed for a highly-oxidized, aged ambient OA [5, 57]. Atmospheric OM constitutes a significant, even dominating, proportion of ambient fine particulate matter at anywhere from 20-90% of the PM mass [58]. It is a complex mixture of various organic compounds. The organic compounds measured in the atmosphere have been estimated to be between 10, 000 to 100, 000 species [59]. Atmospheric OM, however, often is

classified according to different parameters, i.e. based on their sources, formation mechanisms, oxidation status, and volatility. One of the most common classification systems is to divide organic aerosol into primary organic aerosol (POA) and secondary organic aerosol (SOA). POA is organic matter in the condensed-phase which is emitted directly into the atmosphere by various sources [60]. Contrarily, SOA is formed in the atmosphere through chemical transformation of gaseous organic compounds. These compounds then form lower volatile reaction products which subsequently partition into the particle phase [60, 61]. Atmospheric OA can be classified in order of increasing volatility as VOC, IVOC, SVOC, LVOC and ELVOC, meaning volatile, intermediate-volatile, semi-volatile, low-volatile and extremely low-volatile organic compounds [62]. Such a classification system is linked to the saturation vapour pressure and thus, the gas-particle partitioning of the organic components. Another classification system is based on aerosol mass spectrometry (AMS) measurements, which differentiate between “hydrocarbon-like” (HOA) and “oxygenated” organic aerosol (OOA), using the fragment ions at m/z 57 ($C_3H_5O^+$ and $C_4H_9^+$) and m/z 44 (CO_2^+), respectively [63]. HOA was related to primary anthropogenic sources, while OOA was related to secondary sources [64]. A PMF analysis of AMS spectra further separates OOA to LV-OOA, representing the low volatility, more oxygenated fractions, and SV-OOA, representing the semi-volatile, less oxygenated fractions [62, 65].

1.2.3 Secondary organic aerosol (SOA)

SOA accounts for a substantial, and often dominating, proportion of the ambient OA [58, 64]. The chemical complexity of SOA, due to dynamic formation and evolution reactions occurring in the atmosphere, is poorly understood and contributes to the uncertainty of atmospheric aerosol studies [61, 66]. Another aspect adding to this uncertainty and variability is the wide range of interpretation and attribution of SOA in different studies [67]. SOA is defined as liquid or solid particles created in the atmosphere by the transformations of organic gases [60]. These transformations are wide-ranging and can include gas-phase oxidation followed by condensation on pre-existing atmospheric particles (see 1.2.4.1). They can also include reactions involving the condensed-phase and reactions in or on the surface of pre-existing particles or cloud droplets (see 1.2.4.2) [60]. Since these definitions are based on processes rather than properties of organic compounds, they make it challenging to differentiate primary from secondary organic compounds in atmospheric aerosols. For this reason, most of the current knowledge on SOA, including its formation mechanisms, markers or contributing multiphase reactions, is based on laboratory or smog chamber experiments thus, creating serious concerns regarding the validity of results

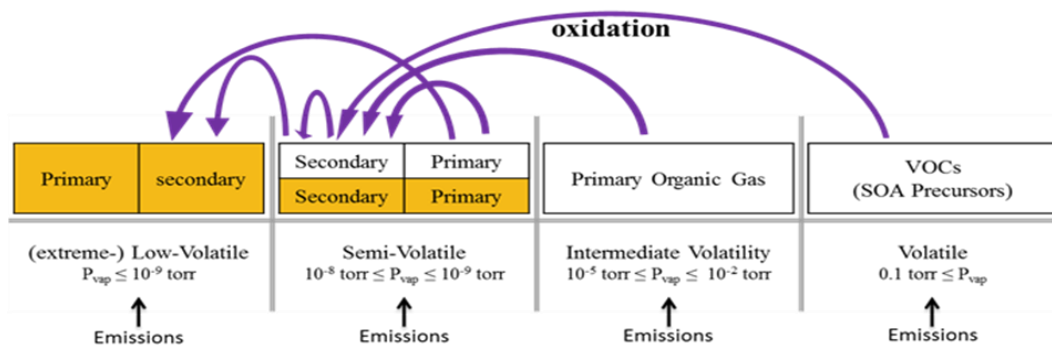


Fig. 6 Schematic image of primary emissions and photochemical oxidation of organic compounds in the atmosphere. Compounds in the particulate phase are highlighted in yellow, while those in the gas phase are not highlighted. Adapted from Fuzzi et al. [5].

when tested in or simply extrapolated to natural conditions in the atmosphere [60]. The gaseous precursors of SOA can be VOC or less volatile organics like IVOC and SVOC, as shown in Fig. 6 [5, 61]. It has been recently recognized that POA consists of a substantial proportion of semi-volatile compounds which can evaporate when diluted and then, undergo photochemical reactions in the gas phase to generate SOA [68]. This material behaves similar to both POA and SOA to some extent; its atmospheric level can be reduced by primary PM controls, but it shows secondary characteristics because it is also generated by photochemical reaction.

1.2.3.1 Reactions in the gas phase

The most commonly studied and likely most important mechanism of atmospheric SOA formation is the oxidation of VOCs to generate products of lower volatility followed by their partitioning into a condensed phase [61]. The gas phase oxidation of VOCs is initiated by atmospheric oxidants, like OH· radical, O₃ and nitrate radical (NO₃·), or through photolysis. The oxidants can participate in further reactions, as well. The initial attack of OH· or NO₃· can either abstract a hydrogen atom or add to a Carbon-Carbon (C=C) double bond [61]. The initial reactions usually lead to the formation of an alkyl or a substituted alkyl radical, whose further reaction will determine the SOA products and yield [69]. Functionalisation and accretion, which can add polarity and/or increase the molecular weight of the product, tend to decrease volatility. Fragmentation also tends to decrease volatility, but by cleaving the C-C bond [70]. A simplified schematic diagram of OH·-initiated VOC degradation pathways is shown in Fig. 7. The (substitute) alkyl radicals (R·) that formed rapidly turn into organic peroxy (RO₂·) radicals and can be further turned into

oxy (RO·) radicals. Varieties of competing reactions may exist for RO₂· and RO·, which makes them critical in generating products of lower volatility. The NO_x level plays an important role in the subsequent reaction of RO₂·; as shown in Fig. 7. The initial oxidation step is also influenced by the NO_x level because it controls the relative proportion of the major oxidizing agents hydroxyl radical, nitrate radical and O₃. Therefore, product distribution and SOA yield were, in turn, also found to be greatly influenced by the NO_x level [61, 71]. The fate of RO· strongly depends on its structure, and thus, on the structure of the parent VOC [71]. Despite a large number of VOC emitted, many are generally believed to be inefficient at the moment of SOA formation. Certain types of VOC were identified as important SOA precursors due to their high reactivity, leading to the production of low volatility products. Cyclic compounds are one of them as their fragmentation can result in ring-opening products, which preserve the carbon number of the parent compound. Moreover, the oxidation of cycloalkanes, aromatic hydrocarbons and cyclic terpenes mainly occur with the addition of functional groups in favour of decreasing volatility [71].

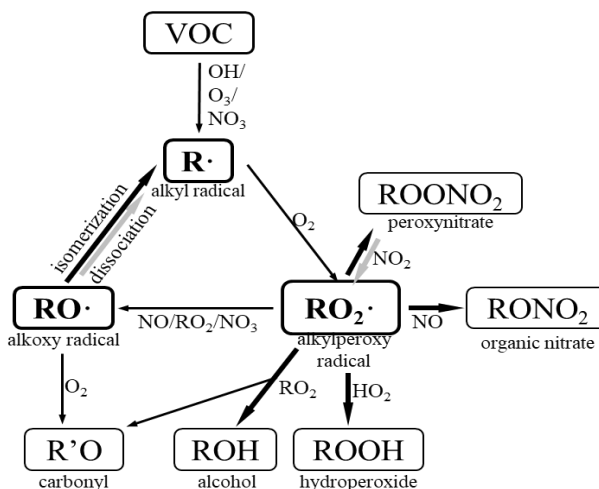


Fig. 7 Simplified representation of the mechanism of atmospheric oxidation of a generic VOC. Bold black arrows denote reactions that can lead to a substantial decrease in volatility; gray arrows denote reactions that increase volatility substantially. Adapted from Kroll et al. [61].

1.2.3.2 SOA formation and aerosol chemical aging occurring in the condensed phase

Atmospheric chemical reactions may also involve the condensed (particle) phase and occur as heterogeneous reaction, multiphase reaction or condensed-phase reaction [60]. The term “heterogeneous reaction” generally refers to reactions at the particle surface, whereas “multiphase reaction” refers to reactions in the particle bulk involving species from the gas phase [6]. These reactions can result in increase or decrease of organic volatility and contribute to SOA formation and chemical aging process of atmospheric aerosols. During its atmospheric lifetime, chemical aging of OA through such reactions continuously changes their physicochemical properties and loading, until all OM is converted to CO and CO₂, or is removed by physical mechanisms (wet or dry deposition) [61]. Both non-oxidative (e.g. “accretion reactions”) and oxidative processes can happen. The former can involve peroxyhemiacetal and hemiacetal formation, aldol condensation, ester formation, organosulphate formation, criegee reactions with alcohol/water/acids, etc., leading to production of compounds with high molecular weight (HMW) and low volatility. Identified products associated with this type of reactions can be HMW species such as oligomers and “humic-like substances” (HULIS), and nitrogen and/or sulphur containing compounds such as organosulphate and nitroxy-organosulphate. Oxidation of organic species in the condensed-phase by atmospheric oxidative agents (OH ; O₃, NO₃ ; etc) is believed to have generally the same chemical mechanism of oxidation in the gas phase, but the branching ratios of different pathways may be variable. It is proposed that autoxidation leads to the formation of highly oxidized multifunctional organic compounds (HOMs) [72, 73]. The abundance of LV-OOA with very high oxidation degree (high O/C ratio) observed could be related to these reactions. The highly oxidized OOA has an O/C ratio approaching 1, much higher than freshly emitted OA (< 0.15 or around 0.3 for biomass burning OC) [5, 57]. It is worth noting that aqueous phase reaction (in cloud, fog, rain or aerosol water) is generally attributed to condensed-phase reaction, but “aqueous-phase” condition typically in the cloud water should be distinguished from condensed-phase condition in the aerosol because there is much higher inorganic salts and other compounds (>> 1M) and minor water in the latter case comparing to the low concentration of solute in former case (< 0.1 M).

Organosulphates is an important type of condensed-phase evolution products found in smog chamber experiments and ambient aerosols. It can be produced through reaction of acidic PM and oxidation products of biogenic precursors (e.g. isoprene and terpenes), with studied mechanism of epoxy-containing products reacting with sulphuric acid in acidic sulphate aerosol [5, 60]. The ubiquity and abundance of organosulphate in aerosols are mostly identified by LC/MS but not GC/MS techniques due to their relative HMW and chemical instability to derivatisation [60]. Oligomers as a type of HMW species are characterised by a regular mass difference pattern (e.g. 12, 14, 16 or 18 Da) in mass spectrometry analysis. They have been detected in SOA generated from the atmospheric oxidation of common VOC precursors including cyclic alkenes (e.g. terpenes), small open-chain alkenes (e.g. isoprene) and aromatic compounds [71]. Determination of the MW range and quantification of oligomer are difficult due to limitation of commonly used mass techniques and lack of authentic standard [5, 71]. HULIS are often found in ambient aerosols, fogs, clouds and rainwater. They show similarity with terrestrial/aquatic humic and fulvic acids (humic substances), particularly their ultraviolet (UV) absorption and fluorescence spectra [74, 75]. Atmospheric HULIS have relatively high but still lower average MW (e.g. < 400 Da) than terrestrial humic substances. They can account for a substantial fraction of OA. Biomass burning is believed to be a primary source of HULIS. In addition, identification of condensed-phase HMW compounds (e.g. from oligomerisation and photo sensitised reaction) can explain a large portion of the

unidentified HULIS source [75]. Aqueous-phase reaction studies have been done for a large number of reduced and oxygenated precursors mainly including C2 and C3 carbonyl compounds (e.g. glyoxal, methylglyoxal, glycolaldehyde), pyruvic acid, methacrolein and methylvinyl ketone from isoprene oxidation, and also for isoprene and α -pinene, etc., either under photochemical or dark conditions. Products may be the above mentioned HMW compounds and also small acids including dicarboxylic acid [76].

1.2.4 Atmospheric organic marker compounds and their relation to sources

Full identification and quantification of single organic compounds are essential for studying sources or unknown processes, although they require sophisticated analytical methods [60]. Source apportionment using receptor models can be achieved by monitoring organic species specific to one or a few sources at the receptor site; these compounds are also called “markers”. The markers or their specific profiles can be very useful in interpreting source factors separated by source apportionment tools, such as positive matrix factorization (PMF, also see section 1.4). The identification and quantification of SOA markers from major biogenic sources and precursors have undergone considerable progress in the last decade and will be discussed in the following section. The chemical compounds or compound classes that are typically found in atmospheric aerosols and are measured in this study will be discussed in the following chapters.

1.2.4.1 PAHs

Polycyclic aromatic hydrocarbons (PAHs) are a series of complex organic compounds made up of carbon and hydrogen with a characteristic fused-ring structure consisting of at least two benzene rings. Fig. 8 shows the molecular structure of four of the PAHs measured in this study. Some PAHs contain other fused rings aside from the six-sided [77]. They are ubiquitous in ambient air and the partition between the gas and particle phase depending on their volatility, with the lighter PAHs in the gas phase and the heavier ones ($\geq 5, 6$ rings) in the particle phase [78, 79]. PAHs and their derivatives are generated during incomplete combustion processes, which can occur naturally in wildfires or during volcanic eruptions, but their dominating mass arises from anthropogenic activities [77, 80, 81]. In general, there are five main categories of PAH sources: domestic, mobile, industrial, open agricultural burning and natural [77]. In urban and near-city environments, vehicular emissions and domestic heating are the major sources of PAHs [79, 82, 83]. Fossil fuels have variable contents of PAHs, which can be released by physical mechanisms rather than combustion, with petroleum products containing the lowest and coal the highest concentrations [82] (and literature therein).

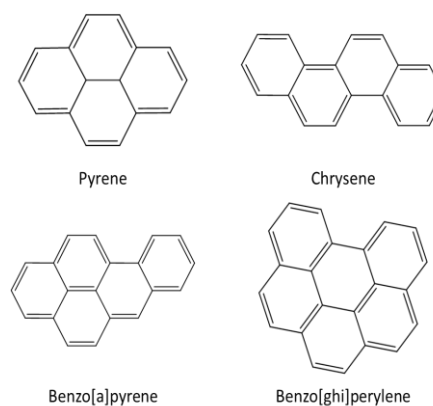


Fig. 8 Molecular structure of four representative PAHs.

1.2.4.2 Hopanes

Hopanes constitute an important class of geohopanoids, which are the diagenetic products of biohopanoids that naturally exist in many plants, ferns, mosses, fungi and bacteria [84]. Hopanoids, including bio- and geo-hopanoids, are a family of triterpenoid hydrocarbons with a pentacyclic skeleton containing four cyclohexanes and one cyclopentane; Fig. 9 displays the general structure of hopanes. The

formation of hopanes requires geological time and the high temperatures reached during the deep sediment burial process, during which many functional groups and some or all carbon atoms of the side chain appear [84]. Hopanes present in fossil fuels, such as coal and crude oil, are believed to be the major source of those hopanes found in atmospheric aerosols, particularly in urban environments [81, 85, 86]. The two most abundant hopanes found in ambient aerosol are 17- $\alpha(H)$,21- $\beta(H)$,29-norhopane and 17- $\alpha(H)$,21- $\beta(H)$ -hopane [81, 87, 88]. Aside from steranes, hopanes have often been used as markers for mobile source emissions, assuming that coal is not widely

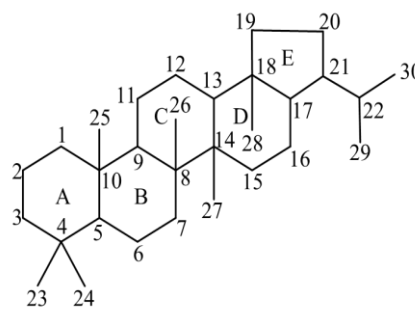


Fig. 9 Schematic image of Hopanes' characteristic structure.

used [88]. It has been found that the distribution patterns of individual hopanes and sterane from vehicular emissions (gasoline and diesel) corresponded well to patterns found in lubricant oil [81, 87]. They belong to the higher boiling fraction of crude oil and are not found in gasoline or diesel fuel; therefore, they are believed to contribute to vehicle exhaust from the lubricating oil [87, 89]. Mandalakis et al. [90] measured the gas particle partition in the urban atmosphere of Athens in July and found the total concentration of twelve α and β hopanes to be 0.2 ng m^{-3} and 1.0 ng m^{-3} in the gas and particle phases, respectively. In places where coal was intensively used in winter, like in East Asia (e.g. China), the measured hopanes' diagnostic ratio indicates a significant contribution stems from coal burning [85]. Hopanes patterns found in lubricating oil and traffic emissions are different from those found in coals of different maturity ranks, which can be used to distinguish the two major source types [81, 86].

1.2.4.3 Anhydrosugars and other polar markers from biomass burning

Biomass burning particles originate mainly from anthropogenic activities, such as residential cooking and heating in urban areas, or combustion in nature occurring during wild fires, agricultural fires and deforestation fires [60]. Primary emissions from biomass burning make significant contributions to the atmospheric OA mass concentration, as occurs in northern European in winter [91-93]. A large number of trace substances are emitted by biomass (i.e. wood in northern European) burning, including both nonpolar and polar compounds [60, 94]. The composition of aerosol from biomass burning depends on both the combustion condition and the chemical composition of the biomass burned [60, 80]. Many of the organic species found in wood smoke can be traced back to the structures or content of the original burnt material [80]. Major compound classes of tree wood include cellulose, hemicellulose, lignin and extraneous, which make up about 40-50%, 20-30%, 20-30% and 4-10% of the dry weight of wood, respectively [80]. Cellulose and hemicellulose provide a supporting mesh, which is reinforced by lignin polymers, responsible for the wood's rigidity [80].

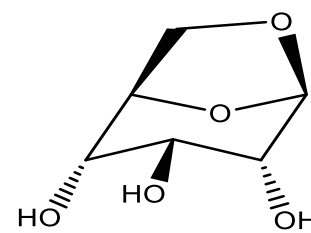


Fig. 10 Molecular structure of levoglucosan

The major pyrolysis products of cellulose and hemicelluloses are anhydromonosaccharides, such as levoglucosan, galactosan, and mannosan. They are widely used as biomass burning marker compounds because they are specific and emitted in considerable amounts [60, 95, 96]. Levoglucosan (see Fig. 10 for its molecular structure) can be detected at a considerable distance from the original combustion source because of its high emission levels [88, 97]. Anhydromonosaccharides are generally believed to be in the

particulate phase due to low vapour pressure. However, the results of May et al. [98] indicate that the semi-volatility of levoglucosan under typical atmospheric conditions with appreciable quantities exists in the gas phase. Xie et al. [99] reported that the median of the gas to particle phase concentration ratio was 0.23 from samples taken in Denver, USA. The atmospheric degradation of levoglucosan should be considered when using it as a marker compound for source apportionment studies as the atmospheric decay of semi-volatiles is supposed to proceed more rapidly than nonvolatiles [98]. Using a smog chamber, Hennigan et al. [100] found the lifetime of levoglucosan to be 0.7- 2.2 days when exposed to 1×10^6 molecules cm^{-3} of $\text{OH} \cdot$ (typical average summertime conditions). Hoffmann et al. [101] estimated a lifetime of 0.5- 3.4 days for levoglucosan using a model study.

Other commonly used biomass burning markers include substituted phenols and substituted methoxyphenols from lignin pyrolysis (e.g. guaiacol, syringol and vanillin) [60, 82]. Resin acids (e.g. abietic acid) and its derivatives (e.g. dehydroabietic acid) are also often found in the ambient aerosol influenced by wood smoke from coniferous trees.

1.2.4.4 Low molecular weight dicarboxylic acids

Among oxygenated organic species in ambient particles, low MW (C2-C9) dicarboxylic acids (DCA) are frequently quantified with the following chemical structures [102]:



Dicarboxylic acids can act as cloud condensation nuclei (CCN) as a result of their high water-solubility and hygroscopic properties; they reduce the surface tension of particles to form CCN [2, 103]. DCA are the most abundant organic compound class in aerosols and can constitute a substantial proportion of water-soluble organic carbons (WSOC) [104-106], with a dominating oxalic acid (C2) concentration, followed by malonic acid (C3) and/or succinic acid (C4) [102, 103, 106-109]. They have been found in a variety of environments such as cities, rural areas, marine environments and polar regions [105, 106, 110]. DCA are present predominately in the atmospheric particle phase, with particle phase proportions close to one due to low vapour pressure [2, 105]. DCA originate from a wide range of sources [110]; primary emissions come from anthropogenic sources, like fossil-fuel combustion including motor vehicle exhausts [111], meat-cooking operations [112], and biomass burning [80], and from biogenic primary sources like oceanic emissions [110]. Nevertheless, a review of previous studies suggests that DCA are mainly derived through the photochemical oxidation of various organic precursors from both anthropogenic (e.g. biomass burning and vehicle emissions) and biogenic (e.g. isoprene, monoterpenes) origin, most likely in the aqueous phase [102, 103, 106]. For instance, it was noted that no direct source of malic acid or tartaric acid was identified [2, 102]. Aqueous-phase productions of C2 are particularly important in aerosol, cloud and fog droplets [106, 107].

1.2.4.5 Nitrophenol and 4-nitrocatechol

Nitrogen-containing organic compounds comprise an important class of OA within which water-soluble organic nitrogen is a large portion (e.g. over 20%) [113]. Of particular interest are nitroaromatic compounds (NACs) which contain at least one nitro group ($-\text{NO}_2$) attached to an aromatic ring which contribute to atmospheric brown carbon [114]. The NAC group includes nitrophenols, nitrocatechols, nitrosalicylic acids, nitroguaiacol and the derivatives of nitrophenols and nitrocatechols [114]. They can absorb light in the UV/VIS range and thus, influence the solar radiation balance [113, 115]. NACs (e.g.

4-nitrocatechol) have been identified in HULIS extracted from PM_{2.5} and correspond to their yellow-coloured substances [115, 116]. NACs have not been extensively studied, but have been found in urban and rural aerosol, rain water and snow samples [110, 113]. The compounds 4-nitrophenol (4-NP) and 4-nitrocatechol (4-NC) have been identified in ambient aerosols with a concentration of less than one to a few hundred ng m⁻³, their structures are shown in Fig. 11

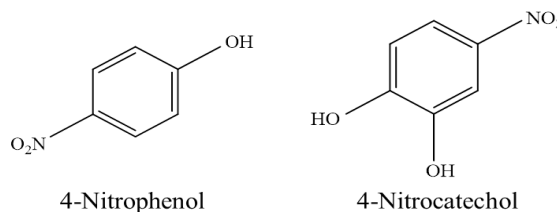


Fig. 11 Molecular structure of 4-nitrophenol and 4-nitrocatechol

[96, 113-119]. During a haze period in Shanghai, China, Li et al. [119] measured 4-NP and 4-NC as ranging from 151-768 and 22-154 ng m⁻³, respectively. The primary sources of 4-NP include vehicle exhaust, coal and wood combustion [117, 119, 120]. It can also be generated by the secondary oxidation of precursors like the mono-aromatics benzene, phenol or benzaldehyde [117, 121-123]. Due to its relatively high vapour pressure, 4-NP showed substantial partitions in the gas phase with a low particulate phase fraction (Fp), but high particulate phase fractions have also been found in some studies [118, 122]. NPs were monitored in a study of the chemical ionisation of AMS using acetate as a reagent ion, and a diurnal pattern with higher levels at night and lower levels in the daytime was observed. The high night-time concentration was attributed to an excess of NP production from NO₃ radical oxidation of phenol at night coupled with the degradation of NP mainly due to photolysis in the daytime [122]. Chow et al. [114] found increased NAC concentrations with elevated night time NO₂ levels, providing more evidence on night time oxidation. 4-NC has often been measured as one of the most abundant NACs in ambient aerosols and is often associated with biomass burning due to their positive correlation with levoglucosan [115, 116, 118]; a relatively wide range of correlation coefficients were found between 4-NC and levoglucosan with *r* values up to 0.9 [113, 114, 118, 119]. Aside from primary emissions, 4-NC was also formed by toluene or benzene oxidation [118, 123, 124]. In ambient aerosols, it was found to highly correlate with methyl-nitrocatechols that have an *r* value > 0.9, indicating similar sources or source processes [96, 113, 115]. Methyl-nitrocatechols can be formed through the photooxidation of *m*-cresol and are suggested to be used as marker compounds for biomass burning SOA [125]. The particle phase fraction of 4-NC was found to be 95% [118].

1.2.4.6 Isoprene oxidation products

An overview of reported isoprene SOA markers has been summarised in Table 1. Molecular speciation activities started after 2004 for isoprene SOA, much later than monoterpene SOA, for which they began in the late 1990s [60]. Before the 2004 discovery of 2-methyltetrols (i.e., the diastereoisomers 2-methylthreitol and 2-methylerythritol) as isoprene oxidation products in the Amazon rainforest, it was believed that the photooxidation of isoprene did not result in SOA because of the high volatility of oxidation products identified in smog chamber experiments [71, 126, 127]. Isoprene is the largest non-methane VOC emitted by vegetation globally, estimated at approximately 600 Tg per year [127]. SOA production from isoprene, therefore, can contribute substantially to the total SOA worldwide [128]. Isoprene is highly reactive due to its two double bonds; laboratory studies confirmed the formation of the markers identified in the atmosphere [129, 130]. Of all the markers shown in Table 1, the mostly widely measured compounds in ambient aerosols are 2-methyltetrols (2-MTs), C5-alkene triols and 2-methylglyceric acid (2-MGA). Their nitrogen- or sulphur-containing derivatives (e.g. organosulphates, nitroxy organosulphates) require specific analytical methods for identification and quantification (i.e.

liquid-chromatography-based method) [131, 132]. The formation of isoprene SOA is complex and not explicitly understood, but in recent years, mechanistic smog chamber studies under diverse experimental conditions have gained insight into the formation of different isoprene markers [60, 128, 133-136]. 2-methyltetrols, their corresponding sulphate esters and C5-alkene triols are produced under low-NO_x (NO_x= NO + NO₂) conditions through the reactive uptake of gas phase epoxydiols (IEPOX) by atmospheric particles [60, 133, 135-137]. Isoprene reacts with OH· and HO₂· radicals to form hydroxy hydroperoxides (ISOPOOH), which further produce isoprene epoxydiols (IEPOX) in the gas phase [128, 133]. It has been noted that the detection of particle-phase IEPOX and its known products (i.e., the 2-methyltetrols and its corresponding sulphur- and nitrogen-containing derivatives) in ambient aerosols provide direct evidence for the chemical interaction of biogenic emissions and anthropogenic pollutants (i.e., SO₂, NO_x), leading to the formation of isoprene SOA [138, 139]. While under high-NO_x conditions (e.g. the increasing influence of anthropogenic emissions), isoprene oxidation shifts from the HO₂-pathway to the NO/NO₂-pathway [128, 135, 139]. The main product of this pathway is 2-MGA. Its derivatives were also identified both in a smog chamber and in ambient aerosols [71] (and literature therein). Recent work by Lin et al. [134] has found that 2-MGA directly forms from the reactive uptake of methacrylic acid epoxide (MAE), which is a gas-phase oxidation product of peroxyethylacrylic nitric anhydride (MPAN); MPAN is a second-generation product of isoprene oxidation under initially high NO_x conditions [134, 135, 140]. In urban environment, both the HO₂-pathway and the NO/NO₂-pathway exist and they compete with each other; this is likely the reason for relatively high 2-MGA levels observed in some urban-influenced sites and spatial heterogeneity of 2-MT observed on a relatively small scale [128, 140-142]. 2-methyltetrols were found to be semi-volatile with a ratio of gas-to-particle phase concentration often close to or higher than one in the summer [99]. Calculated lifetimes of 2-methyltetrols in the gas phase are relatively short, but Hu et al. [143] studied the heterogeneous reaction rate coefficient of ambient IEPOX-SOA with OH radicals and estimated a lifetime of more than 2-weeks for IEPOX-SOA in the particle phase.

1.2.4.7 α -/ β -pinene oxidation products

The key species identified as α - and β -pinene SOA markers are summarised in Table 1. Among these compounds, the ring-retaining cis-pinonic acid and cis-pinic acid have been well established as the major ozonolysis products and resulting from reactions with the OH· radical [71]; they are considered first-generation products [144]. Atmospheric lifetimes for pinonic acid and pinic acid were estimated to be 27 and 32 hours, respectively, using a typical average OH concentration of 1×10^6 radical cm⁻³ [110]. The particle phase fraction of pinonic acid was estimated to be between 30-51%, thus, its concentration within the atmospheric PM is greatly influenced by gas-particle partition [144] (and literature therein). Further reactions generate highly-oxidized, acyclic, polar compounds, which were also observed in the ambient aerosols [71]. With great effort, molecular structures of marker compounds having MW 148 and 204 were elucidated as C5-hydroxydicarboxylic acid, 3-hydroxyglutaric acid (3-HGA) and C8-tricarboxylic acid 3-methyl-1,2,3-butanetricarboxylic acid (3-MBTCA), respectively [145, 146]. 3-MBTCA, which has a very low volatility and long lifetime (estimated at 10 days), is widely considered a suitable marker of aged pinene SOA [60, 147]. The high atmospheric concentrations measured for these compounds in field samples illustrate that complex multi-generation chemistry characterizes the photooxidation of α -/ β -pinene in the ambient atmosphere, while the markers can serve as “clocks” for measuring OA aging [60, 71]. Other markers structurally characterized in pinene SOA are 10-hydroxy-cis-pinonic-acid, lactone-containing terpenylic acid, terebic acid, 2-hydroxyterpenylic acid and 4-hydroxyterpenylic acid [60].

Additionally, organosulphates, nitrooxy organosulphates and high-MW dimers and their structures were also discovered [60].

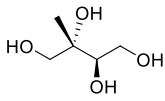
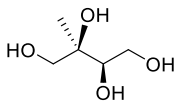
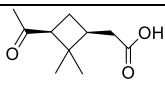
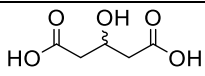
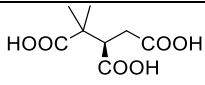
Marker (class)	Individual marker	MW	Selected references
Markers from isoprene oxidation reported between 2004-2009 (also refer to Hallquist et al. [71])			
2-methyltetrol (2-methyl-1,2,3,4-tetrahydroxybutane)	2-methylthreitol (2R,3R) + 2S,3S stereoisomer	136	Claeys et al. 2004 [126] Surratt et al. 2006 [130]
			
	2-methylerythritol (2S,3R) + 2R,3S stereoisomer		
			
2-methyltetrol derivatives	2-methyltetrol organosulphates	216	Surratt et al. 2007 [131]
	2-methyltetrol nitrooxy organosulphates	261	Gomez-Gonzalez et al. 2008 [148]
	2-methyltetrol dinitroxy organosulphates	306	Surratt et al. 2008 [132]
2-methylglyceric acid (2,3-dihydroxy-2-methylpropanoic acid)		120	Surratt et al. 2006 [130]
2-methylglyceric acid SE		200	Gomez-Gonzalez et al. 2008 [148]
C5-alkene triols	Z-2-methyl-1,3,4-trihydroxybut-1-ene	118	Wang et al. 2005 [149] Surratt et al. 2006 [130]
	E-2-methyl-1,3,4-trihydroxybut-1-ene		
	3-methyl-2,3,4-trihydroxybut-1-ene		
Novel markers reported since 2009 are mainly organosulphates related to methacrolein or methyl vinyl ketone			
Markers from pinene oxidation reported before 2007			
cis-pinonic acid		184	Hoffmann et al. 1998 [150] Yu et al. 1999 [151]
cis-pinic acid		186	Glasius et al. 1999 [152]
10-hydroxy-cis pinic acid		200	Larsen et al. 2001 [153]
Markers from pinene oxidation reported after 2007			
3-hydroglutaric acid (3-hydroxypentane-1,5-dioic acid)		148	Claeys et al. 2007 [145]
3-methyl-1,2,3-butanetricarboxylic acid		204	Szmigielski et al. 2007 [146]
Organosulphates and nitrooxy organosulphates	3-hydroxyglutaric acid SE etc.	228	Surratt et al. 2008 [132]
high-MW dimers (refer to Noziere et al. [60])			

Table 1. Overview of main isoprene and pinene SOA markers reported (SE: sulphate ester), and selected references regarding their structural characterization. Only the compounds with molecular structures shown are the ones measured in this study. (Adapted from Noziere et al. [60].)

1.2.5 Size distributions of marker compounds

Size distribution studies of aerosol components provide vital information on their sources, formation pathways, as well as health effects and climate impact. Organic marker species, such as 2-methyltetrols, DCA, levoglucosan, 4-nitrocatechol and the PAHs mentioned above, are mostly found in fine particulate matter (e.g. $PM_{2.5}$, PM_1) [103, 107, 108, 154, 155]. Amador-Munoz et al. [156] found that PAHs ($MW \geq 202$) measured in Mexico City peaked at the finest stage ($PM_{0.49}$) both in dry and wet seasons, with fluoranthene and pyrene containing relatively lower fractions in this size range compared to other heavier PAHs. De Guidi et al. [157] found the highest amount of PAHs in the smallest $PM_{0.5}$ size fraction in PM sampled in Catania, Italy. Di Filippo et al. [158] measured the size distribution of PAHs in PM sampled in Rome, Italy and found the sum of PAHs with $MW > 228$ peaks at $0.4 \mu m$ with the majority of mass accumulated in $< 0.4 \mu m$ size range; the sum of four lighter PAHs (fluoranthene, pyrene, benz[a]anthracene and chrysene) had similar concentrations in 0.06-0.1, 0.1-0.17, 0.17-0.26, 0.26-0.4 and 0.4-0.65 μm size ranges, which were higher than those in other size ranges. However, at a polluted urban centre in Baoji, China, high level of PAHs and hopanes were measured and their corresponding size distribution was found to be largely unimodal, peaking at $0.7-1.1 \mu m$ [85]. Herckes et al. [159] show that the majority of hopanes and pinic acid were measured at $< 0.49 \mu m$ in size at Yosemite National Park, USA; the levoglucosan size distribution, on the other hand, usually peaks at this size range except for one fire-influenced period when the peak shifted to a $0.49-0.95 \mu m$ size range. DCA (C2 - C5) and OC were found to peak at a $0.65-1.1 \mu m$ size range on Okinawa Island, Japan [109]. Zhang et al. [160] found that the size distributions of 2-methyltetrols exhibited a unimodal pattern, peaking in the $0.44-1.0 \mu m$ size range, similar to sulphate and ammonium. At the summit of Mt. Hua in Shanxi, China, the size distributions of the SOA markers 2-methyltetrols, C5-alkene triols, 2-methylglyceric acid, 3-MeTHF-3,4-diols, 3-hydroglutaric acid, 3-MBTCA, malic acid and levoglucosan showed unimodal distributions, peaking at $0.7-1.1 \mu m$. Cis-pinonic acid exhibited a bimodal pattern with a higher peak in coarse mode ($>2.1 \mu m$) and a lower peak of $0.7-1.1 \mu m$. Succinic acid and glutaric acid also showed bimodal distributions with higher peaks of $0.7-1.1 \mu m$ and a lower peaks in coarse mode [161]. At a forest site in northern Japan, 2-methyltetrols demonstrated broader size distributions with a tail into the coarse mode, and in early summer, these size distributions peaked at $1-1.9 \mu m$ while in mid-summer they reduced to $0.39-0.58 \mu m$ with a second peak of $1-1.9 \mu m$ [162]. At the same site, pinonic acid exhibited a bimodal pattern with one peak of $0.39-0.58 \mu m$ and a second broader one in coarse mode. 3-MBTCA peaked at $0.58-1 \mu m$ in both early summer and autumn, while at $0.39-0.58 \mu m$ with a tail at $1.9 \mu m$ in mid-summer [162]. During a haze period in Shanghai, China, levoglucosan and 4-nitrocatechol demonstrated a unimodal distribution, peaking at $0.7-1.1 \mu m$, whereas 4-nitrophenol showed a bimodal distribution with a major peak of $4.7-5.8 \mu m$ and a minor peak of $0.7-1.1 \mu m$ [119].

1.2.6 Spatial and seasonal variability

Spatio-temporal variabilities of organic species in ambient aerosol mainly depend upon the source contribution, forming processes and meteorologically influential factors. Therefore, they can provide insight into these aspects. Primary sources like traffic often result in hot-spot or elevated levels of their source markers at places near the sources. For instance, a typical ranking of anthropogenic pollutants is shown in Fig. 12. Levels increase from a natural background environment to an urban area and kerbside. Markers of SOA are more complex and less studied, demonstrating less spatial heterogeneity in general [144], but they also show individual characteristics with regard to different precursors. Measured PAH

and hopane concentrations in urban centre samples were one to two orders of magnitude higher than those in mountain aerosols and two to three orders of magnitude higher than those in marine samples in China [85]. Atmospheric contributions of PAHs were found to decrease in the following order: street > city background air and suburbs > village > open land [79]. Similarly, Azevedo et al. [163] found a decrease of hopanes in the following order: tunnels > downtown > park and forest. Yan et al. [164] found a much higher concentration of automotive-related primary hopanes and PAHs at highway sites compared to campus and rural sites. Ding et al. [165] found 2-MTs and cis-pinonic acid to show the highest concentration at rural and the lowest at coastal sites. Ding et al. [128] measured isoprene SOA markers at 12 sites across China and also found higher concentrations of 2-MTs at rural sites, but higher concentrations of 2-MGA at urban sites, likely due to the impact of NO_x. The ratio of 2-MTs to 2-MGA was found to be associated with NO_x levels at different sites, with higher levels at rural and remote sites in comparison with urban and suburban sites [141]. High correlations of pinene markers with different monitoring sites up to several hundred miles away suggested a regional impact of pinene SOA [144].

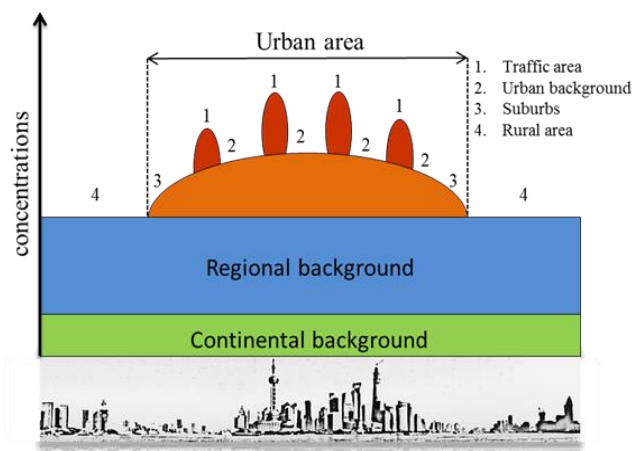


Fig. 12 The concept of continental or regional background, urban increment and local traffic increment. Adapted from Fuzzi et al. [5].

Each season has its characteristic meteorological conditions and corresponding biogenic and anthropogenic sources. Colder seasons are often characterized by low temperatures, low mixing heights and more frequent temperature inversions, leading to the condensation of semi-volatile compounds and the accumulation of gases and particulate matter pollutants. Moreover, fossil fuel or biomass used for domestic heating in winter is an important source of PM often traced by characteristic organic markers (e.g. levoglucosan). For these reasons, levoglucosan and other biomass combustion markers generally show significant increased concentration in colder seasons, which was also observed in PM_{0.49} samples [80, 166-168]. Higher levels of PAHs and hopanes were also observed in winter rather than in summer both at urban traffic and urban background sites in Greece [166]; higher concentrations of PAHs were often observed in winter [93, 157, 167, 169]. However, Yan et al. [164] did not observe significant seasonal variation for hopanes or steranes at all at traffic, campus and rural sites. An increase of hopane in colder periods in Augsburg was attributed to non-traffic sources [93, 169]. A concentration of 4-nitrophenol 8 to 15 times higher and a concentration of 4-NC 310 times higher than average were found in the city of Ljubljana, Slovenia [113]. Kahnt et al. [115] reported the highest levels of nitrophenol and nitrocatechol in winter, followed by autumn, spring and summer at a rural site in Hamme, Belgium. On the other hand, warmer seasons are characterized by high temperatures, elevated radiation levels, and good dispersion conditions, leading to high vegetation emissions and oxidants activities in favour of biogenic SOA formation. Isoprene SOA product 2-methyltetrols generally show maximal concentration during warm seasons and very low or below detection limits in cold seasons. They were found to follow temperature changes closely [142, 162, 164, 165, 170, 171]. Seasonal variability of pinene oxidation products were generally not as extreme as the 2-methyltetrols, and also not as dependent on temperature, with high level

pinene SOA markers observed most often in warmer seasons (e.g. summer and spring) [110, 144, 162, 165, 170, 171].

1.3 Health effects of ambient Particulate Matter: particularly UFP

The general association between airborne particulate matter and adverse health effects is conclusive [172, 173]. Since around 1990, epidemiological studies in the USA, the UK, Canada, Finland, Germany, the Czech Republic, etc. have reported associations between ambient air particulate matter pollution and a wide range of negative health conditions such as respiratory-related restrictions, respiratory hospital admission, mortality, morbidity, asthma attacks, etc. [173] (and literature therein). Some landmark studies on trends in PM health effects are shown in Fig. 13.

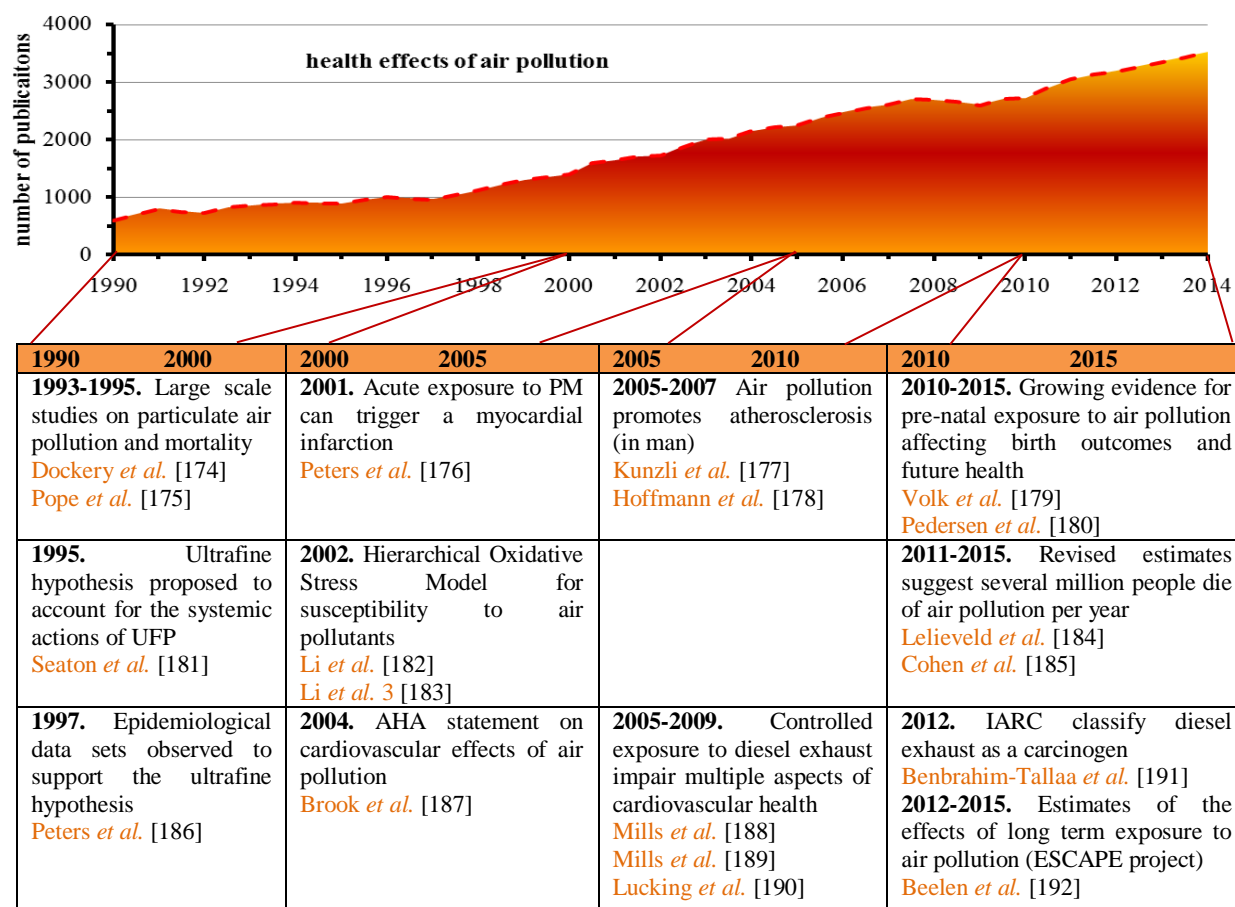


Fig. 13 Time line showing an increased interest in PM health effects research over the last three decades; key studies and research trends are highlighted in the table. Adapted from Stone *et al.* [18].

1.3.1 Epidemiological studies of PM health effects

In 1993 and 1995, two very important cohort-based mortality studies in the United States revealed the health effects of airborne particles [174, 175]. The first study, also known as the Harvard Six Cities study, followed over 8,000 adults from six cities in the USA for 14-16 years [174]. The second study from the American Cancer Society (the ACS study) collected data from over 500,000 adults living in approximately 150 different metropolitan areas and conducted prospective follow-ups from 1982 through 1989 [175].

In both studies, cardiopulmonary and lung cancer mortality were found to be significantly and strongly associated with $PM_{2.5}$ concentrations. A $10 \mu g m^{-3}$ increase of $PM_{2.5}$ was related to 16% (with a 95% confidence interval (CI): 7-26) and 6.2% (95% CI 1.6-11) relative risk increase (RRI) of mortality in the Harvard Six Cities study [193] and the ACS study [194], respectively.

Only a few considering the reproductive and neurological systems [18]. The overall mortality risk was found to be higher for cardiovascular disease than pulmonary disease [4]. Regarding the cardiovascular system, the findings indicate that short-term exposure to elevated $PM_{2.5}$ for a few hours to weeks can trigger cardiovascular disease-related mortality, as well as nonfatal events such as myocardial ischemia, MIs, arrhythmias, heart failure and stroke [4]. However, most studies indicate an increased risk associated with long-term exposure to $PM_{2.5}$ compared to short-term exposure [4, 173]. It has been estimated that exposure to $PM_{2.5}$ caused 4.2 million deaths and 103.1 million disability-adjusted life-years (DALYs) in 2015, with ambient $PM_{2.5}$ being the fifth-ranking mortality risk factor that year [185]. Life expectancy could plausibly be reduced by several months to a few years with long-term exposure to the increased ambient $PM_{2.5}$ concentration currently encountered [4]. It is worth noting that there is no zero-effect threshold value, below which no health effects are expected. Exposure to low level PM (e.g. an average $PM_{2.5}$ concentration of $8.7 \mu g m^{-3}$) in Kotka, Finland, was related to acute systemic inflammation, causing elevated blood inflammatory markers in patients with ischemic heart disease [195]. Children, the elderly and people with pre-existing diseases/conditions are subgroups of population most susceptible to PM exposure. Therefore, further reduction in ambient PM concentration below the current limit would certainly be a benefit to public health [4].

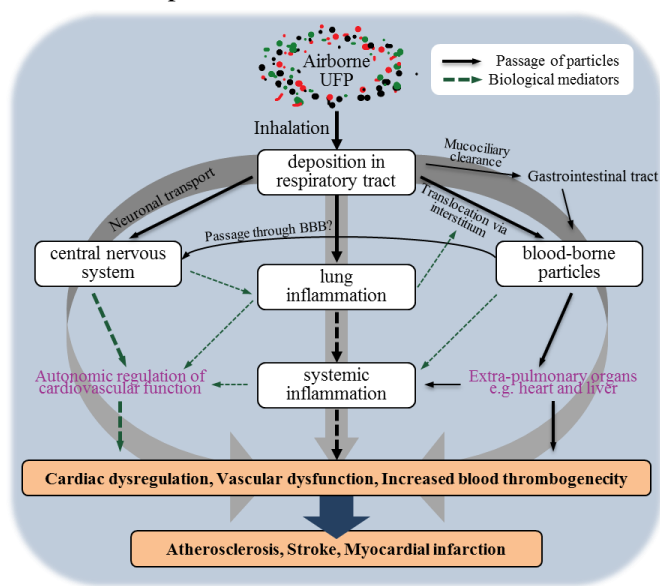


Fig. 14 schematic image illustrating some of the key mechanisms through which inhaled UFP may influence secondary organs and systemic tissues, with emphasis on the mechanism through which inhaled particles may cause cardiovascular events. Adapted from Stone et al. [18].

1.3.2 Toxicological studies of PM health effects

The lack of biological studies cast doubt on the plausibility of a causal relation between PM pollution and health outcomes from epidemiology studies before 1997, particularly regarding the cardiovascular system. Since then, there have been more studies investigating the potential mechanisms of PM to cause adverse health effects [173]. One important hypothesis is that the inflammation resulted from exposure to PM could result in a series of biological effects. This classic hypothesis of inflammation implies that through the uptake of particles inhaled into the lungs by alveolar macrophages, an inflammatory response within the lung (pulmonary inflammation) is triggered. Systemic inflammation, which is strongly related to cardiovascular disease, results from the “spill-over” of inflammatory mediators into the blood. Studies have reported an association between short periods of ambient PM exposure and the daily elevation of a

wide range of inflammatory biomarkers, including the C-reactive protein (CRP), fibrinogen, tumour necrosis factor- α (TNF- α), interleukin (IL)-1, IL-6, etc. [4] (and literature therein). Another important hypothesis of pathophysiological mechanisms proposed that oxidative stress results from excessive reactive oxygen species (ROS: O₂, OH⁻; RO₂; H₂O₂ etc.), which are essentially free radicals generated by PM exposure [4, 196]. ROS can be directly generated by specific particle components (e.g. transition metals or organic species such as semiquinones) *in vivo* through chemical mechanisms on the surface or after metabolic activation through the cytochrome P450 system (e.g. PAH) [4, 197]. It can also be triggered indirectly by other taken-up constituents through the endogenous cellular source upregulation (e.g. upregulation of nicotinamide adenine dinucleotide phosphate [NADPH]) oxidase) or through damage to the organelle function (e.g. mitochondria) [4]. ROS alters the redox state of the cell, thereby triggering a cascade of inflammation-associated events. A three-phase response model was introduced to explain the oxidative stress process. In phase I of relatively low levels of oxidative stress, transcription factors (e.g. nuclear factor erythroid-2, Nrf2) induce antioxidant enzymes to restore cellular redox homeostasis. In phase II of intermediate levels of oxidative stress, after the failure of antioxidants to respond, mitogen-activated protein kinase (MAPK) and NF- κ B (nuclear factor kappa-light-chain-enhancer of activated B cells) cascades are activated to induce a pro-inflammatory response. In phase III of high levels of oxidative stress, the ROS overwhelms the antioxidant defences, resulting in cytotoxic effects and mitochondria damage, and then releases pro-apoptotic factors and induces cellular apoptosis [196, 198]. Two more pathways are also proposed to further explain the cardiovascular effect of PM exposure: “autonomic regulation” and “particle translocation”. Autonomic regulation is caused by the stimulation of the alveolar sensor receptor through exposure to PM (or an inflammatory response). Signals sent to the central nervous system (CNS) alternate the activity of the autonomic nervous system, regulating cardiac function directly and other cardiovascular systems indirectly [18]. Translocation is mainly regarding the entry of ultrafine particles in other vital organs beyond the respiratory system, which will be discussed in following chapter. Using UFP as an example, the aforementioned mechanism can be summarised as shown in Fig. 14.

1.3.3 The association between PM components and PM’s health effect

Despite the fact that many epidemiological studies associate PM exposure with harmful health effects, most do not specify the effects of individual constituents or characteristics of PM. The characteristics that may be important for the health effects of airborne PM include particle size, surface area, sources, etc. [197, 199, 200] while the components studied include single organic compounds, like PAH, sulphate, nitrate, elements like Ni, V, Cu, Zn, Ti, As, Cr, etc., or bulk compositions, like OC, EC, WSOC [201, 202]. Similar to PM health effect studies, both epidemiological and toxicological methods can be applied to investigate effects of specific components or characteristics of PM. Rather than focusing on a single target component, it was proposed that health effects due to simultaneous exposure to multi-component mixtures should be characterized. Studying specific source-originated PM with characteristic components is a multi-pollutant approach of characterizing PM health effects using multiple statistical methods, mainly source apportionment methods [5, 203, 204]. The advantage of a source-orientated health effect study is that the result could be highly relevant to regulations targeting a specific source identified as particularly harmful to human health, covering both primary and secondary pollutants originating from it [203]. The evidence for source-specific health effects is limited, with more existing evidence for combustion-generated aerosols, such as combustion and traffic emission [202, 205-208]. In a study in Phoenix, USA, sources associated with the highest cardiovascular mortality were secondary sulphate

(0 day lag) and traffic (1 day lag) [209]. In Washington, USA, sulphate and coal-related PM_{2.5} were most significantly associated with all-cause mortality (3 day lag for both) [210]. Stanek et al. [211] reviewed the published studies using quantitative methods to investigate the relationship between grouped factors or sources and health effects. They found that cardiovascular effects may be linked to crustal or combustion sources, including traffic, but at that time, no individual source had been identified as unequivocally associated with specific health outcomes from the limited collective evidence available. In Europe, even less multi-pollutant studies were conducted. A study of 3 cities in Sweden demonstrated that long-range transport was the main source of PM exposure, while local emissions were the major cause of premature deaths, the largest contribution stemming from traffic emissions and residential wood combustion [212]. Even fewer studies have investigated the health effects of SOA due to the difficulty in separating, quantifying and characterizing SOA, as mentioned above. Tuet et al. [208] studied the oxidative potential (measured by the Dithiothreitol (DTT) assay) of SOA generated in smog chambers from both biogenic and anthropogenic precursors under various reaction conditions and found that precursors were the main contributors to oxidative stress, with SOA from naphthalene and isoprene oxidation comprising the strongest and lowest oxidative potential, respectively [208]. Comparing to other ambient and experimental studies, SOA from the incomplete combustion of diesel, gasoline and biomass demonstrated the most DTT activity, similar to the result found for naphthalene in their study [208] (and literature therein). Therefore, one major goal of this thesis was to separate between primary and secondary sources using a source apportionment approach based on the specific organic markers introduced in chapters above.

1.3.4 Health effects of (quasi-) UFP

In most urban areas, UFP makes up over 90% of the PNC (1 to 5 x 10⁴ particles cm⁻³ under background conditions), but comprises less than 10% of the PM_{2.5} mass concentration (e.g. between 0.8 and 1.6 ug m⁻³ under background conditions) [5, 213, 214]. Quasi-UFP, including particles with a larger diameter than PM_{0.1}, accounts for an even greater portion of the PNC. If (quasi-) UFP is indeed more toxic than large PM (e.g. coarse particles), the adverse effects are expected to be seen at low mass concentration due to their low contribution to mass concentration [213]. One indication of this came from the London smog episodes from the 1950s to the 1970s, during which the particle mass concentration exposure and daily mortality response curve show a steeper slope at lower concentrations than at higher concentrations [213, 215]. Epidemiology evidence of adverse health effects due to UFP exposure have mostly been based on the PNC and results are not as consistent as for the PM_{2.5}. Due to a lack of evidence, no conclusions could be made regarding a causal relationship between UFP exposure and mortality. It was estimated that a reduction of the UFP concentration by 10,000 particles cm⁻³ would result in a 0.1-2.1% decrease of the all-cause mortality, with uncertainty mainly due to the lack of long-term studies [216]. Therefore, the Ultra-III project, within the frame of which studies in this thesis were conducted, aimed to investigate long-term trends of particle number concentrations as a surrogate of UFP and other pollutants at multiple sites, and model its spatial variability applying land use regression modelling (LUR) so that long-term exposure at different sites can be estimated in epidemiological studies.

From a biological plausibility perspective, there is toxicological evidence that links (quasi-) UFP with *in vitro* biological effects. Several properties of (quasi-) UFP could be related to its more severe and/or independent biological effects, such as surface characteristics, distinct interaction with cells, translocation possibility, etc.. Surface properties of (quasi-) UFP, i.e. high surface-to-volume ratios compared to larger

particles, allow the exposure of hazardous pollutants (metals and organic compounds) on the surface increasing their potential interaction and impact on a biological system after inhalation. This is proposed as one important reason for their high toxicity. Early studies found that smaller and larger particles share the same dose-response curve of inflammatory potential expressed in terms of surface area, but a much steeper slope is shown for UFP than larger particles in terms of mass [213] (and literature therein). Due to their small size, UFP may directly enter different lung cell types instead of the phagocytic pathways. An *in vitro* study found particles taken up into cells via diffusion or adhesive interactions instead of through the endocytic process, and particles within cells were not bound to the membrane and hence, could access cell components such as protein and DNA, enhancing their toxic potential [217]. Electron microscopy found that UFP were localized in mitochondria, thereby inducing major damage [218]. Possible mechanisms or pathways for UFP to influence other organs other than the lungs with emphasis on the cardiovascular are shown in Fig. 14, which is quite similar to the mechanisms proposed for cardiovascular effects caused by PM exposure in general [4, 18]. One mechanism of UFP that causes adverse health effects, particularly regarding the cardiovascular system, is its possibility to translocate through the bloodstream to other vital organs (e.g. liver, brain, etc.) [214, 219, 220]. This specific behaviour of UFP may be indicative of an independent effect. An *in vivo* study of Geiser et al. [217] found inhaled ultrafine titanium dioxide aerosol in all major lung tissue compartments and cells and inside the capillaries, demonstrating its ability of crossing cellular membranes and cell translocation. Elder et al. [172] reported that inhaled Mn oxide as solid UFP can be translocated through the olfactory bulb pathway to the central nervous system and cause inflammatory change in rats. However, epidemiological, toxicological and clinical experts in an elicitation workshop assessed a (very) low to medium likelihood of translocation among 6 pathways tested due to limited evidence (these were mainly animal studies). The dose of translocation might be too low to cause any cardiac effect or it might need to accumulate over a long period of time in order to create any effect, although most experts do believe in the occurrence of translocation [214]. However, the traditional pulmonary and systematic inflammation pathway, similar to the middle pathway in Fig. 14, had the highest rated likelihood (high to very high) of the 6 pathways, while the disturbance of the autonomic nervous system (ANS) regulation pathway is thought to be highly uncertain and difficult to judge [214].

Similarly to the $PM_{2.5}$, there is evidence to link biological effects of (quasi-) UFP to its chemical components and sources. A study by Li N. et al. showed that ambient UFP collected in the Los Angeles basin had the highest potential of inducing cellular oxidative stress markers (cellular heme oxygenase-1:HO-1) and the HO-1 expression was directly correlated to the high OC and PAH content of UFP; also, DTT assay demonstrated the highest ROS activity of UFP [218]. Regarding quasi-UFP, associations were found between ROS activity of the $PM_{0.25}$ and its OC, WSOC and concentrations of water-soluble transition metals, as well as between its DTT activity and chemical species, such as PAHs, hopanes, etc. [221, 222]. DNA damage of the $PM_{0.4}$ winter samples was found to be correlated with the presence of organic compounds [10]. As mentioned earlier, a source-orientated health effect study could be used to target more health-relevant sources. Regarding quasi-UFP, Saffari et al. [13] separated sources contributing to the OC of the $PM_{0.25}$ through a molecular marker based chemical mass balance (MM-CMB) model and found that variability in source strength was the major cause of variability in oxidative potential at different sites. They found that SOA and mobile emission explained 58% of the spatial and temporal variability of the $PM_{0.25}$ oxidative potential in 3 locations. (Quasi-) UFP studies are rare in general, and studies regarding organic composition and its sources are even fewer. Spatial variation

studies of (quasi)-UFP are extremely rare except for investigations of number concentration. The $PM_{0.25}$ mass was found to be relatively, spatially homogeneous in 10 distinct areas in Los Angeles, USA, and an uneven distribution was only found for its EC, nitrate, and a few toxic metals over a short physical distance [223]. Based on the discussion above, this study aims to assess the long-term variation of chemical markers of quasi-UFP, to identify the sources of OC and to investigate the seasonality of source contribution and their spatial-temporal variability at sites with different surrounding environments.

1.4 Source apportionment using receptor modelling

Source apportionment (SA) studies aim at resolving contributions of emission sources and/or formation processes to observed ambient PM concentrations by applying variable measurement strategies followed by data processing techniques. It is an approach that works to relate aerosol observations to sources and their activities; SA is highly relevant for the development of remediation measures [92]. Developments in measurement technology for the chemical characterisation of atmospheric PM and in computer technology for data analysis have enabled substantial improvements in source deconvolution capabilities [224]. Source attribution is mainly based on two models: chemical transport models and receptor models. The former is based upon pollutant emission rates and meteorological data to simulate the dispersion and physiochemical processing of emitted aerosols, so that the concentration at different locations can be calculated [225]. Receptor models, on the other hand, are based on the observations at a sampling site, a so-called “receptor site”, to infer the sources and their contributions to the observed concentrations.

Receptor-oriented SA comprises many tools. Simple techniques include elementary mathematical calculations (e.g. correlation with wind direction, gaseous pollutants or hotspot increments) and physical assumptions (e.g. enrichment factor analysis) [92, 226]. Complex models with pre- and post-data processing and user friendly interfaces are also available [92, 224, 226, 227]. The fundamental principles of receptor modelling are that mass and species conservation can be assumed and a concentration balance analysis can be used to identify and apportion sources of airborne PM [224, 226]. Based on this “mass balance” assumption, an equation can be written to solve the receptor model:

$$x_{ij} = \sum_{k=1}^p g_{ik} f_{kj} + e_{ij} \quad (1)$$

wherein x_{ij} is the measured concentration of the j^{th} species in the i^{th} sample, g_{ik} is the contribution of the k^{th} source to the i^{th} sample and f_{kj} is the concentration of the j^{th} species in the k^{th} source, with e_{ij} as the residue [92]. The traditional approach to obtain a data set for receptor modelling is to utilize measurements of chemical constituents, such as molecular and/or elemental constituents, in a number of samples to attribute a bulk-quantity-like total OC or PM mass concentration, which is termed a “marker-based” technique according to Fuzzi et al. [5, 224]. Alternatively, methods like automated electron microscopy (AMS) can be used to characterize the composition and size of a large number of particles at a low chemical specificity level, termed the “ensemble-based” method by Fuzzi et al. [5, 224]. This thesis used an organic marker-based data set, therefore, only the former method will be described further. Equation 1 is solved differently depending on what a priori information is available [224]. On the basis of known or predefined sources and source profiles (f_{kj}) serving as input in the equation, the appropriate model is the CMB model [5, 92]. The algorithm yields a solution that maximizes the explanatory power of the predetermined profiles, usually from primary source emissions, leaving a residual assumed to be the SOA according to previous research/by many studies [5, 224]. One important characteristic of CMB is

that secondary aerosols must be included not as components of emission source profiles but as specific, single chemical compounds. This absence of mixture with other marker elements is often regarded as a limitation and may lead to a misinterpretation of results [226]. It is worth noting that no established source profile is available for size-segregate samples (e.g. ultrafine particulate matter). The stand-alone software from the United States Environmental Protection Agency (US-EPA) can promote the usage of CMB to some extent, but it has become less popular than PMF analysis in recent years, likely due to the lack of contemporary source profiles for most receptor sites [92, 224]. In this case, other models that does not necessarily require a priori knowledge of source profiles are used, including principal component analysis (PCA), PMF, Unmix, etc. [226]. Among them, PMF is the most widely-used method with independent software [92, 224, 228, 229]. PMF is a type factor analysis considered more efficient than PCA in finding the underlying structure of data with non-negative constrains on source profiles and source contributions [92]. The basic assumption for the PCA of orthogonal components resolved by PCA does not reflect the structure of real world data (many source profiles have a degree of collinearity) [92].

PMF solves equation 1 by minimizing a weighted objective function given by

$$Q = \sum_{i=1}^n \sum_{j=1}^m \left(\frac{e_{ij}}{s_{ij}} \right)^2 = \sum_{i=1}^n \sum_{j=1}^m \left[\frac{x_{ij} - \sum_{k=1}^p g_{ik} f_{kj}}{s_{ij}} \right]^2 \quad (2)$$

wherein s_{ij} is an estimate of the uncertainty for the j^{th} species in the i^{th} sample. The introduction of s_{ij} for each species of each sample as input data allows individual treatment (scaling, weighing) of the measurement matrix [228, 230]. Several algorithms have been used by PMF to find a global minimum Q value, including alternating between the least squares iterative method, PMF2, PMF3 and Multilinear Engine (ME) [92, 224, 228, 230, 231]. The Least square iteration was slow and a faster algorithm computing the profile matrix F and contribution matrix G was subsequently developed (PMF2) [92]. PMF3 was designed to solve trilinear problems [230]. ME was developed in the late 1990s and is a more flexible program that can solve any problem that can be expressed as the sum of products [224, 231]. ME generates a table that specifies the model and then solves it using the Conjugate Gradient Algorithm [92]. With the application of ME in PMF, the rotational ambiguity can be reduced by including additional constraints such as: known source profiles, known source contributions (or lack of contribution), meteorological variables or weekday/weekend [92, 224]. ME flexibility has been exploited to develop dataset-specific models and to process heterogeneous data, like aerosol composition and size distribution, data with different time resolutions or multi-site/multi-type samples [92, 224, 232]. PMF results can also combine with local wind data to analyse point-source impacts from various wind directions, applying conditional probability function (CPF) [92, 233]. The potential source contribution function (PSCF) provides the means to map the source potentials of geographical areas and can be applied to the PMF results for a better interpretation [224, 227, 234].

Since principal component/factor analysis (e.g. PCA, PMF, UNMIX) attempts to apportion the sources on the basis of observations (internal correlations) at the receptor site alone, a common problem is that the resulting components or factors may represent mixtures of emission sources, as opposed to clearly independent source profiles [226]. Specifically, a factor analysis or PCA model cannot distinguish spatially- and temporally-correlated sources. From the PMF or PCA standpoint, spatially- and temporally-correlated sources are perceived as one single source because they almost always impact the receptor site at the same time [227]. Unlike CMB, which may be carried out for a limited number of samples, PMF

requires a substantial number of independent samples (at least 50) and works best with a large dataset in which the number of samples far exceeds the number of analytical variables [92, 235]. It is suggested that a minimum variable-to-observation ratio of 1:3 be maintained to ensure accurate results [235, 236]. Although PMF requires no a priori knowledge of source composition, any information on source emissions characteristics is helpful in discriminating between similar sources [235]. Actually, determining the optimal number of source factors, the assessment of rotational ambiguity, and interpreting factors as potential sources require a profound qualitative understanding of the emissions within the area studied [92].

Belis et al. [92] reviewed the literature on source apportionment of ambient PM in Europe using receptor models, in which 272 records were identified for an estimation of source contribution to PM mass concentration and 60 records to the OC of the PM. According to their analysis, the most commonly used methods are PMF (> 40%), PCA (24%), CMB (18%), and other types of factor analysis without non-negative constraints (7%). A few European studies are based on other methods like the UNMIX model. A descriptive statistical analysis of 243 out of 272 records showed that there were 6 major source categories contributing to the PM mass over Europe. The sources and their median relative contributions are sea/road salt ($5 \pm 3\%$ from 133 records), crustal/mineral dust ($17 \pm 12\%$ from 188 records and $24 \pm 11\%$ for PM₁₀ in urban areas), secondary inorganic aerosol ($20 \pm 7\%$ for sulphate from 87 records and $16 \pm 6\%$ for nitrate from 72 records), traffic ($19 \pm 11\%$ from 216 records), point sources ($15 \pm 6\%$ from 134 records), and biomass burning ($14 \pm 6\%$ from 89 records). Relative sulphate contribution to the PM was found to be the highest during warm seasons due to faster photochemistry and lower wet deposition, while relative contribution from nitrate is the highest during the cold season. Seasonal variation was also identified for the biomass burning source factor with a higher relative contribution in colder seasons (14%) than warmer (3%) due to its association with domestic heating. The crustal/mineral dust source factor showed lower contributions during the cold season. A systematic spatial variability of traffic's relative contribution was observed as increasing from rural sites ($7 \pm 4\%$) to urban ($22 \pm 11\%$) and traffic sites ($27 \pm 12\%$). From their results, it is clear that SOA as a source of atmospheric PM was not resolved by the previous "marker-based" PMF studies. One major reason may be that most studies did not include SOA-related, specific organic markers. Common chemical constituents used for source apportionment are ions and elements, and primary organic markers, like levoglucosan, were generally involved when organic speciation was performed [92, 226]. Elements are good receptor species with respect to atmospheric stability, whereas molecular markers identified from different emission sources (see section 1.2.7) or formed from variety atmospheric processing are much more source specific and can significantly increase the confidence in source interpretation. Therefore, the use of organic chemical species has grown popular in modern source apportionment studies [92, 235]. Particularly, SOA markers are highly valuable in apportioning/delineating/determining the contribution of the SOA. Therefore, these markers are specifically integrated into the chemical speciation analysis in this study and enable the separation and identification of SOA sources and SOA's contributions to the OC of atmospheric quasi-UFP.

Methodology

2.1 Sampling

2.1.1 Sampling system description



Fig. 15 One of the two sequentially-connected RDI and Partisol sampler sets (I) and drum substrate loaded with ambient PM (II: all drums; III: the 3rd stage).

Two sampling sets were used in a field sampling campaign. Each set consisted of a rotating drum impactor (RDI) mounted as a pre-impactor on top of a filter sampler (Partisol™ 2025i Sequential Air Sampler, Thermo Scientific, USA) as shown in Fig. 15. The filter sampler provided 16.7 L min^{-1} of air flow through the RDI. The original filter after the last stage of the RDI could not fulfil the purpose of automatically taking multiple samples because it could not be replaced and stored automatically. Therefore, it was replaced by a Partisol filter sampler, which switched to new sample and stored the sampled filter automatically at a

predefined time interval similar to the RDI. In this way, they were synchronised to start a new sample simultaneously after a 24-h sampling period for one sample, meaning they loaded new filters and rotated them to a new sampling position for the Partisol sampler and RDI, respectively. Such a set-up achieves up to one week of unattended, daily field samples in this study. Quartz fibre filters (QFF: T293, Munktell, Grycksbo, Sweden) were used both as filters in Partisol sampler and as substrate strips covered on RDI drums.

2.1.2 Impactor theory and rotating drum impactor (RDI)

For many years, cascade impactors have been used for the classification of particles by aerodynamic size. Typically, a cascade/multi-stage impactor is made up of a series of stages consisting of a nozzle and an impaction plate as arranged in Fig. 16 [237]. Inside the impactors, particles deposit onto the impaction surface due to an inertial impaction mechanism. Varieties of the impactors have been designed, manufactured, and applied for aerosol studies [238, 239]. RDI is a special category of slit cascade impactors originally designed by Lundgren [240]. A rotating drum is used to hold the substrate in the RDI instead of the conventional flat plate in a normal impactor (Fig. 15: II, III). It can rotate automatically to start a new sample, and the degree and time interval for rotation can be pre-set. In such a manner, time- and

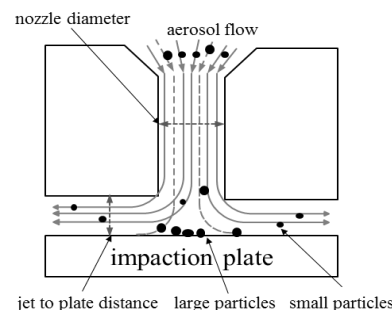


Fig. 16 streamlines and particle trajectories for a typical impactor stage. Adapted from Marple and Willeke [237].

size-resolved PM samples are taken simultaneously. Aerosol flow passing through the nozzle is accelerated and the impaction drum below the nozzle causes a strong bending of the gas stream lines. Large particles which cannot follow the stream lines due to their high inertia will deposit upon the impaction surface, while smaller particles with low inertia pass onto the next stage as aerosol in the gas stream. Hence, the PM entering the impactor is separated by particle size. The midpoint collection diameter ($C_{Dp, 50\%}$) of the collection/penetration efficiency curve where 50% of the particles are collected is often defined as the cut-point diameter. It is worth noting that in reality, the cumulative collection efficiency curve tilted and therefore, the definition of a “nominal” cut-point is based on the assumption that the captured mass (or concentration) of particles $< C_{Dp, 50\%}$ equals the penetrated mass (or concentration) of particles $> C_{Dp, 50\%}$. Aside from size classification, the advantages of the impactor as a sampler compared to filters are: 1) The air stream moves over the sample, not through it as in filtration, reducing any subsequent desiccation and chemical transformations of the collected sample; 2) the theoretical prediction of a cut point; 3) almost complete control of the type of surface with which the particles impact; 4) change the cut-point by varying the key parameters of gas velocity and nozzle dimension [241]. However, there are also disadvantages: 1) only a limited amount of material is available for mass and compositional analysis, as one cannot collect more than a few mono-layers of particles before particle bounce, and mis-sizing become potential problems 2) time multiplied by size resolved sampling yields a large number of samples with low concentration, leading to a great effort and cost of analysis [241].

Although a variety of substrates can be utilized in an impactor, the choice of substrate should meet the requirements of field collection and chemical analysis. For instance, grease or oil can be used to coat an impaction substrate to reduce bounce off and re-entrainment losses, but using such a coating may cause interference with the physico-chemical and biological test of the collected particles [242]. An alternative is to use a porous material such as polyurethane foam (PUF) and QFF as substrate. However, the collection characteristics of such materials should be tested to understand their influence on the cut-points and size distribution of collected particles. It was observed that normally the cut-points were shifted towards smaller diameter and meanwhile sharpness of the cutoff curve was reduced when utilizing such a substrate [242-244].

2.1.3 Test collection characteristic of RDIs

The 3-stage RDIs utilized in this thesis were produced by the Swiss Federal Laboratories for Materials Science and Technology (Empa, Dübendorf, Switzerland), with the nominal cut-points given as 2.5, 1, and 0.1 μm at a nominal flow rate of 16.7 l min^{-1} , respectively, at each stage. Although only a limited number was manufactured, they have already been used in a few scientific studies [245-247]. The $C_{Dp, 50\%}$ testing in the first and second stages done in a previous study are used as a middle cut-point diameter in this one at 2.4 and 1.0 μm , respectively [248]. Very importantly, this study needed to test the $C_{Dp, 50\%}$ of the last stage in order to define the particles captured on the backup filter for chemical speciation.

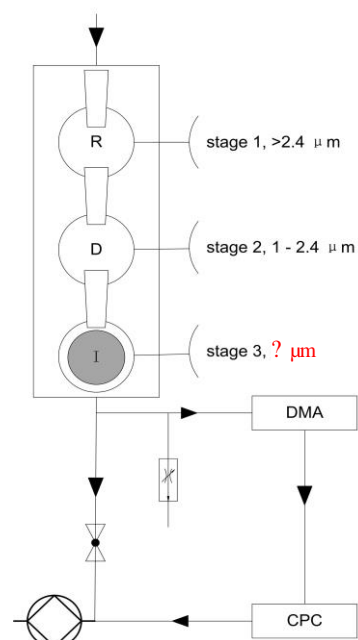


Fig. 17 Experimental set up for testing of RDI cut-point (3rd stage).

To adapt to the chemical analysis method, a collection characteristics of the last stage using QFF as substrate were specifically tested. The experimental setup is shown in Fig. 17. A nominal flow of 16.7 l min^{-1} indoor aerosol was pumped through the RDI. The PM size distribution at the outlet of the RDI was determined by a differential mobility analyser (DMA; model 3081, TSI Inc., Shoreview, USA) sequentially connected to a condensation particle counter (CPC; model 3025A, TSI Inc., Shoreview, USA). Calibration of the DMA connected CPC prior to measurement was done by latex standard spheres (DistriLab, Leusden, The Netherlands) with the RDI dismounted. Each penetration curve has been calculated from paired measurements of size distributions. Reference distributions were determined with empty drum housings by removing all the drums and working size distributions with the drum of the last stage installed. The drum was covered by either QFF or ungreased aluminium foil during operation. C_{Dp} of each size channel was calculated by Eq. (3):

$$C_{Dp} = 1 - \frac{C_{N,withdrum}}{C_{N,nodrum}} \quad (3)$$

Since the pressure at the outlet of the third nozzle was only around -100 hPa, the CPC counting numbers were used in the calculation without correction for the following reasons. According to previous studies, counting efficiency of relatively larger particles most relevant for this study should be almost unaffected at such low pressures [249, 250]. Moreover, both size distributions used in the calculation were measured with the nozzle installed and this would make the pressure comparable in both cases, as it is the nozzle and not the drum, which generates the pressure drop. Two RDIs of identical manufacture and model were tested to check their comparability.

2.1.4 Pilot field sampling

Parallel pilot field sampling was conducted in field after laboratory tests to investigate the comparability of chemical analysis results through the whole process from field sampling to chemical measurement. The pilot sampling period lasted from March 25-April 10, 2014 with two sampling sets working side-by-side at the reference site. The reference site is an ambient aerosol monitoring station located on the campus of the University of Applied Sciences Augsburg (Augsburg, Germany). This monitoring station has been operating for a long time and a more detailed description of it can be found in previous publications [251, 252]. This sampling (lat: 48.358, lon: 10.907) occurred approximately 1 km southeast of the Augsburg city centre. The main items within a 100 m radius are a campus building, tram station and a small company. The closest main road is 100 m to the northeast. The QFF used were baked at $500 \text{ }^\circ\text{C}$ overnight before usage. Samples were taken back to the laboratory on a weekly basis, packed in petri dishes and stored at $-20 \text{ }^\circ\text{C}$ until chemical analysis.

2.1.5 Sampling campaign

A long term sampling campaign lasting from April 11th, 2014 to February 22nd, 2015 was carried out in Augsburg area, with short break periods in between. One sampling set was operated at the reference site mentioned before for continuously sampling (including breaks). Meanwhile, the second sampling set was moved to one of five other sites (master sites) during short sampling periods (2 weeks each) for parallel sampling. Four of the master sites are within the urban area of Augsburg (T1-T3 and B1) and one (T4) in a periphery small town with about 35 km distance from the reference site. T1-T3 and T4 are defined as traffic influenced sites, while B1 is a city background site located in a monastery garden. The characteristics of the master sites influencing the observation in this study will be further explained in the

“Results and discussion” chapter. The distribution of these sites in Augsburg can be found in Fig. 18 and the available profile of each site is shown in Table 2. At each master site, 6 weeks of sampling campaign was divided into three 2-week short campaigns carried out at 3 different seasons, respectively. However, at T1, sampling during the winter period was not successful and at T4, only one short campaign in autumn was successfully completed. Days of successful parallel sampling at both master and reference sites are listed in Table 2, excluding days when only reference site or master site sample are available.

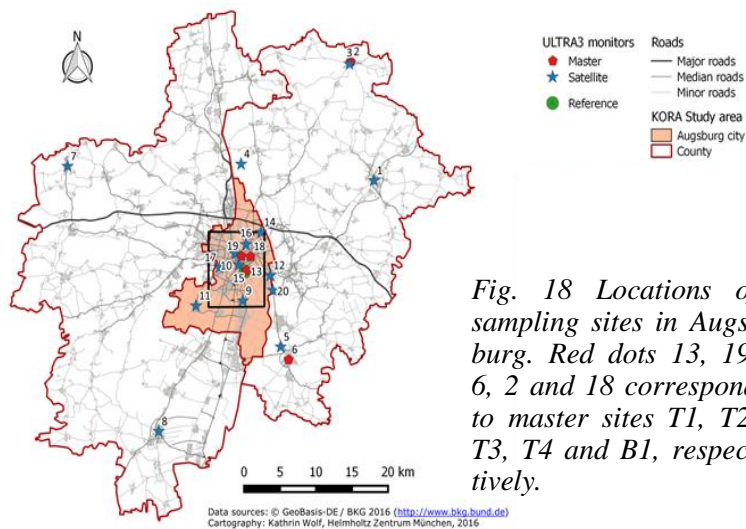


Fig. 18 Locations of sampling sites in Augsburg. Red dots 13, 19, 6, 2 and 18 correspond to master sites T1, T2, T3, T4 and B1, respectively.

2.2 Monitoring of meteorological data and measurement of the PNSD

Meteorological data regarding the air temperature, wind speed and wind direction referred to in this study were monitored by the Bavarian Environmental Agency (Bayerisches Landesamt für Umwelt, LfU). Their monitoring site is located 4 km south of the city centre. The PNSD was measured by a combination of a customized twin differential mobility particle sizer (TDMPs) and an aerodynamic particle sizer (APS) [252]. The size-segregated PNC was calculated for the size ranges of 5-50, 50-360, 360-1000 nm, 1.0-2.4 and 2.4-10 μm . Additionally, the $\text{PM}_{0.36}$ mass was estimated based on two assumptions: the first is the spherical shape of particles allowing size bins to be used to calculate particle volume; the second is that the particle density is 1.5 g cm^{-3} [252].

2.3 Organic compound speciation

The chemical components of QFF samples were analysed utilizing an *in situ* Derivatization Thermal Desorption Gas Chromatography Time-of-Flight Mass Spectrometry (IDTD-GC-TOF-MS) method [253]. A schematic representation of the method is shown in Fig. 19. A 27 mm^2 -sized strip cut from filter samples, or one-fifth (2 mm) of the drum filter strip, was spiked with internal standard mixtures containing isotope-labelled compounds and placed in a clean and deactivated glass-liner for analysis. Sample introduction process was completed by a programmed auto sampler (Combi PAL, CTC Analytics AG, Zwingen, Switzerland), during which the filter in the liner was damped with 10 μl silylation reagent N-methyl-N-trimethylsilyl-trifluoroacetamide (MSTFA). Then, the liner was immediately inserted into the GC-injector (Optic 3, GL Sciences, Eindhoven, The Netherlands). Next, the thermal extraction *in situ* derivatization process of organic species was done in the GC-injector at a temperature of 300 $^{\circ}\text{C}$, during which the carrier gas was enriched with MSTFA and the temperature in GC oven was kept at 70 $^{\circ}\text{C}$. After this process, the temperature ramp of the GC system started. It first heated up to 130 $^{\circ}\text{C}$ at a rapid 80 $^{\circ}\text{C min}^{-1}$ and then, ramped up to 330 $^{\circ}\text{C}$ at 8 $^{\circ}\text{C min}^{-1}$ which it held for 30 min. The capillary column used was the BPX5 (25 m, 0.22 mm ID, 0.25 μm film, SGE, Australia). The column flow was 4 ml min^{-1} and

0.7 ml min⁻¹ during and after desorption, respectively. The TOF-MS record masses ranged from 35- 500m/z with an acquisition frequency of 25 s⁻¹.

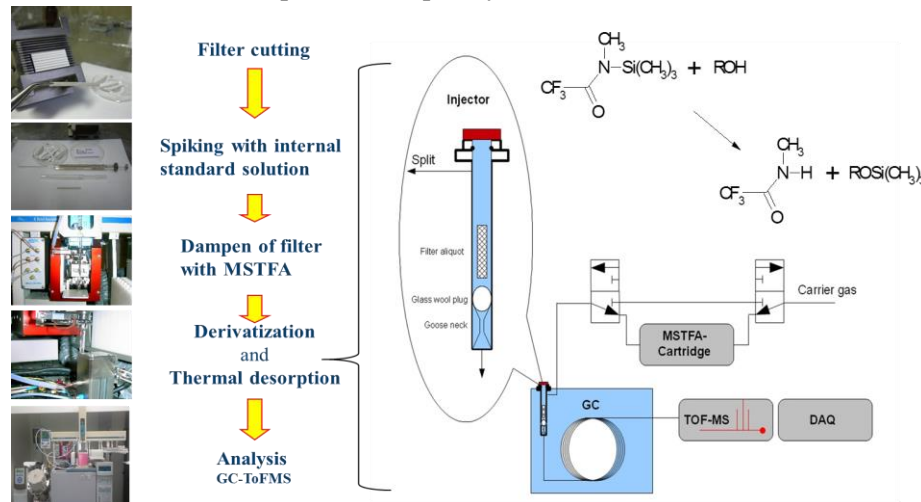


Fig. 19 Analysis procedures and in situ derivatization thermal desorption unit (figure at the right side of the bracket). Silylation reaction of polar organic species with MSTFA is shown at the top right corner. Adapted from Orasche et al. [253].

For the purpose of tracing SOA sources in this study, secondary polar organic compounds were examined and added to the established method as target compounds. These compounds include the SOA markers from isoprene and pinene described in the introduction chapter. This was a very successful extension of the existing method and the key to the successful separation of different SOA sources, which will be discussed below. Quantified/semi-quantified compounds for further data processing include: 17 α (H),21 β (H)-norhopane (29ab), 17 α (H),21 β (H)-hopane (30ab), 9 PAHs including fluoranthene, pyrene, benz[a]anthracene, chrysene, sum of benzo[b]- and [k] fluoranthene, benzo[e]pyrene, benzo[a]pyrene, indeno[1,2,3-cd]pyrene and benzo[ghi]perylene, galactosan, mannosan and levoglucosan, vanillic acid, cis-pinonic acid, 2-methyltetrols (2MTs: 2-methylthreitol and 2-methylerythritol), 3-methyl-1,2,3-butanetricarboxylic acid (3-MBTCA), 3-hydroglutaric acid (3-HGA), malic acid, 4-nitrophenol, 4-nitrocatechol and several DCA, including adipic acid, glutaric acid, succinic acid and fumaric acid. Due to an unidentified technical issue, compounds with more than one acidic functional group could not successfully be analysed for samples collected from the end of July to the middle of October. Both the drum samples and the filter samples from the short pilot field sampling were analysed to compare the two sampling sets (results discussed in Publication 1). For the nearly one-year-long campaign, the drum samples were not analysed, but the samples from the Partisol filter were, in order to focus on the investigation of the seasonality (results discussed in publication 2) and spatio-temporal variability (results discussed in Publication 3) of the quasi-UFP.

2.4 EC/OC analysis

The EC/OC analysis was done via thermal/optical carbon analyser (2001A, Desert Research Institute, Reno, NV, USA) using the IMPROVE-A protocol. In this temperature protocol, a step-wise temperature program is applied to punches of filters in an inert atmosphere of helium gas (>99.99%). OC1, OC2, OC3 and OC4 correspond to OC fractions evaporated at the temperature of 140, 280, 480 and 580 °C, respectively. The EC was measured by adding oxygen to oxidize the elemental carbon at higher temperatures (up to 840 °C).

2.5 PMF analysis

The PMF analysis was performed using the EPA PMF 5.0. One analysis only included the reference site data to investigate seasonal variability of source contributions and is referred to as the PMF_{ref}. The second analysis included data from both the reference site and all master sites to investigate spatio-temporal variability of source contributions and is referred to as the PMF_{mas}. In the PMF_{ref}, organic species, OC2, OC3, OC4, OC and the PNC in size ranges 5-10, 10-30, 30-50, 50-100 and 100-360 nm were used as input parameters. The OC was assigned as a total variable. Since the organic molecular markers are the key indicators for source identification, the OC fractions (OC2, OC3 and OC4) which comprise many organic species and the PNC were defined as weak parameters to decrease their influence on the factor profile, but they are still analysed and receive a distribution among source factors. A few missing data were approximated by median values of the corresponding parameter. The acids for which the analysis of samples from the summer period was unsuccessful were still included in the PMF analysis, but were defined as weak parameters. F_{peak} was applied to test potential rotational possibilities. With an F_{peak} value of 0.5, a rotated model which pulled back a few extreme contributions approaching zero was generated, thus, creating a more reasonable model. This model has minimal influence on factor profiles and changed only 2% of the Q (dQ). The PMF_{mas} had two differences from PMF_{ref} regarding input data. First, as mentioned above, 271 samples from all sites were included in PMF_{mas}, including 109 paired samples from one of the five master sites plus the reference site and 53 unpaired samples mainly from the reference site; this is in comparison to 153 samples total in the PMF_{ref}. Secondly, in the PMF_{mas}, size-segregated PNC data were not used as they were only measured at the reference site and hence, only applicable to the PMF_{ref}. All the other parameters and settings remain the same in both analyses. Results of the F_{peak} 0.5 from the PMF_{mas} were also used for further analysis in this study for the reasons mentioned above, and the dQ was even smaller (0.6%).

Table 2. Summary of sampling site profiles

Site	Description ^a	D ^b	Nbld_ 50 ^c	Abl_ 50 ^c	Abl_ 100 ^c	Green _50 ^d	Green_ 5000 ^d	Paired sample period	Pair N ^e	T(°C) MLH ^f	
										T _f	MLH ^f
Reference			2	NA ^g	NA ^g	0	Refer to T1				
T1	Street	0.1	1	385.6	2273.4	0	0.34	12/7-17/7 17/10-29/10	6 ^e 10	19.6 9.6	726 488
T2	Street	3	1	953.9	2107.0	0	0.36	11/4-23/4 25/7-06/8 05/11-17/11	11 12 12	9.8 19.6 6.5	883 653 478
T3	Street	14	7	1144.8	3055.9	0	0.36	06/5-17/5 03/9-11/9 27/1/15-08/2/15	12 4 ^e 8 ^e	11.8 15.0 1	940 735 592
T4	Street	35	9	1258.2	3404.3	0	0.53	30/9-12/10	8 ^e	14.8	420
B1	City	3	12	1373.0	6907.9	0.4	0.31	27/5-01/6	6 ^e	12.4	626
	Background							14/8-26/8 26/11-08/12	8 ^e 12	14.4 2.1	736 490

^a T1-T4 defined by epidemiology study as street influenced site. B1 defined as city background site. ^b Distance to the reference site (km). ^c Nbld_50: number of buildings within a radius of 50 m. Abl_50 and Abl_100: area of buildings within a radius of 50 m and 100 m, respectively. ^d Green_50 and green_5000: sum of percentage of urban green, forest and semi-natural areas within a radius of 50 m and 5000 m, respectively. ^e Samples were not complete (< 12 days) due to different reasons, such as power failure, nozzle blockage by large materials or insects during sampling, or exclusion from PMF analysis. ^f T (average temperature) and MLH (average mixing height) were monitored by the Bavarian Environmental Agency at a monitoring site 4 km south of the city centre. ^g Not applicable for abld_50 and not available for abld_100.

Results and discussion

3.1 Publication I: Proof of concept and comparability of two sampler sets

3.1.1 Collection characteristics and comparability of cut-points of the 3rd stage of RDI

Fig. 20 shows the collection efficiency curves of the third stages of the two RDIs tested. Based on the morning indoor measurement conditions, an estimated aerosol density of $\rho_p = 1.4 \text{ g cm}^{-3}$ was used to convert the electrical mobility diameter measured by the SMPS system to aerodynamic diameter [251, 254]. The two curves show very similar collection patterns and no systematic shift could be found between them, indicating an overall comparability of the collection behaviours of two RDIs. An Sigmoid function curve was fitted to each collection curve to calculate the $C_{Dp, 50\%}$. *t*-Test applied to repeatedly measured $C_{Dp, 50\%}$ values (10 and 5, respectively) from RDI #1 and RDI #2 did not find any significant difference at a significance level of 0.05. Hence, the cut-points of both RDIs are comparable. The average $C_{Dp, 50\%}$ of the third stage is about $0.30 \mu\text{m}$ in electrical mobility diameter and therefore, $0.36 \mu\text{m}$ in aerodynamic diameter assuming the PM density to be 1.4 g cm^{-3} . This is much larger than the nominal cut-point of $0.1 \mu\text{m}$. The size-segregated PMs sampled in this study are then $\text{PM}_{0.36}$, $\text{PM}_{0.36-1}$, $\text{PM}_{1-2.4}$ and $\text{PM}_{2.4-10}$.

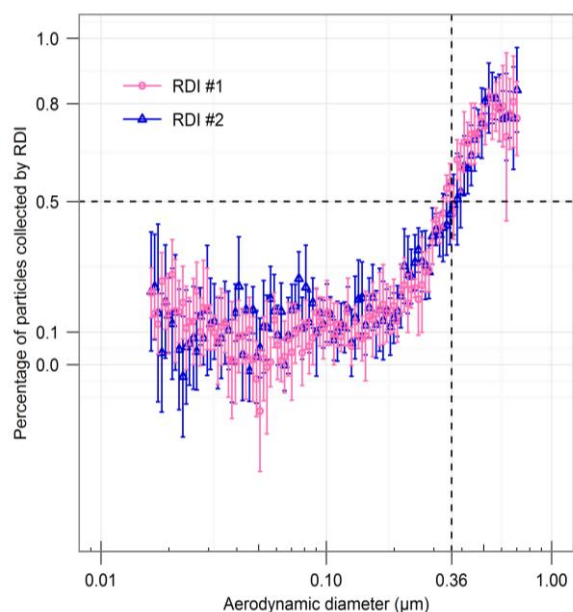


Fig. 20 Collection efficiency curves of the last impaction stage of both RDIs.

3.1.2 Influence on collection efficiency when using the QFF substrate

Fig. 16 shows that collection efficiency reaches a maximum of about 80% at about 600 nm. On the lower diameter side, about 10% of the smallest particles ($< 200 \text{ nm}$) are additionally captured. The test of the aluminium foil substrate demonstrates a lower maximum collection ratio and higher $C_{Dp, 50\%}$ cut-point diameter. This is consistent with observations in previous studies mentioned earlier that porous material substrate leads to a lower midpoint cut-off diameter, mitigated bounce off and re-entrainment artefacts. Grease is not applicable to this study because of its interference with the thermal desorption derivatization chemical analytical method. The use of an aluminium substrate is insufficient due to the low collection capacity and high artefact, at least at the initial sampling period before a substantial loading of PM. The extra collection of particles with the smallest diameter by the QFF is likely due to effects other than impaction. For instance, aerosols can penetrate into the fibre layer at a high velocity [242, 255] or diffuse along the surface of the filter material. In further traveling, the PM may be captured by filtration mechanisms such as interception or diffusion [256]. An increase of the collection ratio with decreasing particle size for particles $< 50 \text{ nm}$ is shown in Fig. 20, which is an indication of the diffusion of these

particles. The central impaction strips from the field campaign are shown in Fig. 15 as they spread out with PM residue observed on both sides. This “shadow”- like PM and the excess collection of the smallest particles may result in a slight underrepresentation of the $PM_{0.36}$ collected by the filter sampler.

3.1.3 Comparability of measured organic species concentrations

For the short pilot sampling period, polar markers, excluding levoglucosan, were quantified only in the smallest $PM_{0.36}$ as the derivatization of these markers was not reproducible for the drum strip samples. In coarse particles $PM_{2.4-10}$, only the 4-ring PAHs, fluoranthene and pyrene, and levoglucosan were detected. When plotting all the measured chemical concentrations from one sampling set against the other, the paired samples coincide with the 1:1 line from PAHs of the lowest concentration to levoglucosan of the highest concentration with limited random variation in both directions. A paired *t*-test of the daily concentration from both sampling sets did not show significant differences for hardly any of the quantified compounds across size ranges ($\alpha = 0.05$). Based on the above, the comparability of parallel sampling and molecular analysis had been verified.

3.1.4 Size distributions of organic species

As the only quantified compounds present in all size fractions, the size distributions of PAHs and levoglucosan will be described briefly as follows. The majority of PAHs are found in $PM < 1\mu m$ and less than 20% PAH in the $PM_{1-2.4}$. HMW (> 4 ring) PAHs were enriched either in the $PM_{0.36}$ or in the $PM_{0.36-1}$. Larger fractions of 4-ring PAHs (about 40-80%) were found in the finest size range $PM_{0.36}$ rather than the HWM PAHs (about 20-60 %). An increased PAH percentage in the $PM_{0.36}$ was observed during the measurement period which coincided with a temperature rise. About 50% of the levoglucosan was found in the finest size range $PM_{0.36}$. It is worth mentioning that for the HMW PAHs, the correlations between PAH in $PM_{0.36}$ and PAHs in other size ranges above $0.36\mu m$ are generally weaker (the majority of *r* values are between 0.5-0.8) than the correlations calculated within each size range ($0.8 < r < 1$). The result indicates that PAH in the smallest size fraction showed different variation patterns than PAHs in other coarser fractions, which might be due to the difference in source contribution.

3.2 Publication II: Seasonality and source apportionment at the reference site

3.2.1 Concentration comparison and seasonal trends

The temporal variation of chemical species and source contributions under substantially different ambient conditions was studied by investigating the samples continuously collected at the reference site for nearly one year. The annual average $PM_{0.36}$ OC concentration was 1.36 ± 0.99 (0.04-4.92) $\mu g m^{-3}$. The $PM_{0.36}$ mass was estimated at 4.57 ± 1.93 (1.02-12.16) $\mu g m^{-3}$. On average, the OC accounts for 31% of the estimated $PM_{0.36}$ mass and the OM 43%-61% when applying the OM/OC conversion factor of 1.4-2. These values are very close to $30.9 \pm 6.5\%$ of the annual average OC fraction in Los Angeles $PM_{0.25}$ samples [257] and 50%-60% of the OM in $PM_{0.25}$ from different sites in California [258]. The EC was measured at a relatively low concentration of 0.25 ± 0.28 (< 0.01 -1.9) $\mu g m^{-3}$ and accounts for 4% of the estimated $PM_{0.36}$ mass on average. Levoglucosan showed an annual average concentration of 75 ± 54 (8-293) $ng m^{-3}$ and levoglucosan-C to OC percentage of 4.4% on average. In winter, a higher mean concentration of $118 ng m^{-3}$ was observed which was similar to the levoglucosan-C OC percentage

of 4.2%. A levoglucosan concentration about 3 times higher than average was found in a previous study of PM_{2.5} in February-March at the same sampling site. Average hopane (29ab and 30ab) concentrations at the reference site were 0.17 ± 0.06 and 0.13 ± 0.05 ng m⁻³, respectively; these were much lower than the street site concentration [259] (and literature therein). This could be due to the low level of traffic influence at the reference site compared to the street site. The hopane concentrations were, however, only slightly lower than the two-year average hopane level in the PM_{2.5} sampled at B1 in 2003-2004 while the nine EPA priority PAHs quantified in this study were about 10% to 20% of the 2-year average concentration of the respective PM_{2.5} PAHs measured at site B1 [93]. This difference between hopane and PAHs might result from their different size distributions, with the hopane mainly in the quasi-UFP size range while the PAHs have higher proportions in coarse mode as indicated by the pilot campaign [260]. The spatial variation of the source contribution might also contribute to these different ratios of hopane and PAHs at the reference site compared to B1. 2-methylerythritol and 2-methylthreitol are highly correlated ($r = 0.96$) with a mean concentration of 0.88 ± 0.58 (< 0.01 -5.17) and 0.32 ± 0.24 (< 0.01 -1.30) ng m⁻³. The average concentration of 2.53 (0.10-21.1) ng m⁻³ for cis-pinonic acid was lower than in the Berlin PM₁ samples [261], but higher than the Mainz PM₃ samples (0.60 ± 1.01 ng m⁻³) [110]. 4-nitrophenol and 4-nitrocatechol levels were much lower than in the PM₃ (2.48 ± 2.12 and 6.40 ± 17.55 ng m⁻³, respectively) samples from Mainz, Germany.

In this study, March, June, September and December were defined as the starting months of spring, summer, autumn and winter, respectively. Seasonal variability was examined using the Kruskal Wallis Test. The PNC in different size ranges did not show significant differences ($p > 0.01$). PAHs, biomass burning (BB) markers and cis-pinonic acid demonstrated the lowest p -values among all seasons, indicating a strong seasonal variation, while OC fractions and hopanes showed higher, yet still significant, p -values, indicating less seasonal variation. The OC2 concentration hierarchy was as follows: winter < autumn < summer < spring. For OC3, it was winter and autumn < spring < summer. Compared to OC2 and OC3, OC4 showed a different result with the highest levels in winter and lower, but comparable levels, in other seasons, indicating a different source and composition of OC4. Molecular markers showed characteristic seasonal variations. Specifically, HMW PAHs, levoglucosan and vanillic acid exhibited their highest concentrations in winter, followed by autumn and then spring, with extremely low levels in summer. On the contrary, cis-pinonic acid concentration levels appeared as follows winter < autumn < spring < summer. 2-MTs also showed maximum levels in summer (July and August), but were not detectable in the colder periods between late October and late April. 4-nitrophenol and 4-nitrocatechol reached maximum concentration in winter. 4-nitrophenol showed much lower levels during the rest of the year, while 4-nitrocatechol was not detected at all in the warmer months.

3.2.2 Correlation matrix between different types of parameters

A Pearson correlation analysis identified many significant ($p < 0.01$) correlations between different parameters, as will be discussed further. Minor to moderate correlations (r : 0.21-0.40) were found between PAHs, levoglucosan, 4-nitrophenol and 4-nitrocatechol and OC4, but not with OC2 or OC3. Cis-pinonic acid, 3-MBTCA, 3-hydroxyglutaric acid, malic acid and adipic acid were well correlated with OC2 (r : 0.54-0.70) and OC3 (r : 0.45-0.60), but not with OC4. The correlation between OC2 and OC3 was strong ($r=0.83$), but neither had any correlation with OC4. The HMW PAHs displayed a moderate correlation with 100-360 nm PNC, but no correlation with the PNC in any other size ranges. Moderate and minor correlations were found between levoglucosan and the PNC in the size ranges of 100-360 nm

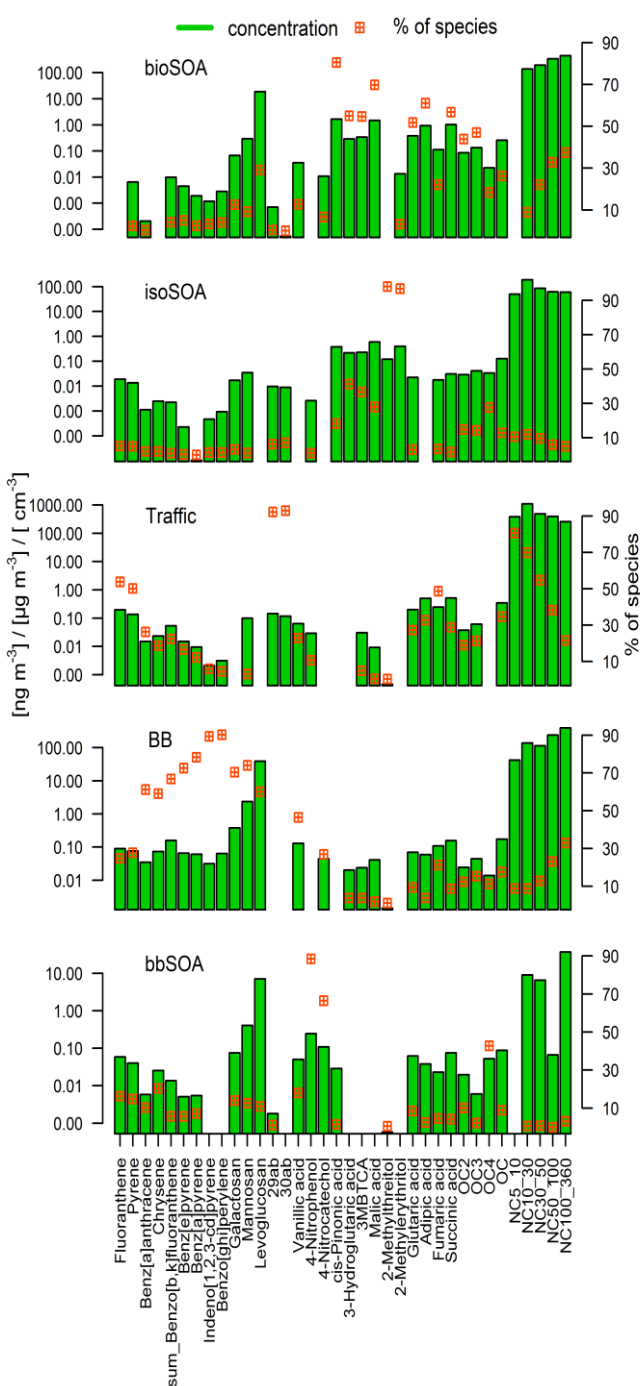


Fig. 21 Source factor profiles identified by PMF_{ref}. (species in ng m^{-3} , OC fractions in $\mu\text{g m}^{-3}$ and particle numbers in cm^{-3})

and 50-100 nm, respectively. Cis-pinonic acid only showed minor correlations to particles in 30-50 and 50-100 nm size ranges. Hopanes and 2-MTs were not correlated with PNC in any size range at all. Temperature was one of the most important meteorological parameters associated with the organic components measured. It was positively correlated to OC2 ($r=0.50$), OC3 ($r=0.55$) and the molecular species cis-pinonic acid, 3-MBTCA, 3-hydroglutaric acid, malic acid, 2-MTs, adipic acid ($r: 0.55-0.86$), but negatively correlated to levoglucosan, 4-nitrophenol and PAHs such as sum_benzo[b,k]fluoranthenes ($r = -0.52, -0.57$ and -0.73 , respectively). O_3 concentration and global radiation (GR) show similar a correlation in terms of temperature with the parameters mentioned above. The impact of the maximum value of the mixing layer height (MLH_{max}), monitored every 10 min, was investigated. Days with 43 (over 30%) missing values were excluded from the analysis. A moderate negative correlation was found between MLH_{max} and PNC in nearly all size ranges except particles <10 nm ($r: -0.31$ to -0.40), HMW PAHs and levoglucosan. While a moderate positive correlation was found between MLH_{max} and cis-pinonic acid, adipic acid, etc., a positive correlation of NO_2 to PAHs, levoglucosan, 4-nitrophenol, OC4, EC and PNC was observed.

3.2.3 PMF analysis results from the PMF_{ref}

Factors found from the PMF analysis were classified based on factor profiles (Fig. 21) and the seasonal variability of contributions to the OC (Fig. 22). The 5-factor solution was found to be most reasonable.

Factor 1 is characterised by high percentages of total cis-pinonic acid, 3-MBTCA, 3-hydroxyglutaric acid, malic acid, OC2 and OC3, and is defined as biogenic secondary organic aerosol (bioSOA). It is associated with the DCA of glutaric acid, adipic acid and succinic acid and particles in the size range 50-360 nm. Its OC contribution demonstrates seasonality similar to cis-pinonic acid, i.e. summer > spring > autumn > winter.

Factor 2 is characterised by 2-MTs and hence, interpreted as isoprene-originated SOA (isoSOA). Like 2-MTs, isoSOA was found almost solely in the summer. Factor 3 is marked by hopanes and defined as the traffic factor. It is associated with elevated concentrations of fluoranthene and pyrene. As shown in Fig. 22, this factor showed the least seasonal variability in OC contribution among all 5 source factors. Factor 4 is characterised by BB markers such as anhydrosugars and vanillic acid. It is, therefore, interpreted as the BB factor. HMW PAHs are also mainly associated with this factor. Its seasonal contribution to OC is in the opposite order of bioSOA and is as follows winter > autumn > spring > summer. This is consistent with the BB period in Augsburg when domestic heating is necessary. Factor 5 is described by high shares of 4-nitrophenol and 4-nitrocatechol and is interpreted as BB-associated SOA (bbSOA). As there are both primary and secondary origins for these two compounds, it was carefully evaluated in this study. Although both compounds showed a moderate correlation to levoglucosan and other wood combustion markers, they followed a different time pattern which was more in accordance with NO_x levels and temperatures, both related to the SOA yield. As with the characteristic markers, the strongest positive correlation was found between bioSOA or isoSOA and temperature, GR and O₃ concentration. This can be explained by the elevated photochemical reaction rate and biogenic vegetation emission rate under high levels of these parameters. On the contrary, BB and bbSOA were negatively correlated with these three parameters, but positively correlated with NO₂ concentration. MLH_{max} was negatively correlated with BB and positively correlated with bioSOA.

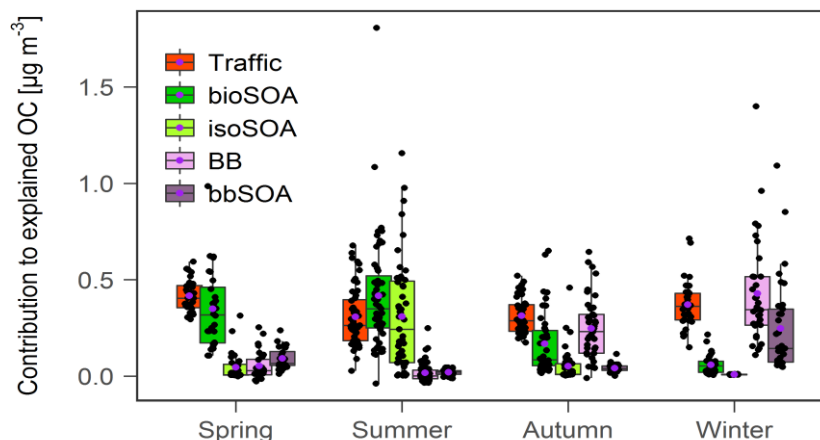


Fig. 22 Seasonal variation of source factors contributing to explained OC concentrations.

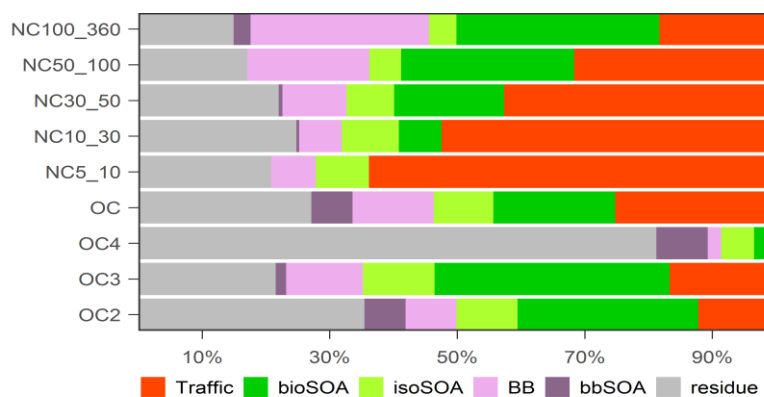


Fig. 23 Percentage contributions of source factors to size-segregated particle number concentrations and OC fractions, and residue which could not be attributed to source factors.

In Fig. 23, the OC and PNC in different size fractions below 360 nm are distributed along the modelled 5 source factors plus the residue. 75-80% of the PNC were explained by these 5 source factors with source-specific patterns. Particularly, the PNC explained by traffic increased from 22% to 81% as the particle size decreases from 100-360 nm to 5-10 nm, which makes traffic the major source of PNC. However, the larger accumulation mode particles stemmed from bioSOA (37% and 33% of particles in 100-360 and 50-100 nm, respectively) and BB (33% of particles in 100-360 nm). IsoSOA was associated with 5-12% particles in different PM size fractions, while negligible particles were explained by bbSOA. On annual average, 66%, 78%, 19% and 73% of OC₂, OC₃, OC₄ and OC are modelled by source factors, respectively. Overall contribution to the OC decreased in the following order: traffic, bioSOA, BB, isoSOA and bbSOA; however, 47% of OC₃ and 44% of OC₂ could be attributed to bioSOA. Therefore, the SOA of biogenic origin (here bioSOA and isoSOA) make the dominating contributions to the PM_{0.36} SVOC, particularly in summer. Semi-volatile OC₂ and OC₃ are modelled much better than the low volatile OC₄ probably because all the species identified by the GC method applied in this study belong to the SVOC. An occurrence of high OC characterized with high OC₂ and OC₃ levels in summer was modelled especially well by the PMF and can mainly be attributed to bioSOA and isoSOA. However, an episode of high OC levels in winter was characterised by high OC₄, and PM_{0.36} and PM_{2.5} concentration was not modelled well by the PMF, leaving high OC₄ residue, which may be due to HMW compounds from the primary BB emission, as well as secondary formations of low volatile OA (e.g. LVOC and/or ELVOC).

3.3 Publication III: Spatio-temporal variability of source contributions

3.3.1 Comparison of results from PMF_{ref} and PMF_{mas}

Source contributions from all sites are modelled by the PMF_{mas} to investigate the spatio-temporal variability. Despite the differences in analysis setup between PMF_{mas} and PMF_{ref} as described in the methodology section, the PMF_{mas} generated an identical number of source factors and very similar individual factor profiles when compared to the PMF_{ref}. 1.04 ug m⁻³ (75%) and 0.99 ug m⁻³ (73%) of the OC was explained by the PMF_{mas} and the PMF_{ref}, respectively. The PMF_{mas} provided source origin information for the OC concentrations in the form of bioSOA, isoSOA, Traffic, BB and bbSOA with the levels 0.35, 0.09, 0.33, 0.2 and 0.08 ug m⁻³, respectively. Regarding the factor profiles, the differences of percentage of each species assigned to an individual source factor between two analyses are in general below 10%, indicating a high uniformity of source composition at the studied area. This warrants the combination of multiple sites into one PMF analysis.

3.3.2 Temporal correlation of source contributions between reference and master sites

In time-series-based health effect studies, the temporal variation at different time scales is often captured by monitoring concentrations at a single site. This approach is reasonable if the Pearson r -value between sites is high, even though the absolute concentrations or source contributions are not the same within the studied area. The temporal variation of source contributions at the master and reference sites for each source factor is shown in Fig. 24, and the calculated Pearson r -values between the pairs of reference-master sites are displayed in Fig. 26. T4 is located in a small town and is the master site furthest from the reference site at a 35 km distance (Table 2 and Fig. 18). Only a limited number of observations were successful at this site. These two reasons may be responsible for the low overall correlation calculated between this site and the reference site, in contrast to other master sites. Except for T4, a Pearson r range from 0.62 to 0.99 ($p < 0.001$) was found between other master sites and the reference site. The BB and bioSOA factors show a Pearson $r > 0.85$ between paired sites. For the autumn and winter periods during which BB made a substantial contribution, the Pearson r for BB is 0.81 ($p < 0.001$, $n=54$). The synchronization of domestic heating activity may be the main reason leading to this high correlation of BB source contributions. The parallel variation of bioSOA could result from similar temporal variation of influential meteorological parameters (temperature, O₃ level and GR) within the study region. The long atmospheric lifetime (up to several days) of the bioSOA identification marker cis-pinonic acid resulted in a long-distance transport capability (discussed below), pointing to more regional impact from this source. The highest r of 0.97 for isoSOA is at T1, less than 100 meters away from the reference site. The Pearson r for isoSOA is 0.93, 0.80 and 0.70 at T2, T3 and B1, respectively. The relatively low temporal correlation of isoSOA at B1 might be due to differences in local precursor sources and influences of

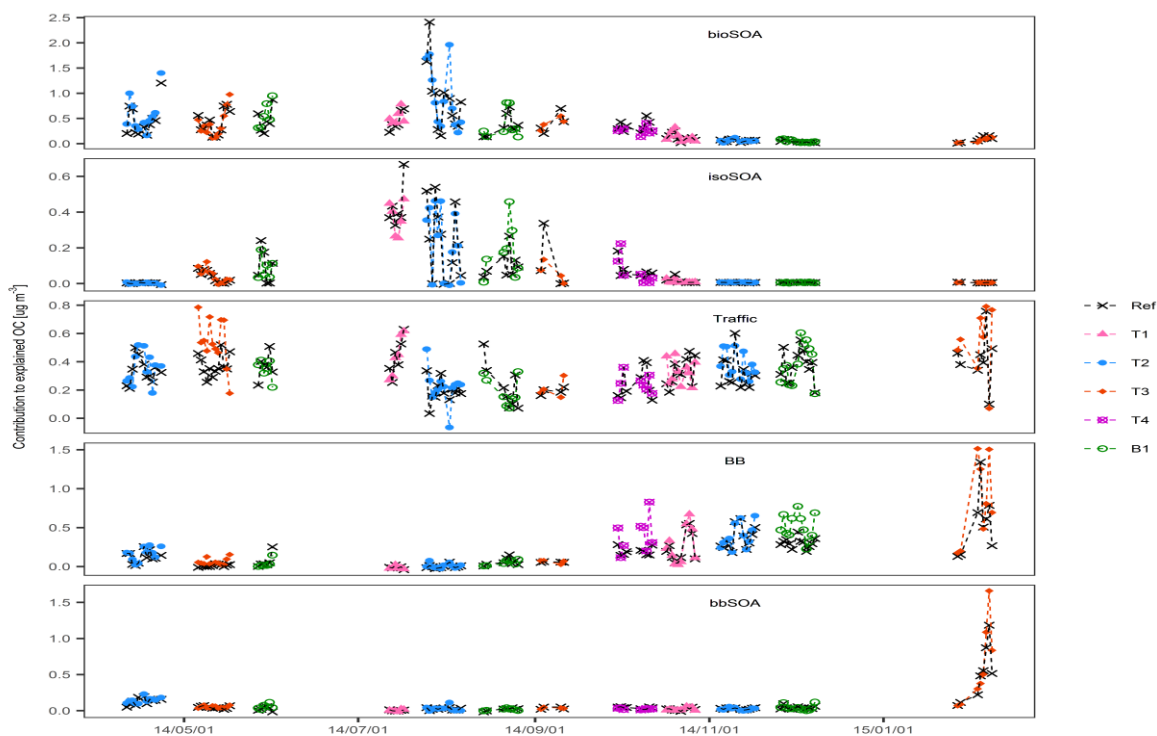


Fig. 24 Comparison of source contributions to OC at the reference site and corresponding parallel sampled master site.

anthropogenic emissions, as will be discussed below. The contribution of bbSOA was low in the warmest period and only increased during the coldest sampling period at T3 (Fig. 26). The calculated r for bbSOA at this high contribution period at T3 is 0.98. Pearson r for the traffic source factor ranges between 0.69 and 0.77 ($p < 0.001$), generally lower than the correlation values of the other source factors. This result is similar to a previous study of PM₁₀ sources in Augsburg [262, 263]. As result from the above- discussed temporal correlations, in time-series studies investigating health effects of quasi-UFP, more caution should be taken when representing a study region with a single monitoring site for source contributions of isoSOA and especially traffic, though it is less risky to apply such an approach to the source contributions of BB, bioSOA and bbSOA.

3.3.3 Spatial variability of sources contributions

A high r -value does not necessarily mean homogeneity of concentrations between two sites. For epidemiological studies on long-term health effects, the absolute exposure level should be accurately evaluated. The coefficient of divergence (COD) was applied to investigate the uniformity of pollutant concentrations and absolute source contributions [262, 264]. This calculation formula is displayed in equation 4, in which the x_{ij} and x_{ik} represent the observation (concentration of species or source contribution in this case) for variable x in the i^{th} of total n samples at the paired sampling sites j and k . COD value ranges from 0 to 1. Heterogeneity increases as the COD value increases, with a COD < 0.2 usually considered to be an indicator of a high level of spatial uniformity.

$$COD_{jk} = \sqrt{\frac{1}{n} \sum_{i=1}^n \left(\frac{x_{ij} - x_{ik}}{x_{ij} + x_{ik}} \right)^2} \quad (4)$$

For the short period measured at T4, the contributions of bbSOA and bioSOA were negligible. bioSOA and traffic show low COD values of 0.17 and 0.20, respectively. BB has a high COD of 0.36 with a higher mean contribution found at T4 compared to the reference site. This may be due to the local domestic heating at T4, which could start early or be more intense in the rural area. With T4 already covered, the following discussion will focus on the other master sites.

bioSOA displayed a high spatial uniformity with low calculated CODs (< 0.2), except for one slightly higher value of 0.23 at site B1. The bioSOA identification marker cis-pinonic acid in the gas phase has an estimated lifetime of two to over three days, and after partition into the particle phase, it can survive for several days before removal through dry or wet deposition [265]. As indicated by Green_5000 in Table 2, the total percentage of urban green, forest and semi-nature area within a radius of 5 km around the sampling site, the vegetation within this radius around the master sites and the reference site are similar. It is expected to be even more comparable within a larger radius; to our knowledge, none of the master sites was influenced by the close proximity to coniferous trees. Therefore, a little local influence on the level of cis-pinonic acid precursor of pinene at these receptor sites is expected. Moreover, the meteorological parameters of temperature, OH· radical concentration and GR-influencing precursor emission and oxidation rate are expected to vary little on a regional scale. Thus, the relative uniformity of bioSOA contribution found in this study can be explained by the dominating of medium- and long-range transported bioSOA in the city of Augsburg. The COD value of isoSOA was much higher at B1 (0.4) than at other master sites (< 0.2), and during the summer period, the absolute isoSOA contribution was 64% higher at B1 than at the reference site. Site B1 is in a monastery garden full of grass and fruit trees. The

total green area within a 50m radius (Green₅₀ in Table 2) is 40% at B1 while it is 0% at the other sites. This could lead to local isoprene emission and SOA formation at B1, but not other sites. Model estimates of NO_x levels are also lower at B1 (27 $\mu\text{g m}^{-3}$) than at the reference site (36 $\mu\text{g m}^{-3}$), probably resulting from different levels of traffic influence. As described earlier, low NO_x favours the formation of 2-MTs while high NO_x favours the formation of 2-methylglyceric acid [130, 266, 267]. Hence, local vegetation coverage ratio and traffic load may contribute to the heterogeneity of isoSOA contributions within urban areas of even a short distance. Traffic showed generally low COD values (< 0.20) with a slightly higher level at T3 (0.21) and B1 (0.20). No significant traffic influence was observed at T1 and T2 although they are both defined as traffic-influenced sites in epidemiology studies. These could be attributed to the positioning of the sampler upwind at these two sites.

T3 shows continuously elevated traffic contributions during the first sampling period in May, as shown in Fig. 24; the dominating wind direction at this time came from the road in the southwest (Fig. 25). At B1, a slightly lower traffic impact was observed just in the month of August. This study also indicates that the spatial variability of traffic contribution to OC is less obvious than the spatial variability of the PNC from traffic emissions. One major reason for this could be the size distribution characteristics of both metrics with the organic markers peaking in relatively larger particles, while the PNC peaks in the smallest particles. BB shows high CODs at sites T3 (0.33) and B1 (0.31) and low CODs below 0.2 at sites T1 and T2. This is consistent with the number

of buildings present (only 1 at T1 and T2 compared to 7 at T3 and 12 at B1) within a 50m radius at these sites as shown in Table 2. This result demonstrates that heterogeneous distribution of living houses is expected to result in spatial heterogeneity of BB source contributions during BB active seasons. bbSOA showed a low COD value of 0.16 between the reference site and T3, and both were observed making significant contributions in the winter period. Unlike BB, bbSOA was less affected by local sources and tends to be spatially homogeneous. As above, a relatively high risk of exposure misclassification exists for isoSOA and BB when using one monitoring site to extrapolate data for a larger study area, while for bioSOA and bbSOA, the risk is lower, and for traffic, the dominating wind direction seems to be an important influential parameter.

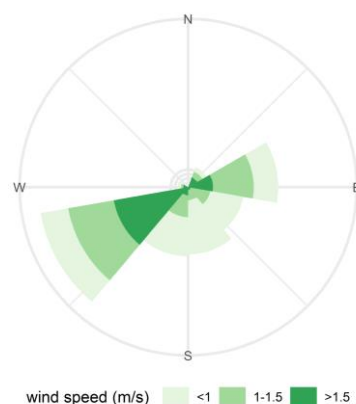


Fig. 25 Windrose at site T3 during 1st sampling period showing wind coming mainly from southwest.

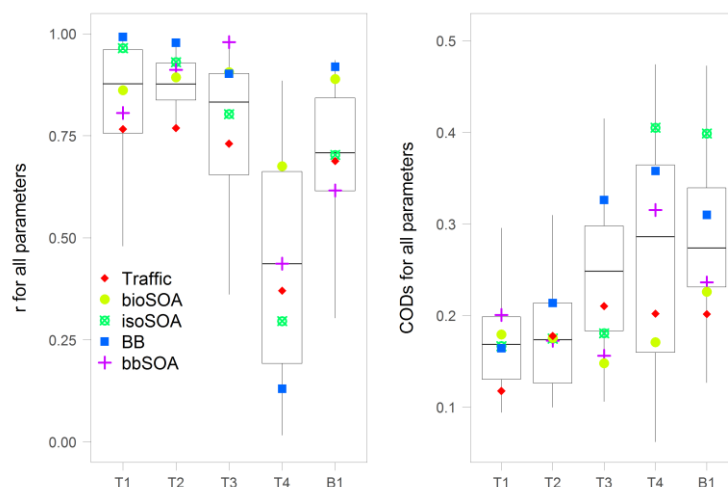


Fig. 26 Calculated Pearson r values (left) and coefficient of divergence (COD, right) for each source factor between the reference site and each master site. Boxplots are generated from the values for all parameters of compound concentration and source contribution, while coloured shaped coded markers represent values for different source factors.

Summary of results

To investigate the seasonal variation and spatio-temporal variability of sources contributing to the OC of quasi-UFP ($PM_{0.36}$), this study conducted a long-term sampling of size-segregated PM in the Augsburg area. Continuous, unattended sampling of 24-h daily samples for up to one week was achieved by connecting RDIs with sequential filter samplers. Two sampling sets enabled parallel sampling simultaneously at two sites and thus, the study of spatio-temporal variability.

The PMF modelling results resolved 5 source factors which explain 75% of the OC concentration from the reference site and 73% from the reference site and all master sites on annual average, including bioSOA, isoSOA, Traffic, BB and bbSOA. The explained OC was mainly attributed to biogenic originated SOA and traffic, and to a lesser extent BB and bbSOA. Particularly, semi-volatile OC2 and OC3 peaks in summer were well modelled by biogenic SOA, which is consistent with the semi-volatile characteristics of both the lower generation SOA markers and the organic markers that can be measured by the IDTD-GC-MS method applied. On the contrary, OC4, especially high OC4 levels in winter, was poorly modelled. The distributions of size-segregated PNC below 360 nm showed source-specific characteristics. As expected, particle number was mainly attributed to traffic because the smallest particles as the dominating contributor to particle number were associated with traffic emissions. About one third of the particles between 100-360 nm and between 50-360 nm were associated with BB and bioSOA, respectively. Seasonal variation of the source contributions of summer maximums for bioSOA and isoSOA is in accordance with the precursor emission and reaction rate mainly driven by high temperature; and the winter maximums for BB and bbSOA were in alignment with domestic heating activity and high NO_x levels with regard to bbSOA.

bioSOA and bbSOA showed high temporal correlation and uniform distribution in the Augsburg region, likely resulting from regional formation and transport. isoSOA showed a weak temporal correlation and less spatial homogeneity at the city background site which contained less traffic impact, but more local vegetation influence. For BB source contributions, a temporal correlation was found to be very strong, but elevated absolute contributions were observed in winter at the two sites with more living buildings in the surroundings. Among the sources, traffic generally showed the weakest correlation over time. The spatial heterogeneity of absolute traffic contribution was also generally low. Among the three sites defined as street-influenced sites, a short period of elevated traffic contribution was observed at only one of the master sites because the road nearby is situated upwind from the sampling site, but this is not the case for the rest of the period. These results indicate that heterogeneous source contributions of quasi-UFP can occur in an urban city with limited space, such as Augsburg.

To summarize the influential parameters to be considered in this health effect study, the amount of primary emissions reaching a specific receptor site depends mostly on the distribution of the respective source and meteorological conditions. The influential factor of SOA variation seems to be more complex. It can involve precursor emissions, reaction pathway/rate, gas-particle partition, product lifetime in the gas and particle phase, etc., with the aforementioned factors having their own influential parameters, such as meteorological conditions, gas molecular concentration, anthropogenic emission, etc. In conclusion, health effect studies focusing on time variation or absolute contribution need to evaluate the temporal correlation or spatial variability of source contributions separately as they are not necessarily consistent.

References

1. Zhang, R.Y., et al., *Formation of Urban Fine Particulate Matter*. Chemical Reviews, 2015. **115**(10): p. 3803-3855.
2. Rozaini, M.Z.H. and H. Abdul-Razzak, *The Chemistry of Dicarboxylic Acids in the Atmospheric Aerosols*, in *Atmospheric Aerosols - Regional Characteristics - Chemistry and Physics*. 2012, InTech: Rijeka. p. Ch. 11.
3. Vu, T.V., J.M. Delgado-Saborit, and R.M. Harrison, *Review: Particle number size distributions from seven major sources and implications for source apportionment studies*. Atmospheric Environment, 2015. **122**: p. 114-132.
4. Brook, R.D., et al., *Particulate Matter Air Pollution and Cardiovascular Disease An Update to the Scientific Statement From the American Heart Association*. Circulation, 2010. **121**(21): p. 2331-2378.
5. Fuzzi, S., et al., *Particulate matter, air quality and climate: lessons learned and future needs*. Atmospheric Chemistry and Physics, 2015. **15**(14): p. 8217-8299.
6. Poschl, U., *Atmospheric aerosols: Composition, transformation, climate and health effects*. Angewandte Chemie-International Edition, 2005. **44**(46): p. 7520-7540.
7. Chen, W.N. and D.W. Fryrear, *Aerodynamic and geometric diameters of airborne particles*. Journal of Sedimentary Research, 2001. **71**(3): p. 365-371.
8. Verma, V., et al., *Physicochemical and oxidative characteristics of semi-volatile components of quasi-ultrafine particles in an urban atmosphere*. Atmospheric Environment, 2011. **45**(4): p. 1025-1033.
9. Amatullah, H., et al., *Comparative cardiopulmonary effects of size-fractionated airborne particulate matter*. Inhalation Toxicology, 2012. **24**(3): p. 161-171.
10. Longhin, E., et al., *Season linked responses to fine and quasi-ultrafine Milan PM in cultured cells*. Toxicology in Vitro, 2013. **27**(2): p. 551-559.
11. Arhami, M., et al., *Organic compound characterization and source apportionment of indoor and outdoor quasi-ultrafine particulate matter in retirement homes of the Los Angeles Basin*. Indoor Air, 2010. **20**(1): p. 17-30.
12. Argyropoulos, G., et al., *Source apportionment of the redox activity of urban quasi-ultrafine particles (PM_{0.49}) in Thessaloniki following the increased biomass burning due to the economic crisis in Greece*. Science of the Total Environment, 2016. **568**: p. 124-136.
13. Saffari, A., et al., *Impact of primary and secondary organic sources on the oxidative potential of quasi-ultrafine particles (PM_{0.25}) at three contrasting locations in the Los Angeles Basin*. Atmospheric Environment, 2015. **120**: p. 286-296.
14. Whitby, K.T., R.B. Husar, and B.Y.H. Liu, *The aerosol size distribution of Los Angeles smog*. Journal of Colloid and Interface Science, 1972. **39**(1): p. 177-204.
15. Harrison, R.M., et al., *Measurement of number, mass and size distribution of particles in the atmosphere*. Philosophical Transactions of the Royal Society of London Series a-Mathematical Physical and Engineering Sciences, 2000. **358**(1775): p. 2567-2579.
16. von Bismarck-Osten, C., et al., *Characterization of parameters influencing the spatio-temporal variability of urban particle number size distributions in four European cities*. Atmospheric Environment, 2013. **77**: p. 415-429.
17. Morawska, L., et al., *Ambient nano and ultrafine particles from motor vehicle emissions: Characteristics, ambient processing and implications on human exposure*. Atmospheric Environment, 2008. **42**(35): p. 8113-8138.
18. Stone, V., et al., *Nanomaterials Versus Ambient Ultrafine Particles: An Opportunity to Exchange Toxicology Knowledge*. Environmental Health Perspectives, 2017. **125**(10).
19. Pey, J., et al., *Source apportionment of urban fine and ultra-fine particle number concentration in a Western Mediterranean city*. Atmospheric Environment, 2009. **43**(29): p. 4407-4415.

20. Gu, J.W., et al., *Source apportionment of ambient particles: Comparison of positive matrix factorization analysis applied to particle size distribution and chemical composition data*. Atmospheric Environment, 2011. **45**(10): p. 1849-1857.
21. Wang, Z.B., et al., *Long-term measurements of particle number size distributions and the relationships with air mass history and source apportionment in the summer of Beijing*. Atmospheric Chemistry and Physics, 2013. **13**(20): p. 10159-10170.
22. Reid, J.S., et al., *A review of biomass burning emissions part II: intensive physical properties of biomass burning particles*. Atmospheric Chemistry and Physics, 2005. **5**: p. 799-825.
23. Janhall, S., M.O. Andreae, and U. Poschl, *Biomass burning aerosol emissions from vegetation fires: particle number and mass emission factors and size distributions*. Atmospheric Chemistry and Physics, 2010. **10**(3): p. 1427-1439.
24. Kirkby, J., et al., *Role of sulphuric acid, ammonia and galactic cosmic rays in atmospheric aerosol nucleation*. Nature, 2011. **476**(7361): p. 429-U77.
25. Hirsikko, A., et al., *Atmospheric ions and nucleation: a review of observations*. Atmospheric Chemistry and Physics, 2011. **11**(2): p. 767-798.
26. Kulmala, M., et al., *Chemistry of Atmospheric Nucleation: On the Recent Advances on Precursor Characterization and Atmospheric Cluster Composition in Connection with Atmospheric New Particle Formation*. Annual Review of Physical Chemistry, Vol 65, 2014. **65**: p. 21-37.
27. Jeong, C.H., et al., *Characteristics of nucleation and growth events of ultrafine particles measured in Rochester, NY*. Environmental Science & Technology, 2004. **38**(7): p. 1933-1940.
28. Nguyen, Q.T., et al., *Seasonal variation of atmospheric particle number concentrations, new particle formation and atmospheric oxidation capacity at the high Arctic site Villum Research Station, Station Nord*. Atmospheric Chemistry and Physics, 2016. **16**(17): p. 11319-11336.
29. Sullivan, R.C. and S.C. Pryor, *Dynamic and chemical controls on new particle formation occurrence and characteristics from in situ and satellite-based measurements*. Atmospheric Environment, 2016. **127**: p. 316-325.
30. Kulmala, M., et al., *Formation and growth rates of ultrafine atmospheric particles: a review of observations*. Journal of Aerosol Science, 2004. **35**(2): p. 143-176.
31. Zhang, X.R., et al., *Observation of aerosol number size distribution and new particle formation at a mountainous site in Southeast China*. Science of the Total Environment, 2017. **575**: p. 309-320.
32. Shen, L.J., et al., *Observation of aerosol size distribution and new particle formation at a coastal city in the Yangtze River Delta, China*. Science of the Total Environment, 2016. **565**: p. 1175-1184.
33. Mordas, G., et al., *Observation of new particle formation on Curonian Spit located between continental Europe and Scandinavia*. Journal of Aerosol Science, 2016. **97**: p. 38-55.
34. Wang, D.F., et al., *Intense secondary aerosol formation due to strong atmospheric photochemical reactions in summer: observations at a rural site in eastern Yangtze River Delta of China*. Science of the Total Environment, 2016. **571**: p. 1454-1466.
35. Jayaratne, R., et al., *Observations of particles at their formation sizes in Beijing, China*. Atmospheric Chemistry and Physics, 2017. **17**(14): p. 8825-8835.
36. Holmes, N.S., *A review of particle formation events and growth in the atmosphere in the various environments and discussion of mechanistic implications*. Atmospheric Environment, 2007. **41**(10): p. 2183-2201.
37. Kontkanen, J., et al., *Measurements of sub-3nm particles using a particle size magnifier in different environments: from clean mountain top to polluted megacities*. Atmospheric Chemistry and Physics, 2017. **17**(3): p. 2163-2187.
38. Reche, C., et al., *New considerations for PM, Black Carbon and particle number concentration for air quality monitoring across different European cities*. Atmospheric Chemistry and Physics, 2011. **11**(13): p. 6207-6227.

39. Dall'Osto, M., et al., *Remarkable dynamics of nanoparticles in the urban atmosphere*. Atmospheric Chemistry and Physics, 2011. **11**(13): p. 6623-6637.
40. Riipinen, I., et al., *The contribution of organics to atmospheric nanoparticle growth*. Nature Geoscience, 2012. **5**(7): p. 453-458.
41. Zhang, R.Y., et al., *Nucleation and Growth of Nanoparticles in the Atmosphere*. Chemical Reviews, 2012. **112**(3): p. 1957-2011.
42. Yli-Juuti, T., et al., *Analysis of sub-3 nm particle growth in connection with sulfuric acid in a boreal forest*. Boreal Environment Research, 2016. **21**(3-4): p. 287-298.
43. Burkart, J., et al., *Organic Condensation and Particle Growth to CCN Sizes in the Summertime Marine Arctic Is Driven by Materials More Semivolatile Than at Continental Sites*. Geophysical Research Letters, 2017. **44**(20): p. 10725-10734.
44. Berland, K., et al., *Spatial extent of new particle formation events over the Mediterranean Basin from multiple ground-based and airborne measurements*. Atmospheric Chemistry and Physics, 2017. **17**(15): p. 9567-9583.
45. Hama, S.M.L., et al., *Sub-micron particle number size distribution characteristics at two urban locations in Leicester*. Atmospheric Research, 2017. **194**: p. 1-16.
46. Putaud, J.P., et al., *A European aerosol phenomenology-3: Physical and chemical characteristics of particulate matter from 60 rural, urban, and kerbside sites across Europe*. Atmospheric Environment, 2010. **44**(10): p. 1308-1320.
47. Bzdek, B.R., M.R. Pennington, and M.V. Johnston, *Single particle chemical analysis of ambient ultrafine aerosol: A review*. Journal of Aerosol Science, 2012. **52**: p. 109-120.
48. Elmes, M. and M. Gasparon, *Sampling and single particle analysis for the chemical characterisation of fine atmospheric particulates: A review*. Journal of Environmental Management, 2017. **202**: p. 137-150.
49. Calvo, A.I., et al., *Research on aerosol sources and chemical composition: Past, current and emerging issues*. Atmospheric Research, 2013. **120**: p. 1-28.
50. Pöschl, U., *Aerosol particle analysis: Challenges and progress*. Analytical and bioanalytical chemistry. 2003. 30-2.
51. Cavalli, F., et al., *Toward a standardised thermal-optical protocol for measuring atmospheric organic and elemental carbon: the EUSAAR protocol*. Atmos. Meas. Tech., 2010. **3**(1): p. 79-89.
52. Chow, J.C., et al., *The dri thermal/optical reflectance carbon analysis system: description, evaluation and applications in U.S. Air quality studies*. Atmospheric Environment. Part A. General Topics, 1993. **27**(8): p. 1185-1201.
53. Chow, J.C., et al., *The IMPROVE_A Temperature Protocol for Thermal/Optical Carbon Analysis: Maintaining Consistency with a Long-Term Database*. Journal of the Air & Waste Management Association, 2007. **57**(9): p. 1014-1023.
54. Bond, T.C., et al., *Bounding the role of black carbon in the climate system: A scientific assessment*. Journal of Geophysical Research-Atmospheres, 2013. **118**(11): p. 5380-5552.
55. Novakov, T. and H. Rosen, *The Black Carbon Story: Early History and New Perspectives*. Ambio, 2013. **42**(7): p. 840-851.
56. Turpin, B.J. and H.-J. Lim, *Species Contributions to PM_{2.5} Mass Concentrations: Revisiting Common Assumptions for Estimating Organic Mass*. Aerosol Science and Technology, 2001. **35**(1): p. 602-610.
57. Aiken, A.C., et al., *O/C and OM/OC ratios of primary, secondary, and ambient organic aerosols with high-resolution time-of-flight aerosol mass spectrometry*. Environmental Science & Technology, 2008. **42**(12): p. 4478-4485.
58. Kanakidou, M., et al., *Organic aerosol and global climate modelling: a review*. Atmospheric Chemistry and Physics, 2005. **5**: p. 1053-1123.
59. Goldstein, A.H. and I.E. Galbally, *Known and unexplored organic constituents in the earth's atmosphere*. Environmental Science & Technology, 2007. **41**(5): p. 1514-1521.

60. Noziere, B., et al., *The molecular identification of organic compounds in the atmosphere: state of the art and challenges*. Chemical reviews, 2015. **115**(10): p. 3919-83.
61. Kroll, J.H. and J.H. Seinfeld, *Chemistry of secondary organic aerosol: Formation and evolution of low-volatility organics in the atmosphere*. Atmospheric Environment, 2008. **42**(16): p. 3593-3624.
62. Donahue, N.M., et al., *A two-dimensional volatility basis set - Part 2: Diagnostics of organic-aerosol evolution*. Atmospheric Chemistry and Physics, 2012. **12**(2): p. 615-634.
63. Zhang, Q., et al., *Deconvolution and quantification of hydrocarbon-like and oxygenated organic aerosols based on aerosol mass spectrometry*. Environmental Science & Technology, 2005. **39**(13): p. 4938-4952.
64. Zhang, Q., et al., *Ubiquity and dominance of oxygenated species in organic aerosols in anthropogenically-influenced Northern Hemisphere midlatitudes*. Geophysical Research Letters, 2007. **34**(13).
65. Lanz, V.A., et al., *Source apportionment of submicron organic aerosols at an urban site by factor analytical modelling of aerosol mass spectra*. Atmospheric Chemistry and Physics, 2007. **7**(6): p. 1503-1522.
66. Pereira, K.L., et al., *Insights into the Formation and Evolution of Individual Compounds in the Particulate Phase during Aromatic Photo-Oxidation*. Environmental Science & Technology, 2015. **49**(22): p. 13168-13178.
67. Fuzzi, S., et al., *Critical assessment of the current state of scientific knowledge, terminology, and research needs concerning the role of organic aerosols in the atmosphere, climate, and global change*. Atmospheric Chemistry and Physics, 2006. **6**: p. 2017-2038.
68. Robinson, A.L., et al., *Rethinking organic aerosols: Semivolatile emissions and photochemical aging*. Science, 2007. **315**(5816): p. 1259-1262.
69. Atkinson, R. and J. Arey, *Atmospheric degradation of volatile organic compounds*. Chemical Reviews, 2003. **103**(12): p. 4605-4638.
70. Chacon-Madrid, H.J. and N.M. Donahue, *Fragmentation vs. functionalization: chemical aging and organic aerosol formation*. Atmospheric Chemistry and Physics, 2011. **11**(20): p. 10553-10563.
71. Hallquist, M., et al., *The formation, properties and impact of secondary organic aerosol: current and emerging issues*. Atmospheric Chemistry and Physics, 2009. **9**(14): p. 5155-5236.
72. Crouse, J.D., et al., *Autoxidation of Organic Compounds in the Atmosphere*. The Journal of Physical Chemistry Letters, 2013. **4**(20): p. 3513-3520.
73. Berndt, T., et al., *Hydroxyl radical-induced formation of highly oxidized organic compounds*. Nature Communications, 2016. **7**: p. 13677.
74. Graber, E.R. and Y. Rudich, *Atmospheric HULIS: How humic-like are they? A comprehensive and critical review*. Atmospheric Chemistry and Physics, 2006. **6**: p. 729-753.
75. Zheng, G.J., et al., *Measurement of humic-like substances in aerosols: A review*. Environmental Pollution, 2013. **181**: p. 301-314.
76. Ervens, B., B.J. Turpin, and R.J. Weber, *Secondary organic aerosol formation in cloud droplets and aqueous particles (aqSOA): a review of laboratory, field and model studies*. Atmospheric Chemistry and Physics, 2011. **11**(21): p. 11069-11102.
77. Ravindra, K., R. Sokhi, and R. Van Grieken, *Atmospheric polycyclic aromatic hydrocarbons: Source attribution, emission factors and regulation*. Atmospheric Environment, 2008. **42**(13): p. 2895-2921.
78. Peltonen, K. and T. Kuljukka, *Air sampling and analysis of polycyclic aromatic hydrocarbons*. Journal of Chromatography A, 1995. **710**(1): p. 93-108.
79. Nielsen, T., et al., *City air pollution of polycyclic aromatic hydrocarbons and other mutagens: Occurrence, sources and health effects*. Science of the Total Environment, 1996. **189**: p. 41-49.
80. Rogge, W.F., et al., *Sources of fine organic aerosol. 9. Pine, oak and synthetic log combustion in residential fireplaces*. Environmental Science & Technology, 1998. **32**(1): p. 13-22.

81. Rogge, W.F., et al., *Sources of fine organic aerosol. 2. Noncatalyst and catalyst-equipped automobiles and heavy-duty diesel trucks*. Environmental Science & Technology, 1993. **27**(4): p. 636-651.
82. Simoneit, B.R.T., *Biomass burning - A review of organic tracers for smoke from incomplete combustion*. Applied Geochemistry, 2002. **17**(3): p. 129-162.
83. Marchand, N., et al., *Polycyclic aromatic hydrocarbons (PAHs) in the atmospheres of two French alpine valleys: sources and temporal patterns*. Atmospheric Chemistry and Physics, 2004. **4**: p. 1167-1181.
84. Populin, T., et al., *Relative hopane content confirming the mineral origin of hydrocarbons contaminating foods and human milk*. Food Additives & Contaminants, 2004. **21**(9): p. 893-904.
85. Wang, G., et al., *Size-distributions of n-alkanes, PAHs and hopanes and their sources in the urban, mountain and marine atmospheres over East Asia*. Atmospheric Chemistry and Physics, 2009. **9**(22): p. 8869-8882.
86. Oros, D.R. and B.R.T. Simoneit, *Identification and emission rates of molecular tracers in coal smoke particulate matter*. Fuel, 2000. **79**(5): p. 515-536.
87. Zielinska, B., et al., *Emission Rates and Comparative Chemical Composition from Selected In-Use Diesel and Gasoline-Fueled Vehicles*. Journal of the Air & Waste Management Association, 2004. **54**(9): p. 1138-1150.
88. Lin, L., M.L. Lee, and D.J. Eatough, *Review of Recent Advances in Detection of Organic Markers in Fine Particulate Matter and Their Use for Source Apportionment*. Journal of the Air & Waste Management Association, 2010. **60**(1): p. 3-25.
89. Simoneit, B.R.T., *Application of Molecular Marker Analysis to Vehicular Exhaust for Source Reconciliations*. International Journal of Environmental Analytical Chemistry, 1985. **22**(3-4): p. 203-232.
90. Mandalakis, M., et al., *Gas-particle concentrations and distribution of aliphatic hydrocarbons, PAHs, PCBs and PCDD/Fs in the atmosphere of Athens (Greece)*. Atmospheric Environment, 2002. **36**(25): p. 4023-4035.
91. Saarikoski, S.K., et al., *Impact of biomass combustion on urban fine particulate matter in Central and Northern Europe*. Water Air and Soil Pollution, 2008. **191**(1-4): p. 265-277.
92. Belis, C.A., et al., *Critical review and meta-analysis of ambient particulate matter source apportionment using receptor models in Europe*. Atmospheric Environment, 2013. **69**: p. 94-108.
93. Schnelle-Kreis, J., et al., *Semi volatile organic compounds in ambient PM(2.5). Seasonal trends and daily resolved source contributions*. Environmental Science & Technology, 2007. **41**(11): p. 3821-3828.
94. Simoneit, B.R.T. and V.O. Elias, *Detecting organic tracers from biomass burning in the atmosphere*. Marine Pollution Bulletin, 2001. **42**(10): p. 805-810.
95. Giannoni, M., et al., *The use of levoglucosan for tracing biomass burning in PM2.5 samples in Tuscany (Italy)*. Environmental Pollution, 2012. **167**: p. 7-15.
96. Iinuma, Y., M. Keywood, and H. Herrmann, *Characterization of primary and secondary organic aerosols in Melbourne airshed: The influence of biogenic emissions, wood smoke and bushfires*. Atmospheric Environment, 2016. **130**: p. 54-63.
97. Simoneit, B.R.T., et al., *Levoglucosan, a tracer for cellulose in biomass burning and atmospheric particles*. Atmospheric Environment, 1999. **33**(2): p. 173-182.
98. May, A.A., et al., *Volatility of Organic Molecular Markers Used for Source Apportionment Analysis: Measurements and Implications for Atmospheric Lifetime*. Environmental Science & Technology, 2012. **46**(22): p. 12435-12444.
99. Xie, M., M.P. Hannigan, and K.C. Barsanti, *Gas/Particle Partitioning of 2-Methyltetrols and Levoglucosan at an Urban Site in Denver*. Environmental Science & Technology, 2014. **48**(5): p. 2835-2842.
100. Hennigan, C.J., et al., *Levoglucosan stability in biomass burning particles exposed to hydroxyl radicals*. Geophysical Research Letters, 2010. **37**.

101. Hoffmann, D., et al., *Atmospheric Stability of Levoglucosan: A Detailed Laboratory and Modeling Study*. Environmental Science & Technology, 2010. **44**(2): p. 694-699.
102. Legrand, M., et al., *Origin of C-2-C-5 dicarboxylic acids in the European atmosphere inferred from year-round aerosol study conducted at a west-10.1029/2006jd008019 east transect*. Journal of Geophysical Research-Atmospheres, 2007. **112**(D23).
103. Yao, X.H., et al., *Characterization of dicarboxylic acids in PM_{2.5} in Hong Kong*. Atmospheric Environment, 2004. **38**(7): p. 963-970.
104. Pavuluri, C.M., K. Kawamura, and T. Swaminathan, *Water-soluble organic carbon, dicarboxylic acids, ketoacids, and α -dicarbonyls in the tropical Indian aerosols C8 - D11302*. Journal of Geophysical Research: Atmospheres, 2010. **115**(D11): p. n/a-n/a.
105. Mochida, M., et al., *Spatial distributions of oxygenated organic compounds (dicarboxylic acids, fatty acids, and levoglucosan) in marine aerosols over the western Pacific and off the coast of East Asia: Continental outflow of organic aerosols during the ACE-Asia campaign*. Journal of Geophysical Research-Atmospheres, 2003. **108**(D23).
106. Kawamura, K. and S. Bikkina, *A review of dicarboxylic acids and related compounds in atmospheric aerosols: Molecular distributions, sources and transformation*. Atmospheric Research, 2016. **170**: p. 140-160.
107. Yao, X., et al., *Size distributions and formation of ionic species in atmospheric particulate pollutants in Beijing, China: I—inorganic ions*. Atmospheric Environment, 2003. **37**(21): p. 2991-3000.
108. Agarwal, S., et al., *Size distributions of dicarboxylic acids, ketoacids, alpha-dicarbonyls, sugars, WSOC, OC, EC and inorganic ions in atmospheric particles over Northern Japan: implication for long-range transport of Siberian biomass burning and East Asian polluted aerosols*. Atmospheric Chemistry and Physics, 2010. **10**(13): p. 5839-5858.
109. Deshmukh, D.K., et al., *Dicarboxylic acids, oxoacids, benzoic acid, alpha-dicarbonyls, WSOC, OC, and ions in spring aerosols from Okinawa Island in the western North Pacific Rim: size distributions and formation processes*. Atmospheric Chemistry and Physics, 2016. **16**(8): p. 5263-5282.
110. Zhang, Y.Y., et al., *Seasonal cycle and temperature dependence of pinene oxidation products, dicarboxylic acids and nitrophenols in fine and coarse air particulate matter*. Atmospheric Chemistry and Physics, 2010. **10**(16): p. 7859-7873.
111. Kawamura, K. and I.R. Kaplan, *Motor exhaust emissions as a primary source for dicarboxylic acids in Los Angeles ambient air*. Environmental Science & Technology, 1987. **21**(1): p. 105-110.
112. Rogge, W.F., et al., *Sources of fine organic aerosol. 1. Charbroilers and meat cooking operations*. Environmental Science & Technology, 1991. **25**(6): p. 1112-1125.
113. Kitanovski, Z., et al., *Liquid chromatography tandem mass spectrometry method for characterization of monoaromatic nitro-compounds in atmospheric particulate matter*. Journal of Chromatography A, 2012. **1268**: p. 35-43.
114. Chow, K.S., X.H.H. Huang, and J.Z. Yu, *Quantification of nitroaromatic compounds in atmospheric fine particulate matter in Hong Kong over 3 years: field measurement evidence for secondary formation derived from biomass burning emissions*. Environmental Chemistry, 2016. **13**(4): p. 665-673.
115. Kahnt, A., et al., *One-year study of nitro-organic compounds and their relation to wood burning in PM₁₀ aerosol from a rural site in Belgium*. Atmospheric Environment, 2013. **81**: p. 561-568.
116. Claeys, M., et al., *Chemical characterisation of humic-like substances from urban, rural and tropical biomass burning environments using liquid chromatography with UV/vis photodiode array detection and electrospray ionisation mass spectrometry*. Environmental Chemistry, 2012. **9**(3): p. 273-284.
117. Harrison, M.A.J., et al., *Nitrated phenols in the atmosphere: a review*. Atmospheric Environment, 2005. **39**(2): p. 231-248.

118. Al-Naiema, I.M. and E.A. Stone, *Evaluation of anthropogenic secondary organic aerosol tracers from aromatic hydrocarbons*. Atmospheric Chemistry and Physics, 2017. **17**(3): p. 2053-2065.
119. Li, X., et al., *Size distribution of particle-phase sugar and nitrophenol tracers during severe urban haze episodes in Shanghai*. Atmospheric Environment, 2016. **145**: p. 115-127.
120. Tremp, J., et al., *Phenol and nitrophenols as tropospheric pollutants: Emissions from automobile exhausts and phase transfer in the atmosphere*. Water Air and Soil Pollution. 1993. 113-123.
121. Sato, K., et al., *AMS and LC/MS analyses of SOA from the photooxidation of benzene and 1,3,5-trimethylbenzene in the presence of NO_x: effects of chemical structure on SOA aging*. Atmos. Chem. Phys., 2012. **12**(10): p. 4667-4682.
122. Yuan, B., et al., *Secondary formation of nitrated phenols: insights from observations during the Uintah Basin Winter Ozone Study (UBWOS) 2014*. Atmospheric Chemistry and Physics, 2016. **16**(4): p. 2139-2153.
123. Borrás, E. and L.A. Tortajada-Genaro, *Secondary organic aerosol formation from the photo-oxidation of benzene*. Atmospheric Environment, 2012. **47**: p. 154-163.
124. Lin, P., et al., *Molecular characterization of brown carbon (BrC) chromophores in secondary organic aerosol generated from photo-oxidation of toluene*. Physical Chemistry Chemical Physics, 2015. **17**(36): p. 23312-23325.
125. Iinuma, Y., et al., *Methyl-Nitrocatechols: Atmospheric Tracer Compounds for Biomass Burning Secondary Organic Aerosols*. Environmental science & technology. 2010. 8453-9.
126. Claeys, M., et al., *Formation of secondary organic aerosols through photooxidation of isoprene*. Science, 2004. **303**(5661): p. 1173-1176.
127. Carlton, A.G., C. Wiedinmyer, and J.H. Kroll, *A review of Secondary Organic Aerosol (SOA) formation from isoprene*. Atmospheric Chemistry and Physics, 2009. **9**(14): p. 4987-5005.
128. Ding, X., et al., *Spatial and seasonal variations of isoprene secondary organic aerosol in China: Significant impact of biomass burning during winter*. Scientific Reports, 2016. **6**: p. 10.
129. Edney, E.O., et al., *Formation of 2-methyl tetrols and 2-methylglyceric acid in secondary organic aerosol from laboratory irradiated isoprene/NO(X)/SO(2)/air mixtures and their detection in ambient PM(2.5) samples collected in the eastern United States*. Atmospheric Environment, 2005. **39**(29): p. 5281-5289.
130. Surratt, J.D., et al., *Chemical composition of secondary organic aerosol formed from the photooxidation of isoprene*. Journal of Physical Chemistry A, 2006. **110**(31): p. 9665-9690.
131. Surratt, J.D., et al., *Evidence for organosulfates in secondary organic aerosol*. Environmental Science & Technology, 2007. **41**(2): p. 517-527.
132. Surratt, J.D., et al., *Organosulfate formation in biogenic secondary organic aerosol*. Journal of Physical Chemistry A, 2008. **112**(36): p. 8345-8378.
133. Paulot, F., et al., *Unexpected Epoxide Formation in the Gas-Phase Photooxidation of Isoprene*. Science, 2009. **325**(5941): p. 730-733.
134. Lin, Y.-H., et al., *Epoxide as a precursor to secondary organic aerosol formation from isoprene photooxidation in the presence of nitrogen oxides*. Proceedings of the National Academy of Sciences, 2013. **110**(17): p. 6718.
135. Surratt, J.D., et al., *Reactive intermediates revealed in secondary organic aerosol formation from isoprene*. Proceedings of the National Academy of Sciences of the United States of America, 2010. **107**(15): p. 6640-6645.
136. Nguyen, T.B., et al., *Organic aerosol formation from the reactive uptake of isoprene epoxydiols (IEPOX) onto non-acidified inorganic seeds*. Atmospheric Chemistry and Physics, 2014. **14**(7): p. 3497-3510.
137. Paulot, F., et al., *Isoprene photooxidation: new insights into the production of acids and organic nitrates*. Atmospheric Chemistry and Physics, 2009. **9**(4): p. 1479-1501.
138. Chan, M.N., et al., *Characterization and Quantification of Isoprene-Derived Epoxydiols in Ambient Aerosol in the Southeastern United States*. Environmental Science & Technology, 2010. **44**(12): p. 4590-4596.

139. Hoyle, C.R., et al., *A review of the anthropogenic influence on biogenic secondary organic aerosol*. Atmospheric Chemistry and Physics, 2011. **11**(1): p. 321-343.
140. Alier, M., et al., *Source apportionment of submicron organic aerosol at an urban background and a road site in Barcelona (Spain) during SAPUSS*. Atmospheric Chemistry and Physics, 2013. **13**(20): p. 10353-10371.
141. Ding, X., et al., *Spatial distributions of secondary organic aerosols from isoprene, monoterpenes, beta-caryophyllene, and aromatics over China during summer*. Journal of Geophysical Research-Atmospheres, 2014. **119**(20): p. 11877-11891.
142. Shen, R.Q., et al., *Seasonal variation of secondary organic aerosol tracers in Central Tibetan Plateau*. Atmospheric Chemistry and Physics, 2015. **15**(15): p. 8781-8793.
143. Hu, W.W., et al., *Volatility and lifetime against OH heterogeneous reaction of ambient isoprene-epoxydiols-derived secondary organic aerosol (IEPOX-SOA)*. Atmospheric Chemistry and Physics, 2016. **16**(18): p. 11563-11580.
144. Ding, X., et al., *Spatial and seasonal variations of secondary organic aerosol from terpenoids over China*. Journal of Geophysical Research-Atmospheres, 2016. **121**(24): p. 14661-14678.
145. Claeys, M., et al., *Hydroxydicarboxylic Acids: Markers for Secondary Organic Aerosol from the Photooxidation of α -Pinene*. Environmental Science & Technology, 2007. **41**(5): p. 1628-1634.
146. Szmigielski, R., et al., *3-methyl-1,2,3-butanetricarboxylic acid: An atmospheric tracer for terpene secondary organic aerosol*. Geophysical Research Letters, 2007. **34**(24): p. 6.
147. Muller, L., et al., *Formation of 3-methyl-1,2,3-butanetricarboxylic acid via gas phase oxidation of pinonic acid - a mass spectrometric study of SOA aging*. Atmospheric Chemistry and Physics, 2012. **12**(3): p. 1483-1496.
148. Gomez-Gonzalez, Y., et al., *Characterization of organosulfates from the photooxidation of isoprene and unsaturated fatty acids in ambient aerosol using liquid chromatography/(-) electrospray ionization mass spectrometry*. J Mass Spectrom, 2008. **43**(3): p. 371-82.
149. Wang, W., et al., *Characterization of oxygenated derivatives of isoprene related to 2-methyltetrols in Amazonian aerosols using trimethylsilylation and gas chromatography/ion trap mass spectrometry*. Rapid Commun Mass Spectrom, 2005. **19**(10): p. 1343-51.
150. Hoffmann, T., et al., *Molecular composition of organic aerosols formed in the α -pinene/O₃ reaction: Implications for new particle formation processes*. Journal of Geophysical Research: Atmospheres, 1998. **103**(D19): p. 25569-25578.
151. Yu, J., et al., *Gas-Phase Ozone Oxidation of Monoterpenes: Gaseous and Particulate Products*. Journal of Atmospheric Chemistry, 1999. **34**(2): p. 207-258.
152. Glasius, M., M. Duane, and B.R. Larsen, *Determination of polar terpene oxidation products in aerosols by liquid chromatography-ion trap mass spectrometry*. Journal of Chromatography A, 1999. **833**(2): p. 121-135.
153. Larsen, B.R., et al., *Gas-Phase OH Oxidation of Monoterpenes: Gaseous and Particulate Products*. Journal of Atmospheric Chemistry, 2001. **38**(3): p. 231-276.
154. Claeys, M., et al., *Polar organic marker compounds in atmospheric aerosols during the LBA-SMOCC 2002 biomass burning experiment in Rondonia, Brazil: sources and source processes, time series, diel variations and size distributions*. Atmospheric Chemistry and Physics, 2010. **10**(19): p. 9319-9331.
155. Duan, J., et al., *Roadside, Urban, and Rural comparison of size distribution characteristics of PAHs and carbonaceous components of Beijing, China*. Journal of Atmospheric Chemistry, 2012. **69**(4): p. 337-349.
156. Amador-Munoz, O., et al., *Solvent extracted organic matter and polycyclic aromatic hydrocarbons distributed in size-segregated airborne particles in a zone of Mexico City: Seasonal behavior and human exposure*. Atmospheric Environment, 2010. **44**(1): p. 122-130.
157. de Guidi, G., et al., *The PAH and Nitro-PAH Concentration Profiles in Size-Segregated Urban Particulate Matter and Soil in Traffic-Related Sites in Catania, Italy*. Polycyclic Aromatic Compounds, 2012. **32**(4): p. 439-456.

158. Di Filippo, P., et al., *Concentrations of PAHs, and nitro- and methyl- derivatives associated with a size-segregated urban aerosol*. Atmospheric Environment, 2010. **44**(23): p. 2742-2749.
159. Herckes, P., et al., *Particle size distributions of organic aerosol constituents during the 2002 Yosemite Aerosol Characterization Study*. Environmental Science & Technology, 2006. **40**(15): p. 4554-4562.
160. Zhang, Z., et al., *Characteristics and applications of size-segregated biomass burning tracers in China's Pearl River Delta region*. Atmospheric Environment, 2015. **102**: p. 290-301.
161. Li, J.J., et al., *Observation of biogenic secondary organic aerosols in the atmosphere of a mountain site in central China: temperature and relative humidity effects*. Atmospheric Chemistry and Physics, 2013. **13**(22): p. 11535-11549.
162. Miyazaki, Y., et al., *Seasonal cycles of water-soluble organic nitrogen aerosols in a deciduous broadleaf forest in northern Japan*. Journal of Geophysical Research-Atmospheres, 2014. **119**(3): p. 1440-1454.
163. Azevedo, D.A., L.S. Moreira, and D.S. de Siqueira, *Composition of extractable organic matter in aerosols from urban areas of Rio de Janeiro city, Brazil*. Atmospheric Environment, 1999. **33**(30): p. 4987-5001.
164. Yan, B., et al., *Roadside, Urban, and Rural Comparison of Primary and Secondary Organic Molecular Markers in Ambient PM_{2.5}*. Environmental Science & Technology, 2009. **43**(12): p. 4287-4293.
165. Ding, X., et al., *Spatial and seasonal trends in biogenic secondary organic aerosol tracers and water-soluble organic carbon in the southeastern United States*. Environ Sci Technol, 2008. **42**(14): p. 5171-5176.
166. Basis, A., et al., *Toxic organic substances and marker compounds in size-segregated urban particulate matter - Implications for involvement in the in vitro bioactivity of the extractable organic matter*. Environmental Pollution, 2017. **230**: p. 758-774.
167. Pietrogrande, M.C., et al., *Seasonal variation and source estimation of organic compounds in urban aerosol of Augsburg, Germany*. Environmental Pollution:our instrumentation, 2011. **159**(7): p. 1861-1868.
168. Pietrogrande, M.C., et al., *Polar organic marker compounds in atmospheric aerosol in the Po Valley during the Supersito campaigns - Part 2: Seasonal variations of sugars*. Atmospheric Environment, 2014. **97**: p. 215-225.
169. Schnelle-Kreis, E., et al., *Analysis of particle-associated semi-volatile aromatic and aliphatic hydrocarbons in urban particulate matter on a daily basis*. Atmospheric Environment, 2005. **39**(40): p. 7702-7714.
170. Ding, X.A., X.M. Wang, and M. Zheng, *The influence of temperature and aerosol acidity on biogenic secondary organic aerosol tracers: Observations at a rural site in the central Pearl River Delta region, South China*. Atmospheric Environment, 2011. **45**(6): p. 1303-1311.
171. Haque, M.M., K. Kawamura, and Y. Kim, *Seasonal variations of biogenic secondary organic aerosol tracers in ambient aerosols from Alaska*. Atmospheric Environment, 2016. **130**: p. 95-104.
172. Elder, A., et al., *Translocation of inhaled ultrafine manganese oxide particles to the central nervous system*. Environmental Health Perspectives, 2006. **114**(8): p. 1172-1178.
173. Pope, C.A. and D.W. Dockery, *Health effects of fine particulate air pollution: Lines that connect*. Journal of the Air & Waste Management Association, 2006. **56**(6): p. 709-742.
174. Dockery, D.W., et al., *An association between air pollution and mortality in six U.S. cities*. N Engl J Med, 1993. **329**(24): p. 1753-9.
175. Pope, C.A., 3rd, et al., *Particulate air pollution as a predictor of mortality in a prospective study of U.S. adults*. Am J Respir Crit Care Med, 1995. **151**(3 Pt 1): p. 669-74.
176. Peters, A., et al., *Increased particulate air pollution and the triggering of myocardial infarction*. Circulation, 2001. **103**(23): p. 2810-5.

177. Künzli, N., et al., *Ambient Air Pollution and Atherosclerosis in Los Angeles*. Environmental Health Perspectives, 2005. **113**(2): p. 201-206.
178. Hoffmann, B., et al., *Residential exposure to traffic is associated with coronary atherosclerosis*. Circulation, 2007. **116**(5): p. 489-96.
179. Volk, H.E., et al., *Traffic-related air pollution, particulate matter, and autism*. JAMA Psychiatry, 2013. **70**(1): p. 71-7.
180. Pedersen, M., et al., *Ambient air pollution and low birthweight: a European cohort study (ESCAPE)*. Lancet Respir Med, 2013. **1**(9): p. 695-704.
181. Seaton, A., et al., *Particulate air pollution and acute health effects*. The Lancet, 1995. **345**(8943): p. 176-178.
182. Li, N., et al., *Use of a stratified oxidative stress model to study the biological effects of ambient concentrated and diesel exhaust particulate matter*. Inhal Toxicol, 2002. **14**(5): p. 459-86.
183. Li, N., et al., *Particulate air pollutants and asthma. A paradigm for the role of oxidative stress in PM-induced adverse health effects*. Clin Immunol, 2003. **109**(3): p. 250-65.
184. Lelieveld, J., et al., *The contribution of outdoor air pollution sources to premature mortality on a global scale*. Nature, 2015. **525**: p. 367.
185. Cohen, A.J., et al., *Estimates and 25-year trends of the global burden of disease attributable to ambient air pollution: an analysis of data from the Global Burden of Diseases Study 2015*. The Lancet. **389**(10082): p. 1907-1918.
186. Peters, A., et al., *Respiratory effects are associated with the number of ultrafine particles*. American journal of respiratory and critical care medicine, 1997. **155**(4): p. 1376-1383.
187. Brook, R.D., et al., *Air pollution and cardiovascular disease: a statement for healthcare professionals from the Expert Panel on Population and Prevention Science of the American Heart Association*. Circulation, 2004. **109**(21): p. 2655-71.
188. Mills, N.L., et al., *Diesel exhaust inhalation causes vascular dysfunction and impaired endogenous fibrinolysis*. Circulation, 2005. **112**(25): p. 3930-6.
189. Mills, N.L., et al., *Ischemic and thrombotic effects of dilute diesel-exhaust inhalation in men with coronary heart disease*. N Engl J Med, 2007. **357**(11): p. 1075-82.
190. Lucking, A.J., et al., *Diesel exhaust inhalation increases thrombus formation in man*. Eur Heart J, 2008. **29**(24): p. 3043-51.
191. Benbrahim-Tallaa, L., et al., *Carcinogenicity of diesel-engine and gasoline-engine exhausts and some nitroarenes*. Lancet Oncol, 2012. **13**(7): p. 663-4.
192. Beelen, R., et al., *Effects of long-term exposure to air pollution on natural-cause mortality: an analysis of 22 European cohorts within the multicentre ESCAPE project*. The Lancet. **383**(9919): p. 785-795.
193. Laden, F., et al., *Reduction in fine particulate air pollution and mortality - Extended follow-up of the Harvard six cities study*. American Journal of Respiratory and Critical Care Medicine, 2006. **173**(6): p. 667-672.
194. Pope, C.A., et al., *Cardiovascular mortality and long-term exposure to particulate air pollution - Epidemiological evidence of general pathophysiological pathways of disease*. Circulation, 2004. **109**(1): p. 71-77.
195. Huttunen, K., et al., *Low-level exposure to ambient particulate matter is associated with systemic inflammation in ischemic heart disease patients*. Environmental Research, 2012. **116**: p. 44-51.
196. Valavanidis, A., K. Fiotakis, and T. Vlachogianni, *Airborne Particulate Matter and Human Health: Toxicological Assessment and Importance of Size and Composition of Particles for Oxidative Damage and Carcinogenic Mechanisms*. Journal of Environmental Science and Health Part C-Environmental Carcinogenesis & Ecotoxicology Reviews, 2008. **26**(4): p. 339-362.
197. Kelly, F.J. and J.C. Fussell, *Size, source and chemical composition as determinants of toxicity attributable to ambient particulate matter*. Atmospheric Environment, 2012. **60**: p. 504-526.
198. Nel, A., et al., *Toxic potential of materials at the nanolevel*. Science, 2006. **311**(5761): p. 622-627.

199. Jalava, P.I., et al., *Heterogeneities in inflammatory and cytotoxic responses of RAW 264.7 macrophage cell line to urban air coarse, fine, and ultrafine particles from six European sampling campaigns*. *Inhalation Toxicology*, 2007. **19**(3): p. 213-225.
200. Araujo, J.A., et al., *Ambient particulate pollutants in the ultrafine range promote early atherosclerosis and systemic oxidative stress*. *Circulation Research*, 2008. **102**(5): p. 589-596.
201. Daher, N., et al., *Characterization, sources and redox activity of fine and coarse particulate matter in Milan, Italy*. *Atmospheric Environment*, 2012. **49**: p. 130-141.
202. Happonen, M.S., et al., *Chemical Compositions Responsible for Inflammation and Tissue Damage in the Mouse Lung by Coarse and Fine Particulate Samples from Contrasting Air Pollution in Europe*. *Inhalation Toxicology*, 2008. **20**(14): p. 1215-1231.
203. Dominici, F., et al., *Protecting Human Health From Air Pollution Shifting From a Single-pollutant to a Multipollutant Approach*. *Epidemiology*, 2010. **21**(2): p. 187-194.
204. Billionnet, C., et al., *Estimating the Health Effects of Exposure to Multi-Pollutant Mixture*. *Annals of Epidemiology*, 2012. **22**(2): p. 126-141.
205. de Kok, T., et al., *Toxicological assessment of ambient and traffic-related particulate matter: A review of recent studies*. *Mutation Research-Reviews in Mutation Research*, 2006. **613**(2-3): p. 103-122.
206. Tainio, M., et al., *Uncertainty in health risks due to anthropogenic primary fine particulate matter from different source types in Finland*. *Atmospheric Environment*, 2010. **44**(17): p. 2125-2132.
207. Sigsgaard, T., et al., *Health impacts of anthropogenic biomass burning in the developed world*. *European Respiratory Journal*, 2015. **46**(6): p. 1577-1588.
208. Tuet, W.Y., et al., *Chemical oxidative potential of secondary organic aerosol (SOA) generated from the photooxidation of biogenic and anthropogenic volatile organic compounds*. *Atmospheric Chemistry and Physics*, 2017. **17**(2): p. 839-853.
209. Mar, T.F., et al., *PM source apportionment and health effects. 3. Investigation of inter-method variations in associations between estimated source contributions Of PM2.5 and daily mortality in Phoenix, AZ*. *Journal of Exposure Science and Environmental Epidemiology*, 2006. **16**(4): p. 311-320.
210. Ito, K., et al., *PM source apportionment and health effects: 2. An investigation of intermethod variability in associations between source-apportioned fine particle mass and daily mortality in Washington, DC*. *Journal of Exposure Science and Environmental Epidemiology*, 2006. **16**(4): p. 300-310.
211. Stanek, L.W., et al., *Attributing health effects to apportioned components and sources of particulate matter: An evaluation of collective results*. *Atmospheric Environment*, 2011. **45**(32): p. 5655-5663.
212. Segersson, D., et al., *Health Impact of PM10, PM2.5 and Black Carbon Exposure Due to Different Source Sectors in Stockholm, Gothenburg and Umea, Sweden*. *International Journal of Environmental Research and Public Health*, 2017. **14**(7).
213. Oberdörster, G., *Pulmonary effects of inhaled ultrafine particles*. *International archives of occupational and environmental health*, 2000. **74**(1): p. 1-8.
214. Knol, A.B., et al., *Expert elicitation on ultrafine particles: likelihood of health effects and causal pathways*. *Particle and Fibre Toxicology*, 2009. **6**.
215. Schwartz, J. and A. Marcus, *Mortality and air pollution in London: a time series analysis*. *Am J Epidemiol*, 1990. **131**(1): p. 185-94.
216. Hoek, G., et al., *Air Pollution Exposure in Europe-Assessment in the ESCAPE study*. *Epidemiology*, 2009. **20**(6): p. S254-S254.
217. Geiser, M., et al., *Ultrafine particles cross cellular membranes by nonphagocytic mechanisms in lungs and in cultured cells*. *Environmental Health Perspectives*, 2005. **113**(11): p. 1555-1560.
218. Li, N., et al., *Ultrafine particulate pollutants induce oxidative stress and mitochondrial damage*. *Environmental health perspectives*, 2003. **111**(4): p. 455.

219. Oberdörster, G., et al., *Translocation of inhaled ultrafine particles to the brain*. Inhalation toxicology, 2004. **16**(6-7): p. 437-445.
220. Oberdörster, G., et al., *Extrapulmonary translocation of ultrafine carbon particles following whole-body inhalation exposure of rats*. Journal of Toxicology and Environmental Health-Part A, 2002. **65**(20): p. 1531-1543.
221. Saffari, A., et al., *Seasonal and spatial variation in reactive oxygen species activity of quasi-ultrafine particles (PM_{0.25}) in the Los Angeles metropolitan area and its association with chemical composition*. Atmospheric Environment, 2013. **79**: p. 566-575.
222. Saffari, A., et al., *Seasonal and spatial variation in dithiothreitol (DTT) activity of quasi-ultrafine particles in the Los Angeles Basin and its association with chemical species*. Journal of Environmental Science and Health Part a-Toxic/Hazardous Substances & Environmental Engineering, 2014. **49**(4): p. 441-451.
223. Daher, N., et al., *Seasonal and spatial variability in chemical composition and mass closure of ambient ultrafine particles in the megacity of Los Angeles*. Environmental Science-Processes & Impacts, 2013. **15**(1): p. 283-295.
224. Hopke, P.K., *Review of receptor modeling methods for source apportionment*. Journal of the Air & Waste Management Association, 2016. **66**(3): p. 237-259.
225. Holmes, N.S. and L. Morawska, *A review of dispersion modelling and its application to the dispersion of particles: An overview of different dispersion models available*. Atmospheric Environment, 2006. **40**(30): p. 5902-5928.
226. Viana, M., et al., *Source apportionment of particulate matter in Europe: A review of methods and results*. Journal of Aerosol Science, 2008. **39**(10): p. 827-849.
227. Hopke, P.K., *Recent developments in receptor modeling*. Journal of Chemometrics, 2003. **17**(5): p. 255-265.
228. Paatero, P. and U. Tapper, *Analysis of different modes of factor analysis as least squares fit problems*. Chemometrics and Intelligent Laboratory Systems, 1993. **18**(2): p. 183-194.
229. Paatero, P. and U. Tapper, *Positive matrix factorization: A non-negative factor model with optimal utilization of error estimates of data values*. Environmetrics, 1994. **5**(2): p. 111-126.
230. Paatero, P., *A weighted non-negative least squares algorithm for three-way 'PARAFAC' factor analysis*. Chemometrics and Intelligent Laboratory Systems, 1997. **38**(2): p. 223-242.
231. Paatero, P., *The Multilinear Engine—A Table-Driven, Least Squares Program for Solving Multilinear Problems, Including the n-Way Parallel Factor Analysis Model*. Journal of Computational and Graphical Statistics, 1999. **8**(4): p. 854-888.
232. Hopke, P., *The Application of Receptor Modeling to Air Quality Data*. Pollution Atmospherique. 2010. 91-109.
233. Kim, E., P.K. Hopke, and E.S. Edgerton, *Source Identification of Atlanta Aerosol by Positive Matrix Factorization*. Journal of the Air & Waste Management Association, 2003. **53**(6): p. 731-739.
234. Polissar, A.V., P.K. Hopke, and R.L. Poirot, *Atmospheric Aerosol over Vermont: Chemical Composition and Sources*. Environmental Science & Technology, 2001. **35**(23): p. 4604-4621.
235. Pant, P. and R.M. Harrison, *Critical review of receptor modelling for particulate matter: A case study of India*. Atmospheric Environment, 2012. **49**: p. 1-12.
236. Thurston, G.D. and J.D. Spengler, *A quantitative assessment of source contributions to inhalable particulate matter pollution in metropolitan Boston*. Atmospheric Environment (1967), 1985. **19**(1): p. 9-25.
237. Marple, V.A. and K. Willeke, *Impactor design*. Atmospheric Environment, 1976. **10**: p. 891-896.
238. Jarvinen, A., et al., *Calibration of the new electrical low pressure impactor (ELPI plus)*. Journal of Aerosol Science, 2014. **69**: p. 150-159.
239. Marple, V., et al., *Second Generation Micro-Orifice Uniform Deposit Impactor, 120 MOUDI-II: Design, Evaluation, and Application to Long-Term Ambient Sampling*. Aerosol Science and Technology, 2014. **48**(4): p. 427-433.

240. Lundgren, D.A., *An aerosol sampler for determination of particle concentration as a function of size and time*. J Air Pollut Control Assoc, 1967. **17**(4): p. 225-9.
241. Cahill, T., et al., *DRUM Quality Assurance Protocols*. 2008.
242. Kavouras, I.G. and P. Koutrakis, *Use of polyurethane foam as the impaction substrate/collection medium in conventional inertial impactors*. Aerosol Science and Technology, 2001. **34**(1): p. 46-56.
243. Lee, S.J., P. Demokritou, and P. Koutrakis, *Performance evaluation of commonly used impaction substrates under various loading conditions*. Journal of Aerosol Science, 2005. **36**(7): p. 881-895.
244. Demokritou, P., et al., *A compact multistage (cascade) impactor for the characterization of atmospheric aerosols*. Journal of Aerosol Science, 2004. **35**(3): p. 281-299.
245. Bukowiecki, N., et al., *Iron, manganese and copper emitted by cargo and passenger trains in Zurich (Switzerland): Size-segregated mass concentrations in ambient air*. Atmospheric Environment, 2007. **41**(4): p. 878-889.
246. Bukowiecki, N., et al., *Trace metals in ambient air: Hourly size-segregated mass concentrations determined by Synchrotron-XRF*. Environmental Science & Technology, 2005. **39**(15): p. 5754-5762.
247. Richard, A.C.J., *Determination of trace elements in ambient aerosols with synchrotron induced X-ray fluorescence spectrometry and subsequent source apportionment*. 2011, ETH Zürich, Switzerland: Zürich. p. 1-169.
248. Bukowiecki, N., et al., *Deposition Uniformity and Particle Size Distribution of Ambient Aerosol Collected with a Rotating Drum Impactor*. Aerosol Science and Technology, 2009. **43**(9): p. 891-901.
249. Hermann, M. and A. Wiedensohler, *Counting efficiency of condensation particle counters at low pressures with illustrative data from the upper troposphere*. Journal of Aerosol Science, 2001. **32**(8): p. 975-991.
250. Seifert, M., et al., *Operation and performance of a differential mobility particle sizer and a TSI 3010 condensation particle counter at stratospheric temperatures and pressures*. Journal of Aerosol Science, 2004. **35**(8): p. 981-993.
251. Pitz, M., et al., *Quality control and quality assurance for particle size distribution measurements at an urban monitoring station in Augsburg, Germany*. Journal of Environmental Monitoring, 2008. **10**(9): p. 1017-1024.
252. Pitz, M., et al., *Seasonal and diurnal variation of PM(2.5) apparent particle density in urban air in Augsburg, Germany*. Environmental Science & Technology, 2008. **42**(14): p. 5087-5093.
253. Orasche, J., et al., *Technical Note: In-situ derivatization thermal desorption GC-TOFMS for direct analysis of particle-bound non-polar and polar organic species*. Atmos. Chem. Phys., 2011. **11**(17): p. 8977-8993.
254. Pitz, M., et al., *Variability of apparent particle density of an urban aerosol*. Environmental Science & Technology, 2003. **37**(19): p. 4336-4342.
255. Rao, A.K. and K.T. Whitby, *Non-ideal collection characteristics of inertial impactors—II. Cascade impactors*. Journal of Aerosol Science, 1978. **9**(2): p. 87-100.
256. Sillanpaa, M., et al., *Field and laboratory tests of a high volume cascade impactor*. Journal of Aerosol Science, 2004. **34**(4): p. 485-500.
257. Hasheminassab, S., et al., *Source apportionment and organic compound characterization of ambient ultrafine particulate matter (PM) in the Los Angeles Basin*. Atmospheric Environment, 2013. **79**: p. 529-539.
258. Kam, W., et al., *Size-segregated composition of particulate matter (PM) in major roadways and surface streets*. Atmospheric Environment, 2012. **55**: p. 90-97.
259. Li, F., et al., *Organic speciation of ambient quasi-ultrafine particulate matter (PM_{0.36}) in Augsburg, Germany: Seasonal variability and source apportionment*. Science of The Total Environment, 2018. **615**(Supplement C): p. 828-837.

260. Li, F.X., et al., *Semi-continuous sampling of health relevant atmospheric particle subfractions for chemical speciation using a rotating drum impactor in series with sequential filter sampler*. Environmental Science and Pollution Research, 2016. **23**(8): p. 7278-7287.
261. Wagener, S., et al., *Spatial and seasonal variations of biogenic tracer compounds in ambient PM10 and PM1 samples in Berlin, Germany*. Atmospheric Environment, 2012. **47**: p. 33-42.
262. Gu, J.W., et al., *Spatial and temporal variability of PM10 sources in Augsburg, Germany*. Atmospheric Environment, 2013. **71**: p. 131-139.
263. Qadir, R.M., et al., *Spatial and temporal variability of source contributions to ambient PM10 during winter in Augsburg, Germany using organic and inorganic tracers*. Chemosphere, 2014. **103**: p. 263-273.
264. Cyrus, J., et al., *Spatial and temporal variation of particle number concentration in Augsburg, Germany*. Science of the Total Environment, 2008. **401**(1-3): p. 168-175.
265. Shrivastava, M., et al., *Global transformation and fate of SOA: Implications of low-volatility SOA and gas-phase fragmentation reactions*. Journal of Geophysical Research-Atmospheres, 2015. **120**(9): p. 4169-4195.
266. Lin, Y.H., et al., *Isoprene Epoxydiols as Precursors to Secondary Organic Aerosol Formation: Acid-Catalyzed Reactive Uptake Studies with Authentic Compounds*. Environmental Science & Technology, 2012. **46**(1): p. 250-258.
267. Worton, D.R., et al., *Observational Insights into Aerosol Formation from Isoprene*. Environmental Science & Technology, 2013. **47**(20): p. 11403-11413.

Appendix

1. LIST OF ABBREVIATIONS	57
2. LIST OF FIGURES	60
3. LIST OF TABLES	62
3. CURRICULUM VITAE	63
4. PUBLICATION LIST	64
5. PUBLICATIONS FOR THE CUMULATIVE DISSERTATION	65

1. LIST OF ABBREVIATIONS

2-MGA	2-methylglyceric acid
3-HGA	3-hydroxyglutaric acid
3-MBTCA	C8-tricarboxylic acid 3-methyl-1,2,3-butanetricarboxylic acid
4-NC	4-nitrocatechol
4-NP	4-nitrophenol
ACS	American Cancer Society
AMS	aerosol mass spectrometry
ANS	autonomic nervous system
APS	aerodynamic particle sizer
BC	black carbon
CCN	cloud condensation nuclei
$C_{Dp, 50\%}$	midpoint collection diameter
CI	confidence interval
CMB	chemical mass balance
CMD	count median diameter
CNS	central nervous system
COD	coefficient of divergence
CPC	condensation particle counter
CPF	conditional probability function
CRP	C-reactive protein
D_{Ac}	aerodynamic diameter
DALY	disability-adjusted life-years
DCA	dicarboxylic acid
DMA	differential mobility analyzer
DPF	diesel particulate filter
DTT	Dithiothreitol
EC	elemental carbon
ELVOC	extremely low-volatile organic compound
F_p	particle phase fraction
GR	global radiation
HMW	high molecular weight
HOA	hydrocarbon-like organic aerosol
HOM	highly oxidized multifunctional organic compound
HULIS	humic-like substances
IDTD-GC-TOF-MS	<i>In situ</i> Derivatization Thermal Desorption Gas Chromatography Time-of-Flight Mass Spectrometry
IEPOX	isoprene epoxydiols
IL	interleukin
ISOPOOH	hydroxy hydroperoxides
IVOC	intermediate volatile organic compound

LUR	land use regression modeling
LVOC	low-volatile organic compound
MAE	methacrylic acid epoxide
MAPK	mitogen-activated protein kinase
ME	Multilinear Engine
MLX	mixing layer height
MM-CMB	molecular marker based chemical mass balance
MPAN	peroxymethylacrylic nitric anhydride
MSTFA	N-methyl-N-trimethylsilyl-trifluoroacetamide
MW	molecular weight
NAC	nitroaromatic compounds
NADPH	nicotinamide adenine dinucleotide phosphate
Nrf2	nuclear factor erythroid-2
OA	organic aerosol
OC	organic carbon
OM	organic matter
OOA	oxygenated organic aerosol
PAH	polycyclic aromatic hydrocarbon
PCA	principal component analysis
PM	Particulate matter
PM _{0.1}	particulate matter with an aerodynamic diameter of less than 100 nm
PM _{0.36}	particulate matter with an aerodynamic diameter of less than 360 nm
PM ₁₀	particulate matter with an aerodynamic diameter of less than 10 µm
PM _{2.5}	particulate matter with an aerodynamic diameter of less than 2.5 µm
PMF	positive matrix factorization
PM _x	particulate matter with an aerodynamic diameter of less than x µm
PNC	particle number concentration
PNSD	particle number size distribution
POA	primary organic aerosol
PSCF	Potential source contribution function
PUF	polyurethane foam
QFF	quartz fibre filter
quasi-UFP	quasi ultrafine particulate matter
RDI	rotating drum impactor
RO ·	oxy radical
RO ₂ ·	peroxy radical
ROS	reactive oxygen species
SA	source apportionment
SE	sulphate ester
SOA	secondary organic aerosol
SVOC	semi-volatile organic compound
TC	total carbon
TDMPS	twin differential mobility particle sizer

TNF- α	tumour necrosis factor- α
UFP	ultrafine particulate matter
US-EPA	United States Environment Protection Agency
UV	ultraviolet
VIS	visible
VOC	volatile organic compound
WSOC	water soluble organic carbon

2. LIST OF FIGURES

Fig. 1 Schematic image of the formation, growth and processing of atmospheric aerosol. Adapted from Zhang et al. [1].	1
Fig. 2 Schematic example of number and mass size distribution of the same aerosol population. Nucleated fresh particles can increase in size through condensation and coagulation, and decrease through evaporation. Modified from Fuzzi et al. [5].	2
Fig. 3 A schematic example of the composition of UFP (e.g. in urban environment). Adapted from Stone et al. [18].	3
Fig. 4 Average composition of PM ₁₀ and PM _{2.5} at rural and urban sites across Europe. OM calculated as OC*1.4, its contribution to PM was therefore probably underestimated. Adapted from Fuzzi et al. [5] and Putaud et al. [46]	5
Fig. 5 Thermochemical and optical classification of EC, BC and OC. Adapted from Poeschl et al. [50].	6
Fig. 6 Schematic image of primary emissions and photochemical oxidation of organic compounds in the atmosphere. Compounds in the particulate phase are highlighted in yellow, while those in the gas phase are not highlighted. Adapted from Fuzzi et al. [5].	7
Fig. 7 Simplified representation of the mechanism of atmospheric oxidation of a generic VOC. Bold black arrows denote reactions that can lead to a substantial decrease in volatility; gray arrows denote reactions that increase volatility substantially. Adapted from Kroll et al. [61].	8
Fig. 8 Molecular structure of four representative PAHs.	10
Fig. 9 Schematic image of Hopanes' characteristic structure.	11
Fig. 10 Molecular structure of levoglucosan.	11
Fig. 11 Molecular structure of 4-nitrophenol and 4-nitrocatechol	13
Fig. 12 The concept of continental or regional background, urban increment and local traffic increment. Adapted from Fuzzi et al. [5].	17
Fig. 13 Time line showing an increased interest in PM health effects research over the last three decades; key studies and research trends are highlighted in the table. Adapted from Stone et al. [18].	18
Fig. 14 schematic image illustrating some of the key mechanisms through which inhaled UFP may influence secondary organs and systemic tissues, with emphasis on the mechanism through which inhaled particles may cause cardiovascular events. Adapted from Stone et al. [18].	19
Fig. 15 One of the two sequentially-connected RDI and Partisol sampler sets (I) and drum substrate loaded with ambient PM (II: all drums; III: the 3 rd stage).	26
Fig. 16 streamlines and particle trajectories for a typical impactor stage. Adapted from Marple and Willeke [237].	26
Fig. 17 Experimental set up for testing of RDI cut-point (3 rd stage).	27
Fig. 18 Locations of sampling sites in Augsburg. Red dots 13, 19, 6, 2 and 18 correspond to master sites T1, T2, T3, T4 and B1, respectively.	29

Fig. 19 Analysis procedures and in situ derivatization thermal desorption unit (figure at the right side of the bracket). Silylation reaction of polar organic species with MSTFA is shown at the top right corner. Adapted from Orasche et al. [253].	30
Fig. 20 Collection efficiency curves of the last impaction stage of both RDIs.	32
Fig. 21 Source factor profiles identified by PMFref. (species in ng m^{-3} , OC fractions in $\mu\text{g m}^{-3}$ and particle numbers in cm^{-3}).	35
Fig. 22 Seasonal variation of source factors contributing to explained OC concentrations.	36
Fig. 23 Percentage contributions of source factors to size-segregated particle number concentrations and OC fractions, and residue which could not be attributed to source factors.	36
Fig. 24 Comparison of source contributions to OC at the reference site and corresponding parallel sampled master site.	38
Fig. 25 Windrose at site T3 during 1 st sampling period showing wind coming mainly from southwest.	40
Fig. 26 Calculated Pearson r values (left) and coefficient of divergence (COD, right) for each source factor between the reference site and each master site. Boxplots are generated from the values for all parameters of compound concentration and source contribution, while coloured shaped coded markers represent values for different source factors.	40

3. LIST OF TABLES

Table 1. Overview of main isoprene and pinene SOA markers reported (SE: sulphate ester), and selected references regarding their structural characterization. Only the compounds with molecular structures shown are the ones measured in this study. (Adapted from Noziere et al. [60]).	15
Table 2. Summary of sampling site profiles	31